DEVELOPMENT AND EXPERIMENTAL VALIDATION OF AN ACID MINE DRAINAGE PREDICTION TOOL BASED ON MINERAL PARTICLES

Mafeni Samuel Ramatsoma

A Dissertation submitted to the Faculty of Engineering and the Built Environment, University of the Witwatersrand, in fulfillment of the requirements for the degree of Master of Science.

September 2024

Declaration

I, Mafeni Samuel Ramatsoma declare that this Dissertation is my own, unaided work. It is being submitted for the Degree of Master of Science at the University of the Witwatersrand, Johannesburg. It has not been submitted before for any degree or examination at any other University.

_____

September 2024

ABSTRACT

Acid Mine Drainage (AMD) is an environmental hazard that is generated as a by-product of mining-related activities. It is an acidic metal-rich water formed when sulfide minerals react with oxygen and water. Due to different ore types at different mines, kinetic AMD models are often 'calibrated' with kinetic humidity tests done with the target mine site ore. However, most of these tests require several months to complete. This study aimed to investigate ways to reduce the time required to conduct kinetic humidity tests, and to develop a mineral particles-based kinetic AMD model. An Accelerated Humidity Cell (AHC) is proposed in this study. It was tested with two ore types and performed better (produced 24% more acidic-leachates) than normal humidity cells. The particles-based model was developed and tested with experimental data and gave promising results. It is recommended that the proposed model and AHC be further tested with other ore types.

Conference and/or Symposia presentations arising from this study

Ramatsoma, S., Chetty, D., Bazhko, O. and Govender, V. 2022, "Acid mine drainage prediction with the aid of accelerated humidity cell tests" SAIMM, Mine-Impacted Water Conference, 12-13 October, online conference.
https://www.saimm.co.za/media/com_eventbooking/AMD%20Conference%202022%20Preliminary%20Programme-27092022.pdf

Acknowledgments

A warm thank you to the following people and organisation for their contribution to this study:

- Mintek; Mintek funded this project and the Mintek facilities were used during this study.
- Prof Jean Mulopo and Prof Kevin Harding for the assistance, patience and guidance.
- The Mintek research team of the main project from which this study was initiated: Dr Deshenthree Chetty, Ms Veruska Govendor, and Dr Olga Bazhko.

TABLE OF CONTENTS

LIST OF FIGURES

LIST OF TABLES

NOMENCLATURE

A	Arrhenius equation pre-exponential factor	1/s
C_{o2}	Concentration of oxygen	kg/m^3
$c_{wf,i}$	Concentration of species i in water	kg/m^3
D	Column Diameter	m
D_e	Oxygen diffusion coefficient	m^2/s
D_w	Water Oxygen diffusion coefficient	m^2/s
D_2	Oxygen diffusion coefficient within mineral grain	m^2/s
E_a	Activation energy	J/mol
f_m	Bacteria/microbiological factor	(-)
g	Gravitational acceleration	m/s^2
h	Matric potential	m
H	Henry's law constant	(-)
$\boldsymbol{k}$	Reaction rate constant	1/s
K	Hydraulic conductivity	m/s
K_i	Initial Hydraulic conductivity	m/s
k'	Intrinsic permeability	m^2

K_s	Hydraulic conductivity at saturation	m/s
L_s	Sulfide liberation	(-)
L_c	Carbonate liberation	(-)
m_i	Sulfide mass oxidized at discrete layer i	kg
m_o	Total sulfide oxidized	kg
N	Total number of discrete layers	(-)
N_p	Total number of particles in the ore bed/heap	(-)
n	van Genuchten constant n	(-)
PS	Pyrite/Sulphur mass ratio	(-)
R_p	Particle radius	m
R	Gas constant	J/(K.mol)
r	Reaction rate	mol/(L.s)
r_c	Non-reacted particle radius	m
S	Inflow (source) or outflow (sink) fluid flux	$m^3/(s.m^3)$
S_e	Effective saturation	(-)
t	Time	s

T	Temperature	°C
$\boldsymbol{T}$	Absolute temperature	K
V_{total}	The overall ore bed/heap total	m^3
$V_{p,total}$	The total volume occupied by particles	m^3
x	Position in x direction	m
$X_{p,i}$	Volume fraction of particle size class/range i	m^3/m^3
y	Position in y direction	m
z	Position in z direction	m

Greek letters

α	van Genuchten alpha	(-)
ε	Effective factor	(-)
θ	Water volumetric content	m^3/m^3
θ_{eq}	Air volumetric equivalent content	m^3/m^3
θ_a	Air content	m^3/m^3
θ_a	Water volumetric content	m^3/m^3
θ_r	Residual water content	m^3/m^3

θ_s	Water volumetric content at saturation	m^3/m^3
μ	Viscosity	$N.s/m^2$
ρ	Density	kg/m^3
φ	Porosity	(-)

CHAPTER 1. INTRODUCTION

1.1. Background

Globally, it is of critical concern to address the environmental effects of mining and mining-related activities. New and existing mines are now obliged to put plans in place to deal with the detrimental waste that could be generated during and after the mining activities. Acid Rock Drainage (ARD), in a broader context, Acid Mine Drainage (AMD) is one of the environmental concerns that must be addressed. It is an acidic metal-rich water that is formed when sulfide-bearing minerals or phases are exposed to oxygen and water (Erguler & Erguler, 2020, Becker *et al.*, 2015; Sapsford *et al.*, 2009).

About 5800 abandoned mine dumps were reported in China in 2018 (Wang *et al*., 2020). In Japan, of the 5487 abandoned and/or closed mines reported in 2000, several of them were generating AMD (Herrera *et al*., 2007). In South Africa, there were approximately 5906 abandoned mine dumps in 2009 as listed in the report of the South African Auditor General (2009); the South African Auditor General was consulted in 2024 also, and they confirmed that they had not done a follow up report yet i.e. their records still shows that there are approximately 5906 abandoned mine dumps in South Africa. Hence, accurate and cost-effective AMD prediction models are crucial to assist the South African government in classifying and prioritizing the critical abandoned mine dumps (i.e. the ones at or close to peak AMD production) for remediation. Erguler and Erguler (2020) stated that AMD simulations are crucial not only after the mining operations but even before, and during the mining operations to develop remediation processes for the potential AMD hazard. This is also supported by the study by Leiva *et al.* (2021) that investigated the effect of possible AMD formation (i.e. sulphate content) on the paste tailings storage design.

Literature studies have also shown that valuable by-products can be extracted from AMD (Ayoraet *et al.*, 2015). Therefore, it is also crucial to be able to predict the rate of acid production to aid with the prediction of how much byproducts can be extracted in a financially viable manner.

To safely dispose of the mine plant tails-to-tails dumps, it is also crucial to know whether the ore will generate any acid, and when and how much acid will be generated. Static test methods are most commonly used to predict if any acid will form (Karlsson *et al.*, 2021; Yeheyis *et al.*, 2009). The major disadvantage of the static AMD prediction models currently used in the industry is that they do not give the occurrence profile nor the estimated time of when the mine dump or tailings facilities will generate more acid if indeed it will. The 'when' and 'how much' are crucial for prioritising resources for management and mitigation of AMD potential if more than one mine tails dumps are considered. To address this, experimental kinetic tests and/or model predictions are used to predict when and how much acid will be formed. However, experimental kinetic tests which are typically laboratory-based columns, humidity cells, and field-based test pads, take time (several months to years) to get meaningful results. It was suggested by the United States Environmental Protection Agency (1994) that kinetic tests should be run for periods of at least 20 weeks, and this has been observed to be the least required time in most studies and some studies required even more time (Parbhakar-Fox *et al.*, 2013; Sapsforda *et al.*, 2008; GARD Guide, 2012).

According to Chetty *et al.* (2020), there is an opportunity to improve AMD predictions by including the modelling and simulation of changes in the system's individual particle properties over time. The study by Bernardes de Souza and Mansur (2011) showed that an AMD prediction model that uses a single average particle size can over-predict or under-predict if the selected particle size is wrong.

1.2. Aim and Objectives

1.2.1. Aim

This study aimed to investigate methods for reducing the time required to obtain meaningful experimental kinetic humidity test results, that can be used along with mathematical models for AMD prediction. Additionally, it sought to develop an AMD prediction tool that uses multiple input particle sizes. Therefore, the overall aim was to enhance the efficiency and accuracy of predicting acid mine drainage.

1.2.2. Objectives

1. To develop hardware and/or systems to accelerate the experimental kinetic humidity tests. This included:
   1.1. Designing and building a custom humidity cell that can directly regulate its environmental conditions (e.g. temperature) with a control system.
   1.2. Conducting experimental kinetic tests with the custom-built humidity cell and with a conventional humidity cell using two different ore types
   1.3. Comparing the results from the custom humidity cell with the conventional humidity cell to determine if the kinetic humidity test results were accelerated by or in the custom humidity cell.

2. To develop a kinetic AMD prediction model that incorporates multiple particle sizes from ore samples (i.e. mineral particles-based AMD prediction tool). This included:
   2.1. Developing a technique to handle multiple particle size inputs (at least four particle sizes) in the AMD prediction model
   2.2. Testing the developed model's prediction capabilities using the experimental data obtained from the tests conducted in Objective 1.2.
   2.3. Comparing the developed multiple particle sizes based model with a model that uses a single particle size as typically used in literature studies such as Ma *et al*. (2019), and Bernardes de Souza and Mansur (2011).

1.3. Scope

This investigation presents the customized humidity cell recommended for accelerating the kinetic humidity tests which are often used along with mathematical models for kinetic AMD prediction. The customized humidity cell was tested with two ore types and compared with standard kinetic humidity cell tests. The experimental kinetic test results were then compared with the model predictions. The main distinctive feature of the model presented in this study is the incorporation

of multiple mineral particle sizes in the model and how the particle sizes can be used to select the mesh cell sizes when solving the infiltration or fluid flow models used for AMD prediction.

1.4. Structure of the Document

The layout of the seven chapters presented in this document is as follows:

Chapter 1 summarises the background of the research, the problem statement, the research aim and objectives, and methods.

Chapter 2 presents a literature review on the principle of AMD formation and neutralization, and a brief overview of its impact on the environment and society. The AMD kinetic tests, and recent models for static and kinetic AMD predictions are also presented in this chapter.

Chapter 3 discusses the difference between the typical kinetic humidity cell and the proposed customised humidity cell that is supposed to aid with accelerating the kinetic tests. The proposed minerals particles-based AMD predictor that is meant to enhance the AMD prediction accuracy is also presented in this chapter.

Chapter 4 describes the methodology followed to conduct experimental tests and simulations which were used to evaluate the proposed custom humidity cell and the mineral particles-based AMD prediction models presented in Chapter 3, and to compare them with the relevant literature techniques presented in Chapter 2.

Chapter 5 presents the results obtained from the experimental tests and simulations conducted as per the methodology in Chapter 4.

Chapter 6 discusses the results obtained from Chapter 5 and any other possible areas of improvement.

Chapter 7 presents the overall conclusions from this research and recommendations for future work.

CHAPTER 2. LITERATURE REVIEW

2.1. AMD Overview and its Impact on the Environment

2.1.1. Principle of AMD

AMD is commonly associated with the mining of minerals such as gold, copper, and nickel (Bouzahzah *et al*., 2015). In most cases, pyrite is a common sulfide mineral found in tailings and oxidises to produce acid. The general reaction equation for acid mine drainage formation from sulfide ores is given below using pyrite as an example (Dold, 2014; Garland, 2011; Sangita *et al.*, 2010; Weber *et al*., 2006; Kreger, 2004):

$$4\mathrm{FeS_2\ (s)} + 15\mathrm{O_2\ (g)} + 14H_2\mathrm{O\ (l)} \rightarrow 4\mathrm{Fe(OH)_3\ (s)} + 8H_2SO_4\ \mathrm{(aq)} \qquad 2.1$$

The following sulfides also undergo a similar chemical reaction i.e. they can produce acid when they react with water and oxygen: Arsenopyrite, Pyrrhotite, Chalcopyrite, and Chalcocite (Dold, 2014; Simate & Ndlovu, 2014; Sangita *et al.*, 2010).

The acid neutralization reaction by carbonate minerals can be summarized as follows (Mauren *et al.*, 2020; Ma *et al.*, 2019; Fusi *et al.*, 2015; Fusi *et al.*, 2012):

$$\mathrm{CaCO_3\ (s)} + \mathrm{H_2SO_4\ (aq)} \rightarrow \mathrm{H_2O\ (l)} + \mathrm{CO_2\ (g)} + \mathrm{CaSO_4}(s) \qquad 2.2$$

Although the process of AMD formation is known to occur naturally, heavy mining activity in recent years has proven to promote AMD generation by increasing the number of sulfides exposed to water and oxygen (Amos *et al.*, 2014). Mine dumps or waste-mined material (e.g. spent ore from heap leach operations, tailings, etc.) with the right mineralogical composition have the potential to generate acid (US EPA, 1994).

2.1.2. Factors Affecting AMD Formation

The following factors have been observed to affect the AMD formation:

- Micro-organism

  Some bacteria (microorganisms) are known to accelerate AMD production by assisting in the breakdown of sulfide minerals (Sánchez-Andrea *et al*., 2014; Nancucheo *et al.*, 2017). Microorganisms such as *Thiobacillus* and *Acidithiobacillus ferrooxidans* are found in sulfide mineral tails and assist in oxidising the sulfide minerals i.e. increases the rate of acid formation (Sangita *et al.*, 2010, Özçelik, 2007). The acidity of the medium increases the effectiveness of these bacteria (Sangita *et al.*, 2010).

- Ore Mineralogy

  The ore mineral composition plays a major role in AMD formation as highlighted by Guseva *et al.* (2018). Guseva *et al.* (2018) stated that the Fe-sulfides are predominately associated with inert minerals which makes them only accessible after they have been further ground down. The acid-generating (sulfide) minerals and acid-neutralising (carbonate) minerals determine how much acid can be theoretically produced if all other conditions or reactants are met (US EPA, 1994).

- Particle size and porosity

  Fine particle sizes imply high minerals liberation and/or high surface area i.e. the rate of acid formation will be high as the available sulfide minerals would be exposed (Erguler & Erguler, 2020; Erguler *et al.*, 2014; Bradham & Caruccio, 1997; US EPA, 1994). Coarse grain material allows air circulation; however, fine grain material exposes more surface area for oxidation (Ferguson and Erickson 1988). Low porosity slows down the movement of both air and water. Therefore, grain material that is not too fine and not too coarse will yield optimal acid formation as the grain material will expose enough mineral surface area and the overall porosity will be enough for optimal movement of both water and air required for acid formation. Erguler and Erguler (2020) stated that particle size,

temperature, and pH are crucial for AMD modelling and simulation, and the effects of bacteria can be included at pH values below 4.

- Ore pH

  The ore/material pH activates bacteria that act as catalysts for AMD formation (Sangita *et al.*, 2010). The *Metallogenium* and *Thiobacillus ferrooxidans* bacteria are activated at a pH of 3.5 to 4.5 and below 3.5 respectively (US EPA, 1994). The acid neutralization potential is also pH-dependent (Ma *et.al,* 2019).

- Environmental conditions

  As shown in Equation 2.1, water and air (oxygen) are prerequisites for AMD formation from sulfide minerals. The area seasonal changes (i.e. wetting and drying cycles) directly affect the water and oxygen required for AMD formation; high or frequent wetting (rainfall) flushes oxidation products out of the system i.e. high acid drainage, while an intense drying cycle increases the accumulation of acid in the ore bed (US EPA, 1994). The environmental temperature also affects the rate of reaction, high temperatures increase the rate of sulfide mineral oxidation (Erguler & Erguler, 2020; Bradham & Caruccio, 1997).

2.1.3. Impact of AMD on the Environment and Society

Several studies have shown that AMD (including some mining dumps effluents such as heavy metals and cyanides) has serious ecological and human health implications (Khorasanipour, 2015; Edraki *et al.*, 2014; Simate and Ndlovu, 2014). AMD products and/or by-products contaminate surface and groundwater with soluble metals and cause a decrease in the water pH (Erguler & Erguler, 2020).

The following environmental impacts of AMD were listed by the United States Environmental Protection Agency in 1994:

> *"The acid formation in mine dumps causes some of the metals such as arsenic, cadmium, copper, silver, and zinc to also leach out and these metals along with the acid formed are*

harmful to the environment. Hence, the long-term prediction of AMD for historic mines must be improved for better management/action plans to deal with the formed acid if any."

In South Africa, all mining companies are required by law to also ensure the safe disposal of the pollutants generated (DWA, 2010).

2.2. AMD Prediction

2.2.1. Static Prediction

Static AMD Prediction is used to quickly check if the ore will produce acid or not (Karlsson *et al.*, 2021; Yeheyis *et al.*, 2009; US EPA, 1994). It is used to determine the ore sample's total acid-generating and neutralising potential (US EPA, 1994). The ore's ability to produce acid and the ability to neutralise it is called the Acidity Potential (AP) and the Neutralization Potential (NP) respectively (US EPA, 1994). AP is evaluated based on the ore sample's total sulfide content available to react to form acid while NP is based on the carbonate content available to react with the generated acid (ASTM 2018, NP de Mello *et al.*, 2006). If all the sulfide content reacts to form acid leads to over-estimation if the ore samples have sulfur-bearing minerals such as gypsum ($CaSO_4$) which does not react to form acid (ASTM 2018). Elghali *et al.* (2023) suggested the following corrected equations for AP and NP that include mineralogical data.

$$Avaialable\ AP = L_s \times 31.25 \times wt\%S - sulfide \qquad 2.3$$

$$Available\ NP = L_c \times 83.3 \times wt\%C - carbonate \qquad 2.4$$

Where L_s and L_c represent the extent of sulfide and carbonate liberation.

Chetty *et al.* (2020) proposed the following equation for static AMD prediction:

$$AMD_{value} = AP \times m \times R \times L \qquad 2.5$$

Where AMD_{value} is the total H_2SO_4 that the mineral can produce (measured in kg/t). m, R and L are the mineral mass percentage, relative reactivity, and free surface percentage liberation

respectively. AP is the acid production potential (measured in kg H_2SO_4/t), and it is calculated using the following equation:

$$AP = \text{AFC} \times 98 \times \text{MW} \times 1000 \qquad 2.6$$

Where AFC and MW are acid formation or consumption (measured in mol acid per mol mineral reacted), and mineral molecular weight (measured in g/mol) respectively.

A negative AMD_{value}implies that the mineral is consuming acid while a positive value would imply that the mineral has the potential to produce acid (Chetty *et al.,* 2020). The overall ore sample is then determined by calculating the sum of all individual minerals AMD_{value} (Chetty *et al.,* 2020).

The major disadvantage of static AMD prediction models is that they do not give the occurrence profile nor the estimated time of when the mine dump will generate more acid if indeed it will. This is crucial for prioritising mine tails dumps that are at the peak acid formation rate if several mine dumps are considered for meaningful management and mitigation of AMD potential.

2.2.2. Kinetic AMD Prediction – Kinetic Test

Kinetic tests are usually conducted along with or to aid model predictions to determine the AMD occurrence profile over time (Sibarani & Damayanti, 2006). The four main kinetic test methods are humidity cells, humidity columns, field-based test pads, and Sohlet Cell (Sibarani & Damayanti, 2006). These are discussed here as follows:

Humidity Cell Tests

Humidity cells and column tests are the most commonly used kinetic test methods (Sibarani & Damayanti, 2006). A schematic diagram of a typical humidity cell is shown in the figure below.

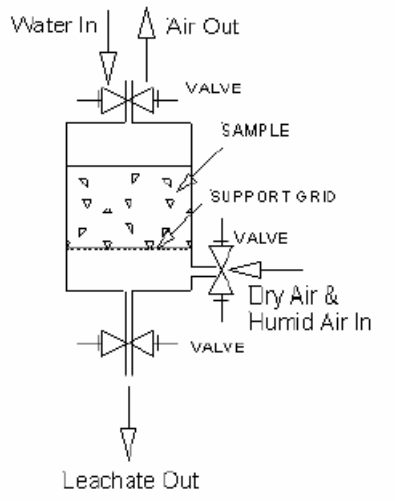

Figure 2.1: Schematic diagram of a humidity cell (Mills, 1998; Sibarani & Damayanti, 2006)

Most literature studies follow the ASTM procedures as standard guidelines for conducting kinetic humidity cell tests (Therriault *et al.*, 2015; Sibarani & Damayanti, 2006).

The following guidelines for conducting humidity cell tests were obtained from ASTM (2018):

- Ore sample should be at least 1 kg
- The leach water should remain constant throughout the test duration.
- The ratio of leach volume to sample is recommended to be 0.5:1 or 1:1, depending upon the efficiency of sample wetting and the amount of effluent required for chemical analyses
- Weekly leachate samples should be collected and analysed for
    - pH, alkalinity/acidity, conductivity, sulphate
    - iron sulfide
    - Cation and anion concentrations, calcium carbonate, magnesium carbonate contents, etc.
    - Metals and trace metals concentrations

- Minimum duration of 20 weeks but some ore samples may require a longer period
- Oxygen can be supplied to samples in the individual humidity cells separately or it can be split from the main source into individual cells
- The weekly cycles of water and air additions to the cell(s) can be performed as follows:
    - Option A: 3 days of dry air (less than 10 % relative humidity) and three days of water-saturated air (approximately 95 % relative humidity). The leach water is added on Day 7. Because of the excess amount of air added, this option helps to reduce saturation by evaporating the water remaining in the sample pores and promotes oxygen/air diffusion rate. However, it could eject some of the finer particles formed from the system when large particles weather down and break into smaller particles. The test is conducted at a normal temperature of around 25°C. An example of the setup is given in Figure 2.3.
    - Option B: Air (Oxygen) is not pumped into the system, it is added by diffusion of ambient air. The cell(s) are stored in an enclosure for 6 days. The enclosure environmental conditions are kept at constant (controlled) relative temperature and humidity. The enclosure should be able to achieve a temperature of around 62°C. The leach water is also added on Day 7. The enclosure should be big enough to host multiple cells if required. This option results in more water retention which increases the chances for acid neutralisation by carbonate minerals. An example of the setup is given in Figure 2.2.
- The weekly cycles and/or analysis can be spaced such that there are more initially, and fewer later in the test, e.g. the sampling week's numbers could be as follows: 0, 1, 2, 4, 6, 8, 10, 12, 14, 16, 18, and 20.

ASTM (2018) also recommended that the ore sample (head ore and any other sample after and during the tests) chemical composition and mineralogy should be compared to ensure that the chemistry is consistent with mineralogy and vice versa.

Figure 2.2: Examples of humidity cells test setup (ASTM, 2018)

[Image removed due to copyright concerns]

Figure 2.3: Examples of humidity cells test setup with Separatory Funnel Rack (ASTM, 2018)

[Image removed due to copyright concerns]

In terms of the cell design, ASTM (2018) recommends the following:

- For samples with all particle sizes less than 6.3 mm, a humidity cell, if cylindrical, is recommended to have an inner diameter of 10.2 cm and a height of 20.3 cm.
- For cells that will be used to conduct tests with particle sizes less than 150- µm, the humidity cells are recommended to have a 20.3 cm inner diameter and a height of 10 cm.
- The bottom of the cell should be perforated to allow for extraction of the leachate into the bottom compartment of the cell.
- A filter media is recommended to ensure that solids remain in the cells ore bed when the added leach water drains to the bottom compartment
- A separatory funnel can be used to add the weekly leach water
- The cells can be moved to a drying oven if it is required to operate them at a higher temperature.
- For tests that require air to be pumped into the cell, an airflow rate of 1 to 10 L/min/cell is recommended.
- A fan can also be used for air circulation within the enclosure

Column Tests

Leach column tests are similar to humidity cells except that the material bed height is much higher in leach columns. Water is added to the column and then allowed to dry in order to simulate the wetting or drying cycle (United States Environmental Protection Agency, 2011, Sibarani & Damayanti, 2006). The amount of water added depends on the column size and it can range from 89 to 1090 (Erguler & Erguler, 2020). Water addition should be done carefully to avoid piping i.e. water seepage between the bed material and the column walls (Erguler & Erguler, 2020; Sibarani & Damayanti, 2006). Each cycle is suggested to last for a period of 7 days i.e. 1 week (United States Environmental Protection Agency, 2011; Sibarani & Damayanti, 2006). The leachate analysis and sampling procedure for leach columns is similar to humidity cells (United States Environmental Protection Agency, 2011). A schematic example of the kinetic column test is shown in the figure below:

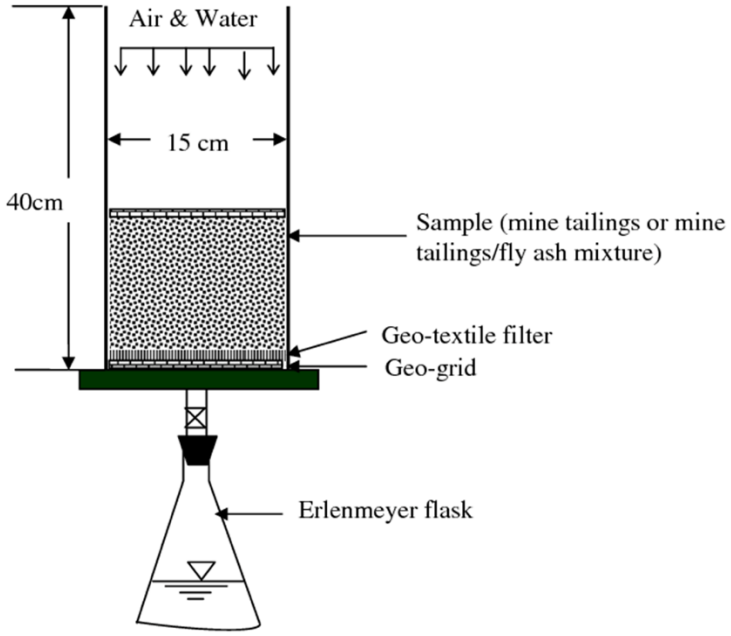

Figure 2.4: An example of a column humidity cell test setup (Yeheyis *et al*., 2009).

Soxhelet Extraction Tests

Soxhelet Extraction tests are conducted with a Soxhelet extraction apparatus (Sibarani & Damayanti, 2006). The sample is placed in a thimble and leached with the recirculated condensate from the leachate water which is boiled in the distillation flask or reservoir (Coastech Research Inc., 2008; US EPA, 1994). These tests are meant to assist with acid consumption reaction kinetics (Coastech Research Inc., 2008). However, they are considered to be a bit more complex compared to humidity cells and/or column cells, especially the results interpretation or translation to kinetic AMD prediction (Coastech Research Inc., 2008; Sibarani & Damayanti, 2006). Hence, they are rarely used (Coastech Research Inc., 2008).

Shake Flask Tests

Shake Flask Tests or Batch Reactor tests are conducted in a flask to study parameters like pH, temperature, sulphate, and metal release (Sibarani & Damayanti, 2006; US EPA, 1994). A sample of about 250g is mixed with 500 ml of distilled water in a flask and stirred continuously by shaking

the flask (Coastech Research Inc., 2008; Sibarani & Damayanti, 2006; US EPA, 1994). If sampling is required during the tests, additional fresh water must be added to the flask to maintain the volume and this complicates the interpretation of the results (Sibarani & Damayanti, 2006; US EPA, 1994). These tests are relatively simple compared to Soxhelet Extraction Tests. However, similar to the Soxhelet, they also cannot be used to study the fluid flow (infiltration rate) profile that can be expected at the target mine site.

British Columbia Research Confirmation Test

These tests are intended to confirm if the bacteria can catalyse enough reactions to meet their acid demands and, as a result, confirm if the ore can generate acid (US EPA, 1994). However, they do not take into account the ore's acid neutralisation potential (US EPA, 1994). The following test procedure was obtained from the US EPA (1994) and Coastech Research Inc. (2008):

1. The ore sample's particle sizes should be 100% passing 400 mesh screen.
2. The ore sample should be between 15 to 35g
3. The tests are conducted by adding sulphuric acid to bacteria cultures in a flask, periodically until the pH is stable between 2.5 and 2.8
4. 5 ml of ferrooxidans cultures are then added to the flask
5. The flask should then be placed on a shaker at 35 °C
6. The flask pH should then be monitored and if it is above 3.5, the test should be terminated, and if not, the sample should be halved and then agitated for up to 72h before the next pH reading is taken.
7. Repeat steps 5 to 6 until the pH is above 3.5 or the test duration (step 8) is reached.
8. The test duration is about 3 to 4 weeks.

Field-based Test Pads

These tests are conducted outdoors, with the sample exposed to ambient conditions and large sample volumes are used (US EPA, 1994). The procedure for conducting these tests was documented by Sibarani and Damayanti (2006) and the US EPA (1994), and is as follows:

- Sample size could be as large as 1000 metric tons
- The sample is loaded on an impervious liner to catch the solution that is to be collected by the leachate vessel
- The leachate is then analysed similarly to the humidity cells
- Climate changes (temperature, rainfall, wind speed, etc.) need to be monitored as they directly affect the AMD production rate for these tests
- These tests are normally the longest out of all the tests

Summary of Experimental Kinetic AMD Tests

From this section i.e. Section 2.2.2, it should be noted that the Soxhelet Extraction test, Shake Flask test, and the British Columbia Research Confirmation test cannot be used to investigate or validate the prediction fluid flow model (i.e. infiltration rate) results. This may explain why they are rarely used as the main kinetic tests along with a model.

The humidity cells, column tests, and field-based test pads can be used to investigate all the possible parameters needed to 'calibrate' or validate the kinetic AMD prediction model parameters without additional experimental tests. The field-based test pads are expected to have a longer experimental time because they can only be run with ambient conditions. Hence, this is the reason why humidity cells and column tests are the commonly used kinetic tests. Due to the challenges with fluid channeling between the walls of the column and the material bed that occurs with column tests, it could be postulated that humidity cells are probably more favorable than column tests. Hence, they were selected for further improvement in this study.

2.2.3. Kinetic AMD Prediction – Model Predictions

A kinetic AMD prediction model would generally include the following:

- Fluid flow model – infiltration model (s)
- Reaction kinetics model, including bacterial activities
- Environmental conditions – seasonal changes (temperature, air, etc.)

The following sub-section reviews some of the fundamental or hybrid kinetic AMD prediction models.

Liquid Fluid Flow

The Richards equation is commonly used for modelling the liquid fluid flow through the packed bed of particles/material i.e. tails ore heap (Bonn, 2019; Baoqin 2017). The one-dimensional (1D) fluid flow model is given in Equation 1 (Bonn, 2019; Baoqin 2017):

$$\frac{\partial \theta}{\partial t} = K(\theta)\frac{\partial^2 h}{\partial z^2} + \frac{\partial K}{\partial z} * \frac{\partial h}{\partial z} + \frac{\partial K}{\partial z} \pm S \qquad 2.7$$

Where:

θ is the water volumetric content (m^3/m^3)

K is the hydraulic conductivity (m/s)

h is the matric potential (m)

t is the time (s)

S is the inflow (source) or outflow (sink) fluid flux ($m^3/(s.m^3)$)

z is the depth position in z direction (m)

The overall three-dimensional (3D) Richards fluid flow model i.e. the expansion of Equation 2.7 to 3D model is as follows (Botros *et al.*, 2012):

$$\frac{\partial \theta}{\partial t} = \nabla \cdot K(h) \nabla h + \frac{\partial K(h)}{\partial z} \pm S \qquad 2.8$$

The hydraulic conductivity (K) can be modelled using the Maulem-van Genuchten model (Baoqin, 2017).

$$K = \begin{cases} K_s \dfrac{(1-(\alpha|h|^{nm}[(1+(|h|)^n)]^{-m})^2}{[(1+(\alpha|h|)^n)]^{\frac{m}{2}}} & h<0 \\ K_s & h \geq 0 \end{cases} \qquad 2.9$$

Where:

K_s is the hydraulic conductivity at saturation (m/s).

α (in 1/m), n (-), and m (-) are material-specific van Genuchten constants.

The saturated conductivity changes as a function of temperature (T in °C), can be determined using the following Kozeny–Carman equation (Zhang *et al.*, 2021):

$$K_s(T) = k' \frac{\rho g}{\mu} \quad 2.10$$

with gravitation acceleration (g in m^2/s) and permeability (k' in m^2) as constants, and the density (ρ in kg/m^3) and viscosity (μ in $N.s/m^2$) as a function of temperature. The matric potential (h) modelled as follows:

$$h = \frac{((S_e^{\frac{1}{-m}} - 1)^{\frac{1}{n}})}{\alpha} \quad 2.11$$

The van Genuchten (1980) constants α, n, and m are material-specific. Their values as given in Table 2.1 for a wide range of materials. The material/soil type classification can be done based on the material particle size distribution using the textural triangle shown in Figure 2.5 (Moreno-Maroto & Alonso-Azcárate, 2022). The particle size for sand soil is from 2.0 mm to 0.05 mm, silt is 0.05 mm to 0.002 mm and clay is particles less than 0.002 mm (Moorberg & Crouse, 2017).

The van Genuchten constant n is related to m as follows:

$$m = 1 - \frac{1}{n} \quad 2.12$$

The dimensionless effective saturation (S_e) can be determined as follows (Bonn, 2019):

$$S_e = \frac{\theta - \theta_r}{\theta_s - \theta_r} \quad 2.13$$

Where:

θ_r is the residual volumetric water content (m^3/m^3)

θ_s is the water volumetric content at saturation (m^3/m^3)

The overall fluid flow model is generally solved using finite difference approximation. The challenge involved in solving this equation is the selection of the size of the discrete layers as it determines the accuracy of the solution. The discrete layers could be chosen such that they are equally spaced discrete layers, variable or adaptive discrete layers (Farthing & Ogden, 2017). Li (2022) gives guidance on the critical mesh size and time step for ensuring convergence in the numerical results. Farthing and Ogden (2017) found that space and time discretisation affects both computational effort and accuracy, and the adaption of space and time is beneficial.

Table 2.1: van Genuchten parameters for different soil types (Bona, 2019)

Soil Type	**van Genuchten parameters**				
	θ_s (-)	θ_r (-)	α (cm^{-1})	n (-)	K_s (cm/h)
Sand	0.43	0.045	0.145	2.68	29.7
Loamy Sand	0.41	0.057	0.124	2.28	14.59
Sandy Loam	0.41	0.065	0.075	1.89	4.42
Silt Loam	0.45	0.067	0.02	1.41	0.45
Loam	0.43	0.078	0.036	1.56	1.04
Sandy Clay Loam	0.39	0.1	0.059	1.48	1.31
Silt Clay Loam	0.43	0.089	0.01	1.23	0.07
Clay Loam	0.41	0.095	0.019	1.31	0.26
Sandy Clay	0.38	0.1	0.027	1.23	0.12
Silty Clay	0.36	0.07	0.005	1.09	0.02
Clay	0.38	0.068	0.008	1.09	0.2

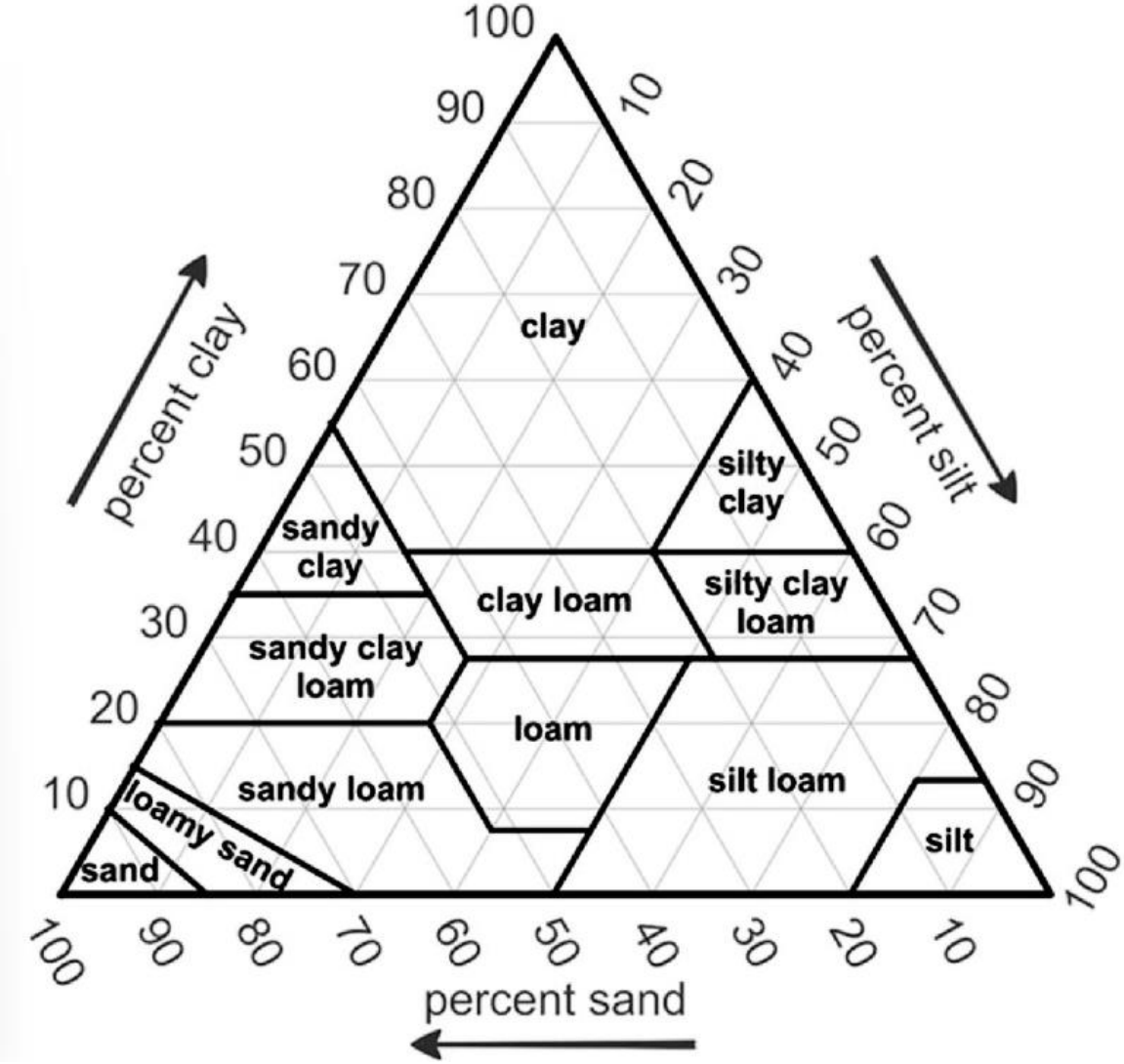

Figure 2.5: Soil type classification – Textural triangle (Moreno-Maroto & Alonso-Azcárate, 2022)

Gas diffusive Flow

Air (Oxygen) diffusion through the liquid media (water) between the solid particles is the main gas of interest for kinetic AMD modelling. Bernardes de Souza and Mansur (2011) proposed that

it be considered as a diffusive flow through a porous media and the concentration of oxygen (C_{o2} in kg/m^3) be modelled as follows:

$$\theta_{eq}\frac{\partial C_{o2}}{\partial t} = D_e\frac{\partial^2 C_{o2}}{\partial z^2} - S_0 \qquad 2.14$$

where θ_{eq} is the air volumetric equivalent content (m^3/m^3),as given in 2.15 with θ_a, $\theta_{w,}$ and H as air content (m^3/m^3), water content (m^3/m^3), and Henry's law constant (-) respectively. D_e is the oxygen diffusion coefficient (m^2/s). S_0 is the oxygen consumption (kg.m^{-3}.s^{-1}), which can be determined using 2.16 if it is assumed that the principle of shrinking radius (r_c in m) applies when the sulfide mineral particles are oxidised (Bernardes de Souza & Mansur, 2011):

$$\theta_{eq} = \theta_a + \frac{\theta_w}{H} \qquad 2.15$$

$$S_0 = D_2\frac{3(1-\theta)}{{R_p}^2}\left(\frac{r_c}{R_p - r_c}\right)\frac{C_{o2}}{H}f_m \qquad 2.16$$

where D_2 (in m^2/s), f_m (-), H (-),and R_p (in m) are the oxygen diffusion coefficient within the mineral grain, microbiological factor, Henry law constant, and particle radius respectively.

Ma *et al.* (2019) proposed that the movement of oxygen and other ions in the solution phase be modelled as follows:

$$\frac{\partial}{\partial t}(C_{wf,i}) - \nabla.(D_i\nabla C_{wf,i}) = S_{mf,i} \qquad 2.17$$

where $C_{wf,i}$ is the concentration for species i in the solution phase (kg/m^3), and D_i is the corresponding species diffusion coefficient (m^2/s). $S_{mf,i}$ is the species consumption or generation rate (kg.m^{-3}.s^{-1}).

Particle-Chemical Reactions Kinetics

For the chemical reactions, Bernardes de Souza and Mansur (2011) proposed that the sulfide minerals particles be modelled as follows with the principle of shrinking core radius:

$$\frac{\partial r_c}{\partial t} = -\frac{D_w(1-\theta)}{\varepsilon \rho_s} \frac{R_p}{r_c(R_p - r_c)} \frac{C_{o2}}{H} f_m \qquad 2.18$$

where D_w(in m^2/s), ε (-), and ρ_s (in kg/m^3) are water oxygen diffusion coefficient, effective factor, and particle density.

The oxidised pyrite mass at each discrete layer j i.e. m_j (in kg) and time interval, Δt, can then be modelled as follows (Bernardes de Souza & Mansur, 2011).

$$m_j = \frac{PS}{\varepsilon} \frac{S_{o,j}\,(1-\theta)\pi D^2 H \Delta t}{4N} \qquad 2.19$$

with D (in m), N (-) and PS (-) are the cell column diameter, number of discrete layers, and pyrite/sulfur mass ratio respectively.

Bernardes de Souza and Mansur (2011) also proposed that the pH and sulphate concentration in the leachate/solution in the system be estimated using Equations 2.21 and 2.19.

$$\text{pH} = -log\left(\frac{\frac{m_o}{120}}{\frac{\pi D^2 H\theta}{4}}\right) \quad 2.20$$

$$C_{SO_4{}^{-2}} = \frac{\frac{2m_o}{120}}{\frac{\pi D^2 H\theta}{4}} \quad 2.21$$

with m_o as the sum of all discrete layers oxidized pyrite mass (kg).

Heat Transfer

For heat transfer, Ma *et al*. (2019) proposed that the following equation that includes the effect of cyclic ambient conditions be used:

$$c_p\rho\frac{\partial T}{\partial t} + c_w\rho_w\nabla\text{T}.\boldsymbol{q}_w - \nabla.(k\nabla\text{T}) = Q_h \quad 2.22$$

where T, c_p, c_w , ρ, ρ_w, k, and Q_h are temperature (K), specific heat capacity ($\text{J}\cdot\text{kg}^{-1}\cdot\text{K}^{-1}$), heat capacity for water ($\text{J}\cdot\text{kg}^{-1}\cdot\text{K}^{-1}$), effective mass density (kg), water density (kg), effective thermal conductivity ($\text{J.s}^{-1}.\text{m}^{-1}.\text{K}^{-1}$) and the heat (J/s) generated from the geochemical reactions respectively. And $\boldsymbol{q}_w$ is the Darcy velocity (m/s).

CHAPTER 3. DEVELOPED ACID MINE DRAINAGE PREDICTION TOOLS

3.1. Customised Humidity Cell Design

The modified humidity cell that is proposed in this study is shown in Figure 3.1. The main difference compared to the typical humidity cells (examples shown in Figure 2.1 and Figure 3.2) is that it allows for direct automatic control of temperature, pressure (aeration rate), and/or humidity. It also allows for direct circulation of air between the cell's top and bottom compartments if required. This cell can also be reconfigured to run as a normal/typical humidity cell by closing or opening the airline valves and/or changing the compressed air inlet from bottom to top. The control system would also need to be set to control to the desired temperature, humidity, and/or pressure. The sensors (temperature, pressure), spray water addition point, and/or the heating element position can be interchanged depending on the test requirements. A cone-shaped bottom leachate collection compartment with one drainage line was also tested in this study for ease of leachate collection.

The proposed cell's top compartment (i.e. from the drilled filter support at the bottom of the sample to the top of the cell) has internal dimensions of 30 cm long x 19 cm wide and a height of 15 cm. The cell can accommodate a maximum bed height of 10cm if required. The dimensions were chosen such that the minimum specifications suggested by ASTM (2018) for humidity tests with particles passing 150 µm are still met.

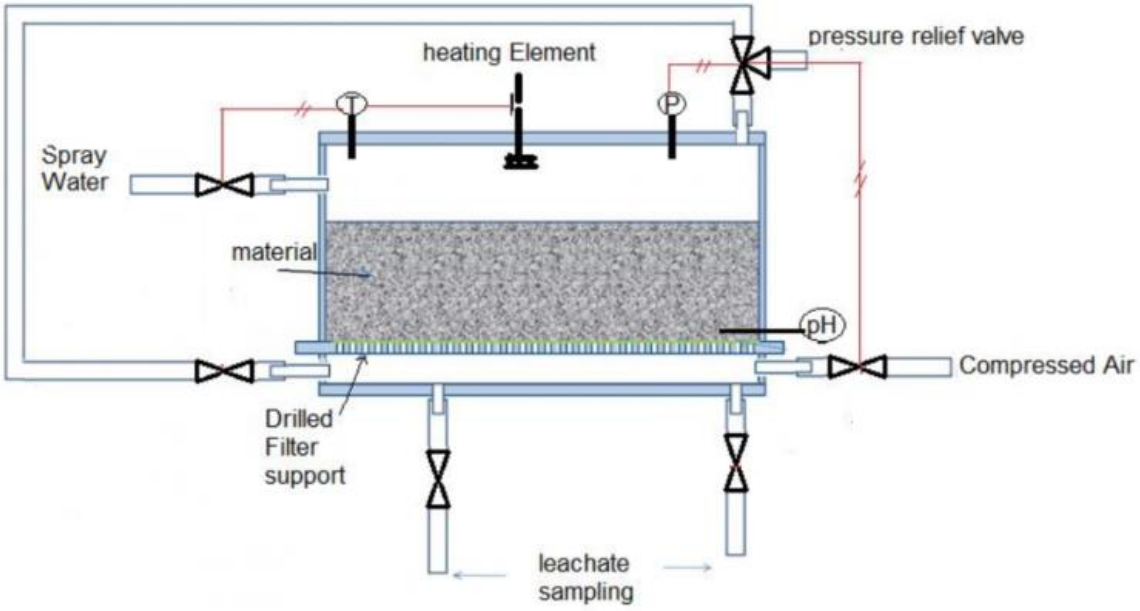

Figure 3.1: Proposed Modified Humidity Cell

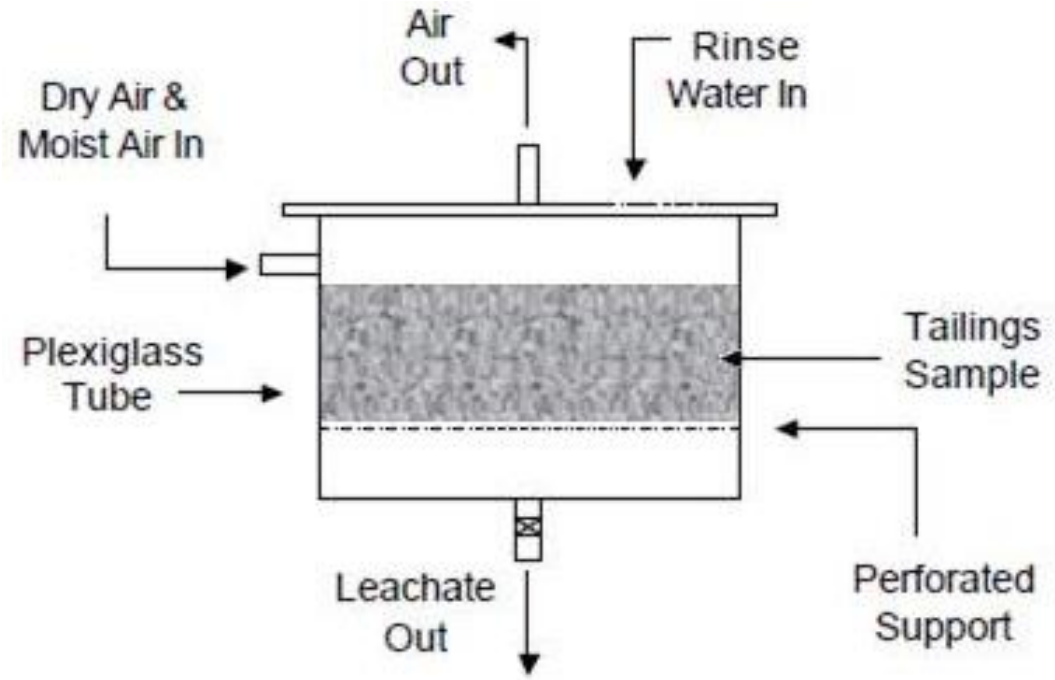

Figure 3.2: Typical Humidity cell (Geochmic, 2022; ASTM, 2018; MEND, 2009)

3.2. Mineral Particles-based AMD Predictor

The following subsections give an overview of the models used and the software architecture of the developed acid mine drainage predictor. Note that the literature models described in Section 2.2.3 were used as a basis for the developed acid mine drainage prediction tool. The main features added to the developed acid mine drainage prediction tool are as follows:

- Incorporation of the particle size distribution in the model instead of using one particle size as done in literature studies, e.g. model by Bernardes de Souza and Mansur (2011). For the proposed prediction tool, up to four particle size classes can be included i.e. the particle size distribution can be divided into four particle size classes/range.
- Using the particle size classes to automatically determine the ore bed/heap mesh cell sizes
- Tracking each particle in the ore bed/heap leach. The fluid flow and chemical reactions are modelled on each particle.

3.2.1. Liquid Fluid Flow

The 3-Dimensional Richards equation as given in 2.2.3 was used in this study for modelling the fluid flow through the packed bed of particles/material (i.e. tails ore heap). The overall fluid flow model was solved using finite difference approximation. This method requires that the system be divided into discrete layers or mesh cells. The layers/mesh cells could be of uniform equally spaced discrete layers, variable or adaptive discrete layers (Farthing and Ogden, 2017). The final choice in most cases is a compromise between accuracy and processing speed (Farthing and Ogden, 2017). Li (2022) gives guidelines for determining the critical mesh size and time step for ensuring convergence in the numerical results. Farthing and Ogden (2017) found that space and time discretisation affects both computational effort and accuracy and the adaption of space and time produces benefits. The concluding remarks of the study by Farthing and Ogden (2017) which reviewed numerical solutions of Richards' equation emphasised that there is still an opportunity for improving the numerical solution of Richards' equation. Quoting Farthing and Ogden (2017),

"We hope to see continued development and research into the numerical solution of Richards' equation".

In this study, it is proposed that the mesh cells size/volume c_i in m^3 i.e. the system discrete layers, be determined based on the particle volumes $V_{p,i}$ (m^3) and porosity φ (-) using equation 3.1.

$$c_i = V_{p,i}\left(\frac{1}{1-\varphi}\right) \qquad 3.1$$

The difference between the proposed and the typical equally spaced discrete layers is shown in Figure 3.3 with a system of 5 particles (p1 to p5) of different sizes. Note that with the conventional equally spaced discrete layers, multiple particles can be classified or belong to one cell.

Typical mesh cell sizes or discrete equally spaced layers (Bonan, 2019)	Proposed mesh cell sizes or discrete layers based on the particle sizes
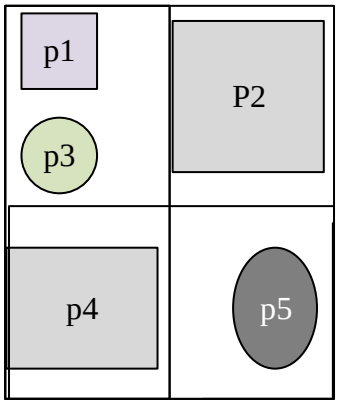 • p1 and p3 are sharing a mesh cell	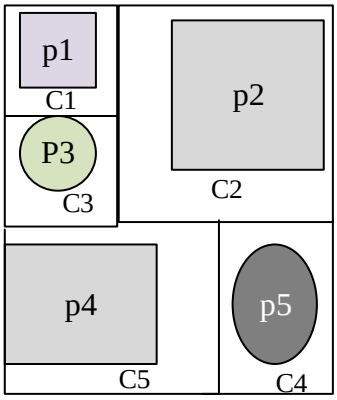 • No particles sharing mesh cell(s), each particle is within its mesh cell.
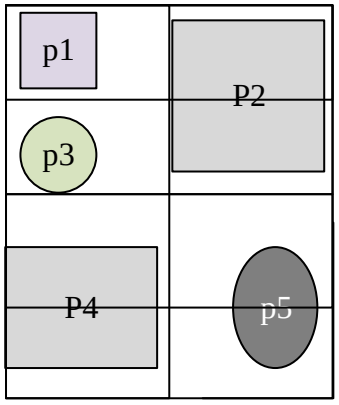 • p2, p4 and p5 belong to multiples cells	

Figure 3.3: Dimensional illustration of the proposed particle size based adaptive mesh cell sizes vs typical uniform mesh size

Instead of picking random or calculated static mesh cell sizes to predict the water or leachate drainage, the input particle sizes are used to calculate the mesh cell size with the proposed approach.

3.2.2. Gas Diffusive Flow

The gas diffusion model (Equation 2.14) described in Section 2.2.3 has been added to the developed acid mine drainage predictor.

3.2.3. Particle-Chemical Reaction Kinetics

The particle-chemical reaction model given in Section 2.2.3 has been added to the developed acid mine drainage prediction software. This was used to model the rate of acid formation.

The rate of acid neutralisation by carbonate minerals (Equation 2.2) was modelled similarly to the study by *Mauren et al. (*2020). However, instead of using the acid molar concentration only in the reaction rate equation as done by *Mauren et al. (*2020), both the acid and carbonate minerals molar concentrations were used in this study since they are both limiting factors. As a result, the acid neutralisation reaction rate by carbonate minerals was modelled as follows:

$$\boldsymbol{r} = \boldsymbol{k}[Acid]^{a}[Carbonate\ mineral]^{\boldsymbol{b}} \qquad 3.2$$

where a and b are reaction rate orders for the acid-consuming carbonate mineral and the reactant acid.

The study by *Mauren et al. (*2020) recommended a first-order reaction rate with respect to the acid molar concentration. As a result, the reaction rate orders a and b were given values of 1 in this study, implying a first-order reaction rate with respect to the reactants, but an overall second-order reaction rate.

From Equation 3.2, the rate of acid neutralization and carbonate mineral consumption were determined as follows:

$$\frac{d[Acid]}{dt} = -\boldsymbol{k}[Acid]^{a}[Carbonate\ mineral]^{\boldsymbol{b}} \quad 3.3$$

$$\frac{d[Carbonate\ mineral]}{dt} = \frac{u}{v}\frac{d[Acid]}{dt} \quad 3.4$$

where *u and v* are the chemical reaction stoichiometry coefficients for the carbonate mineral and acid respectively. Based on Equation 2.2, *u* and *v* have values of 1.

The Arrhenius equation, as given in Equation 3.5, has been added to account for the impact of temperature on the mineral particle reactions (Fogler, 1999)

$$\boldsymbol{k} = Ae^{\frac{-E_a}{RT}} \quad 3.5$$

where *A* is the pre-exponential factor or frequency factor, *R* is the gas constant and *T* is the absolute temperature and E_a is the activation energy.

3.2.4. Software Architecture

The software presented in this section was developed by the author of this document (i.e. as part of the MSc project) and as mentioned in the above sections, the literature models were used as the basis for this software and adjustments were added to these models as indicated in Sections 3.2.1 to 3.2.3. The software user interface layout and inputs handling (i.e. using excel file for any additional inputs required) was done with reference to the Mintek AMD Predictor v2.0 because this research was funded by Mintek and the findings from this project (including some of the developed software algorithms) are to be incorporated into the main Mintek project i.e. for improving the Mintek AMD Predictor v2.0. The acid mine drainage prediction software developed in this study is referred to as the Mine Dumps Acid Estimator (MiDAE). It uses the input particle size classes/ranges, ore classification, and the ore bed/heap dimensions (height, length, and width)

to reconstruct the full ore bed for simulations. The ore classification is done using Figure 2.5. This is also used to determine the porosity if the porosity value is not specified in the input data file (see Appendix F, Figure F. 1for an example of input data required and Figure F. 2 for the developed software interface). Currently, a maximum of four size classes can be specified as inputs. These sizes are specified as inputs along with the percentage for each size class/range. Using the porosity, bed dimension, and particle size classes, the total number of particles (N_p) in the ore bed is then calculated by the software using Equation 3.6 below:

$$N_p = \sum_{i=1}^{4} \frac{X_{p,i}\, V_{p,total}}{V_{p,i}} \tag{3.6}$$

where $X_{p,i}$ is the volumetric fraction of particle size class/range i and the total number of particle size classes is 4. The total volume occupied by particles ($V_{p,total}$) in the overall ore bed/heap system volume (V_{total}) is determined as follows (Softusvista, 2022):

$$V_{p,total} = V_{total}(1 - \varphi) \tag{3.7}$$

The process that the software follows when reconstructing the ore bed is summarised in Figure 3.4 below. It should be noted that each vertical strip of single particles contains all the input particle size classes and the particles are placed such that they form groups or sections that represent the input particle size distribution. Each particle is also given a unique identification number and/or position as shown in Figure 3.5. From Figure 3.5, note that this is a system (mine tails dump or experimental ore bed) with a volume of *jmn* (height *n*, length *j*, and width *m*).

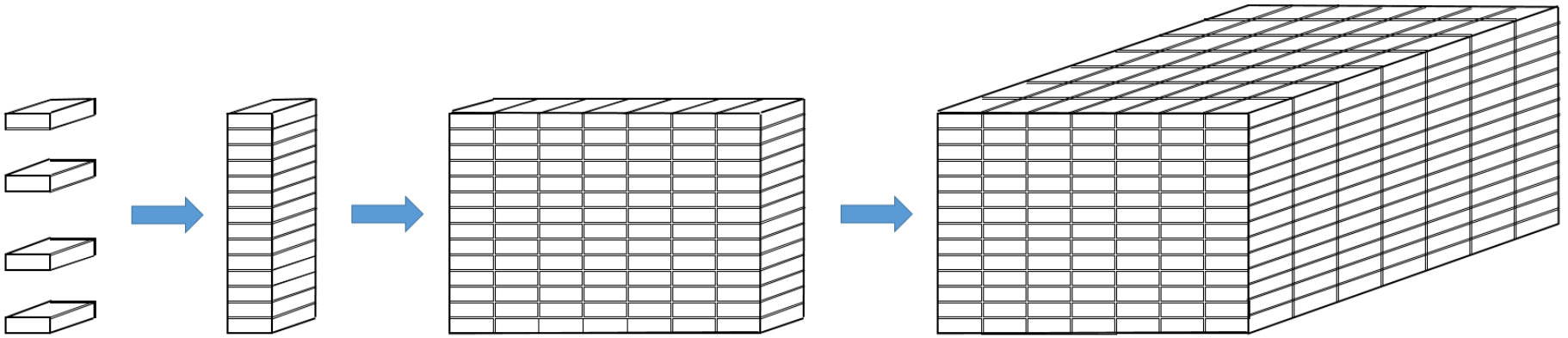

Figure 3.4: From four Particle size classes to full mesh or full ore bed

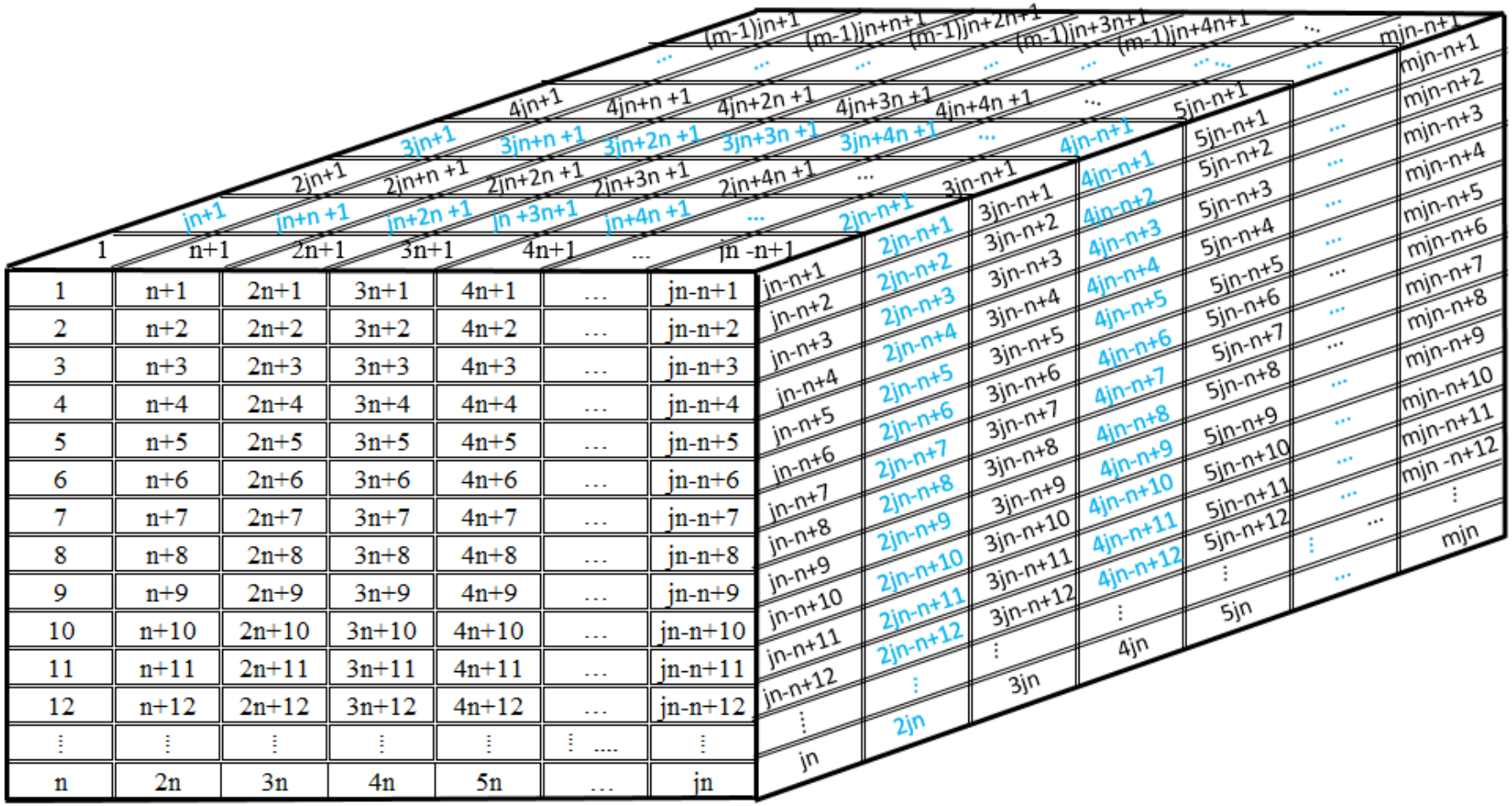

Figure 3.5: Particle identification numbers and position.

One of the major challenges in solving the Richards Equation or models for kinetic acid mine drainage prediction is balancing between accuracy and the processing speed for large systems (Farthing and Ogden, 2017). This often requires the use of supercomputers or computers with more than standard Random-access memory (RAM) and Central Processing Unit (CPU). The standard computer RAM and CPU sizes are given by Micron Technology (2022). To tackle this problem, in this study, the software has been designed such that the simulation of one large ore bed/heap can be divided and done simultaneously by multiple standard computers on the same network. The results/progress data is stored and shared from the main PC or the selected central location on the network. Dividing the ore bed/heap system into multiple subsystems that communicate with each other is also expected to be faster because it implies parallel processing for everything.

Figure 3.6 below shows how the developed software (MiDAE) will divide the ore bed if it is specified that it should run with four instances. Note that the ore bed division is only done by the overall simulation initiator which is numbered as Instance 1 (Main Instance). The size of the Instances (i.e. number of vertical layers of single particle strips) depends on the ore bed size. If the computer that launched the Main Instance is not big enough to accommodate the rest of the Instances, the remaining Instances can be run on different computers that are on the same network as the main Instance or main computer. The Instance Links are vertical layers of single particle strips that switch their affiliation between the two adjacent Instances on each simulation cycle. In Figure 3.6, Instance Link 1 will switch its affiliation between Instances 1 and 2, Instance Link 2 for Instances 2 and 3, and Instance Link 3 for Instances 3 and 4. These Instance Link layers are meant to facilitate fluid movement between the Instances. During the simulation, only one instance can have the authority to update the contents (i.e. fluid flow to or from, particle-chemical reactions, etc.) of the Instance Links at a time and for only one cycle. After the Instance has included the Instance Link layer in the cycle, it sends an Authority of 0 to the “InstanceSchedulerLink” file to let the adjacent Instance know that it is done with its cycle/turn with the instance Link layer. Additionally, before the adjacent layer takes over, it checks that the value in the “InstanceSchedulerLink” file is 0 which implies that the Instance Link layer is available. The Adjacent Instance also sends its identification number to the “InstanceSchedulerLink” to imply that it has locked the Instance Link for the next simulation cycle. A watchdog has also been added to keep track of the time that the Instance Link layer

has been locked, if this is too long, the requesting Instance will attempt to overwrite the authority so that it can take control. This is done to avoid situations whereby the Instance Link layer could have been locked by an inactive Instance.

It should also be noted that even if the instances are launched on the same computer, having multiple instances implies parallel processing for everything i.e. the overall simulation time is expected to be shorter as compared to having one or few instances.

The MiDAE software/code flow diagram is shown in Figure 3.7 below. Refer to Appendix G for the software code files mentioned in Figure 3.7.

Appendix H gives an example of how to simulate or predict acid mine drainage of a large ore bed/heap system with multiple MiDAE Instances on the same computer and/or on two different computers on the same network. In this example, four MiDAE Instances are used.

.

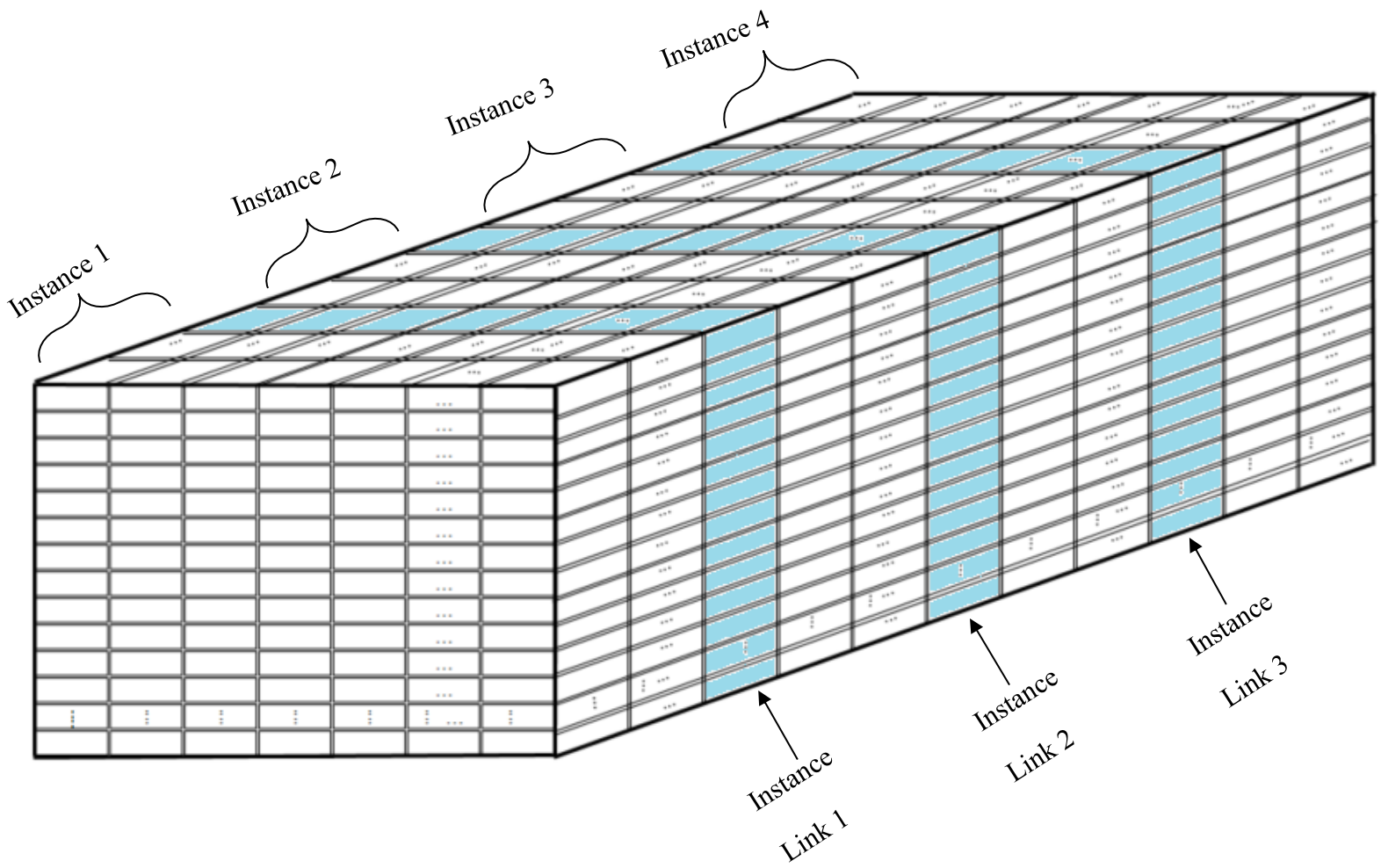

Figure 3.6: Simulation instances and Instance links

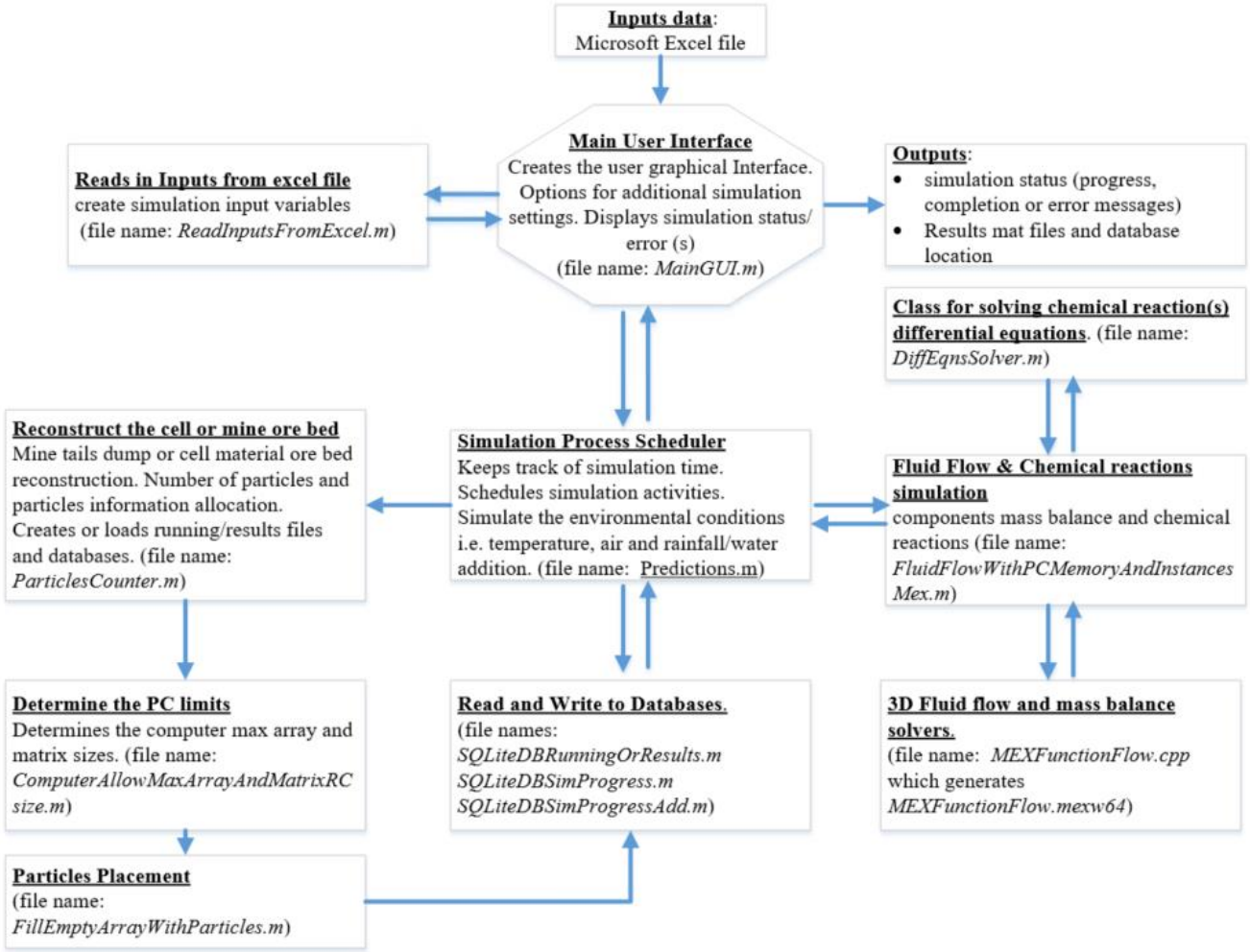

Figure 3.7: MiDAE software source code files interaction or flow diagram

CHAPTER 4. METHODOLOGY

The subsections below presents experimental as well as simulation procedure. The experimental procedure were mainly for evaluating the proposed customised humidity cell against the conventional humidity cell i.e. to determine if the proposed customised humidity cell could be used to accelerate the AMD formation. The experimental tests were also used to generate data that was used for evaluating the proposed multiple particle sizes based AMD Prediction model (i.e. minerals particles based AMD prediction model). The simulation procedure was mainly for evaluating the proposed minerals particles based AMD prediction model as compared to the single particle size used in literature i.e. to determine if the proposed model prediction accuracy is better than the single particle size models used in literature studies.

4.1. Experimental Setup

The actual experimental setup with the custom humidity cells is shown in Figure 4.1 (See Appendix A and Appendix B for the final design and a list of the main instrumentation used, respectively). A Micro850 Allen-Bradley PLC was used for signal processing and/or scaling. The communication between the PLC and the process control system software (Mintek StarCS) was established using the Kepware KEPserverEX OPC server.

All the sensors and actuators were wired to the PLC i.e. the signal from all the sensors or measured variables (temperature, pressure, and relative humidity) was sent to the PLC. The signal to the actuators from the control system was sent from the process control system via the PLC to the actuators or manipulated variables (electric heaters, water pump, and air fan). Process control strategies for temperature and humidity were implemented by customising the existing Mintek StarCS control modules (Advanced PID and fuzzy logics) with the electric heater and air fan as manipulated variables. The Mintek StarCS control system setup implemented and used is shown in Appendix B.

It should be noted that the PLC and/or the computer can be replaced by cheaper equipment such as Raspberry Pi or Arduino. However, with the number of sensors and actuators involved, these

alternatives would have required a significant amount of time to set up. Hence the PLC was chosen because it is convenient to work with. Also, the Mintek StarCS software for data logging and process control was selected because it is robust, used worldwide for minerals processing plants process control and simply because it was offered for free by Mintek during this investigation and the findings from this study will also be integrated into the main Mintek project which funded this study. However, any other control system can be configured according to the number of humidity cells, instrumentation or process parameters to be controlled and/or measured, and then wired/connected to the cell's PLC or the control system can also be implemented in the PLC itself which was not ideal for this study due to time constraints.

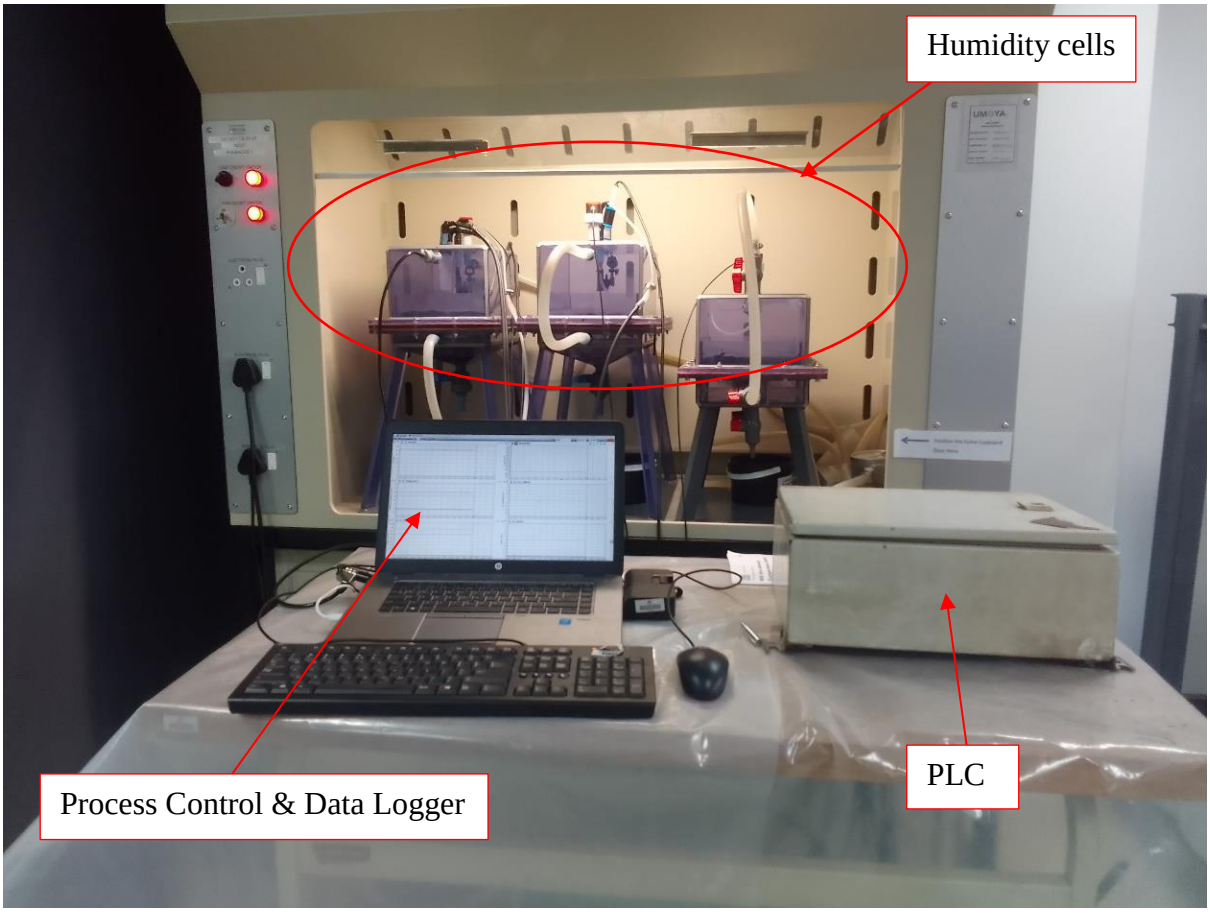

Figure 4.1: Experimental setup used in this work

4.2. Experimental Method

The ASTM (2018) guidelines were used as a basis and modified for this application (i.e. not followed entirely) as they are not for mine tails i.e. not applicable for this application.

Two ore samples from different mines were sourced. Table 4.1 below shows the summarised ore content for both ores. Sub-samples for each ore type were screened to determine the particle size distribution (PSD) and sent for mineralogical characterisation. The PSDs and mineralogical data are given in Appendix C and Appendix D respectively. Note that the ore's particle sizes were below 300 µm, which is expected for most mine tails dump ore.

Table 4.1: Summarised chemical composition of ore types 1 and 2

Chemical Composition	Ore Type 1	Ore Type 2
Total Sulphur (%)	1.95	0.80
Fe (%)	5.06	2.04
Cu (%)	0.42	2.18
Ca (%)	1.32	12.5
Mg (%)	1.25	1.66
Si (%)	29.85	20.7
Al (%)	7.94	4.24
Other	52.21	55.88

The humidity cell tests were conducted with 2 kg ore samples per cell. The weekly leach water addition to the cells was 200 ml and it was added on the 7^{th} day of each week using the flooding method (a timer was set on the pump such that it delivers 200 ml – calibrated using a stopwatch and a bucket). The pre-test runs with the modified humidity cell were done with 500 ml weekly water addition, but this was observed to be too much flooding and it generated more leachate. Too much flooding closes the pores and results in less oxygen diffusion (ASTM, 2018). It was then reduced until the final amount of 200 ml weekly water addition, which was observed to not cause too much flooding for all the test cells. A continuous air supply was provided at a rate of 2.36 x 10^{-4} m^3/s (measured from the source – electric fan), through a 10 mm inner pipe diameter into the humidity cells i.e. equivalent to a wind speed of 10.8 km/h. The air supply could be varied automatically, but it was maintained at a constant level during the tests so that the impact of temperature could be investigated. A weekly leachate collection was done to determine the cumulative leachate volume, and pH, and for chemical analysis. The test duration was 11 weeks. The difference between the tests conducted is summarised in Table 4.2. It would have been ideal to conduct multiple repeats, but due to a limited budget, especially for ore chemical and mineralogical analysis and leachates chemical composition analysis, this was not possible.

Table 4.2: Experimental tests conducted

Test Number	Test type	Ore type	Additional/Special conditions
1	Accelerated Humidity Cell (AHC)	Ore type 1	• Done at 40°C
2	Reference Humidity Cell (HC)	Ore type 1	• Done at 14-25°C (room temperature)
3	Accelerated Humidity Cell (AHC)	Ore type 2	• Done at 40°C
4	Reference Humidity Cell (HC)	Ore type 2	• Done at 14-25°C (room temperature)

The maximum temperature of 40°C for the AHC experiments was chosen for this study to avoid chemical and physical changes in some mineral species as suggested by ASTM (2018), and Morin and Hutt (1997). If tests are to be done above 40°C, these chemical and physical changes must be accounted for in the data analysis or simulation (ASTM, 2018).

The experimental test results were then compared to the model predictions. The procedure followed and the parameters used for the model simulations are described in section 4.3 below.

4.3. Simulation Procedure

The first objective of the simulations was to validate the developed acid mine drainage prediction tool described in Section CHAPTER 3. above with the experimental test conditions and/or results.

The second objective was to compare the proposed model which uses multiple particle sizes with a model that uses a single particle size as used in literature studies (e.g. Bernardes de Souza and Mansur, 2011).

The simulation inputs for both multiple particle size inputs and a single particle size (D50) input model are given in Appendix F Table F. 1 and Table F. 2 respectively. From these tables, it should be noted that for multiple particle size inputs, the particle size distribution of both ore types was divided into four size classes. Based on the particle size distributions of both ore type 1 and type 2 samples (Appendix C), they were classified as sandy-loam soil using the Textural Triangle given in Figure 2.5. The van Genuchten properties of sandy-loam soil, as given in Table 2.1, were then used in the fluid flow model simulations i.e. the software has all the van Genuchten properties for different soil types as given in Table 2.1. The average particle size (D50) was approximately 32 µm and 53 µm for ore type 1 and type 2, respectively. For these simulations, the sulfide minerals mass percentage included Pyrite, Pyrrhotite, and Chalcopyrite. The carbonate minerals' mass percentage included Calcite and Dolomite. The rain amount is based on the amount of water added (in liters) per square ore bed area i.e. 0.2 L added per square area of 0.053 m^2 in this study. The simulations were done with computers with a RAM of 16 GB, 32 GB, and 256 GB RAM (all these computers were made available for this study by Mintek). As discussed in Section 3.2.4, the software allows for the simulated system to be divided into multiple instances which can be shared by computers with relatively small amounts of RAM (e.g. 16 GB RAM computer) on the same network. However, it should be noted that more RAM (e.g. 256 GB RAM) allows for simulations with few MiDAE instances which could be convenient for the user. A total of eight different simulations as shown in Appendix F Table F. 1 and Table F. 2 were done (HC and AHC simulations for ore type 1 and 2 by the single particle size model, and simulations by the multiple particle size model).

CHAPTER 5. RESULTS

5.1. Experimental Results

A visual comparison between the HC and AHC ore bed after the 11-week experimental test duration is given in Appendix E. As expected, the AHC is drier than the HC ore bed/heap because it was exposed to high temperatures.

The approach by Erguler and Erguler (2020), and García *et al.* (2005), of interpreting the kinetics test results with the aid of cumulative plots was also used in this study. Erguler and Erguler (2020) found that the instant leachate contents (e.g. SO_4^{2-}, Ca^{2+}, Mg^{2+}, etc.) including pH, do not directly correlate with time but their cumulative values do. The instant pH values were found to be unsteady by Erguler and Erguler (2020) due to the simultaneous occurrence of the oxidation and neutralization reactions, and as a result, instant pH values were not recommended for evaluating the rate of AMD generation but cumulative pH values were recommended for this purpose.

The cumulative leachate collected during the experimental tests is shown in Figure 5.1 and Figure 5.2. It can be seen from these figures that the Accelerated Humidity Cells (AHC) generated more leachate as compared to the reference Humidity Cells (HC). All the AHC tests generated leachate after week 1 while the HCs started after week 5. Ore type 1 HC started generating leachate after 6 weeks while ore type 2 started after 5 weeks. The AHCs started generating leachate much earlier than HCs because they are running at higher temperatures. Higher temperatures affect the hydraulic conductivity and as a result, increase the infiltration rate (Braga *et al.*, 2007). Braga *et al. (*2007) found that higher temperatures can increase the infiltration rate by as much as 56 %. In this study, the increased temperature increased the infiltration rate by at least 47% and 24% for ore type 1 and ore type 2, respectively.

Besides the fact that the reference HCs tests were operating at lower temperatures compared to the AHCs, the other reason as to why they started generating leachate much later could be attributed to the ore bed field capacity and the weekly water addition. The soil/ore bed field capacity is the maximum amount of water the soil/ore bed can hold before the water starts draining due to gravity

(US DA, 2008). In the case of the reference HCs, it does imply that the weekly water addition was much lower than the ore bed field capacity. However, as stated in the experimental method, Section 4.2, increasing the weekly water addition beyond 200 ml resulted in too much flooding for the AHCs, and too much flooding hinders oxygen/air diffusion as it closes the ore bed pores. Because all the experimental tests had to be conducted with the same weekly water addition, the weekly water addition was not increased even though it did show that it was lower than the field capacity for the reference cells.

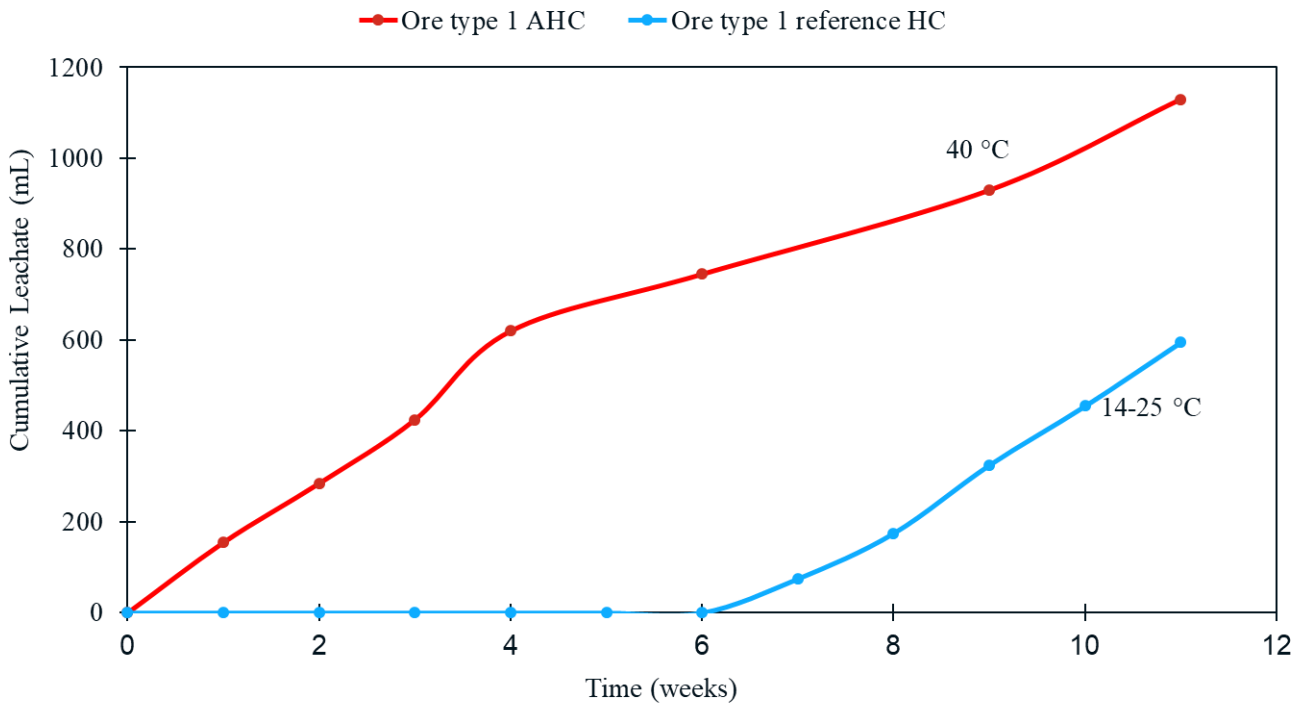

Figure 5.1: Cumulative Leachate of Accelerated Humidity Cell (AHC) vs Reference Humidity Cell (HC) for Ore type 1

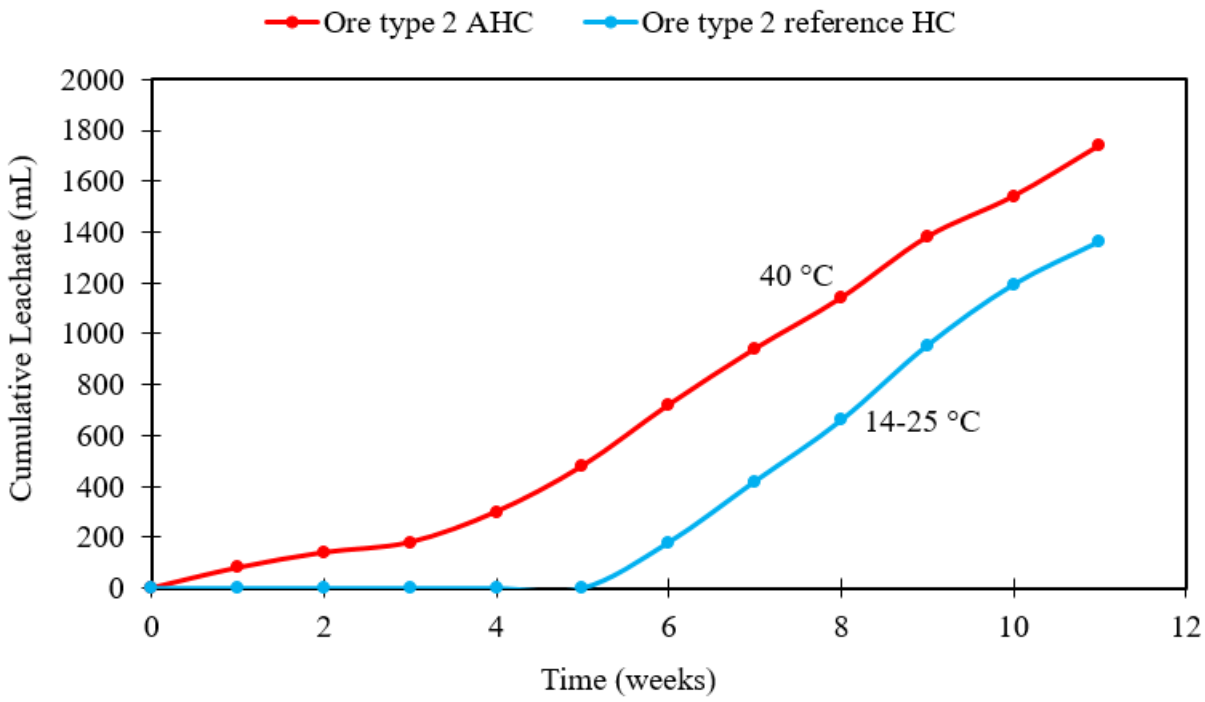

Figure 5.2: Cumulative Leachate of Accelerated Humidity Cell (AHC) vs Reference Humidity Cell (HC) for ore type 2

The leachate pH profiles for both AHCs and HC are given in Figure 5.3 and Figure 5.4 for ore type 1 and ore type 2 respectively. For both ore type 1 and type 2, it can be noted that the overall leachate pH was lower for the AHCs compared to HC tests. It should also be noted that the overall leachate amount of ore type 2 was higher than that of ore type 1. This can be attributed to the fact that ore type 2 had slightly smaller amounts of fine particles (approximately 36% less than 38µm) than ore type 1, which had approximately 53% particles less than 38µm. As described in Section 2.2.3, Equations 2.20 and 2.21, the relationship between pH and sulphate concentration is such that pH decreases with increased sulphate concentrations. Therefore, the obtained pH profiles suggest that the sulphate generation i.e. acid generation in AHC cells was higher than that of HC cells for both ore types.

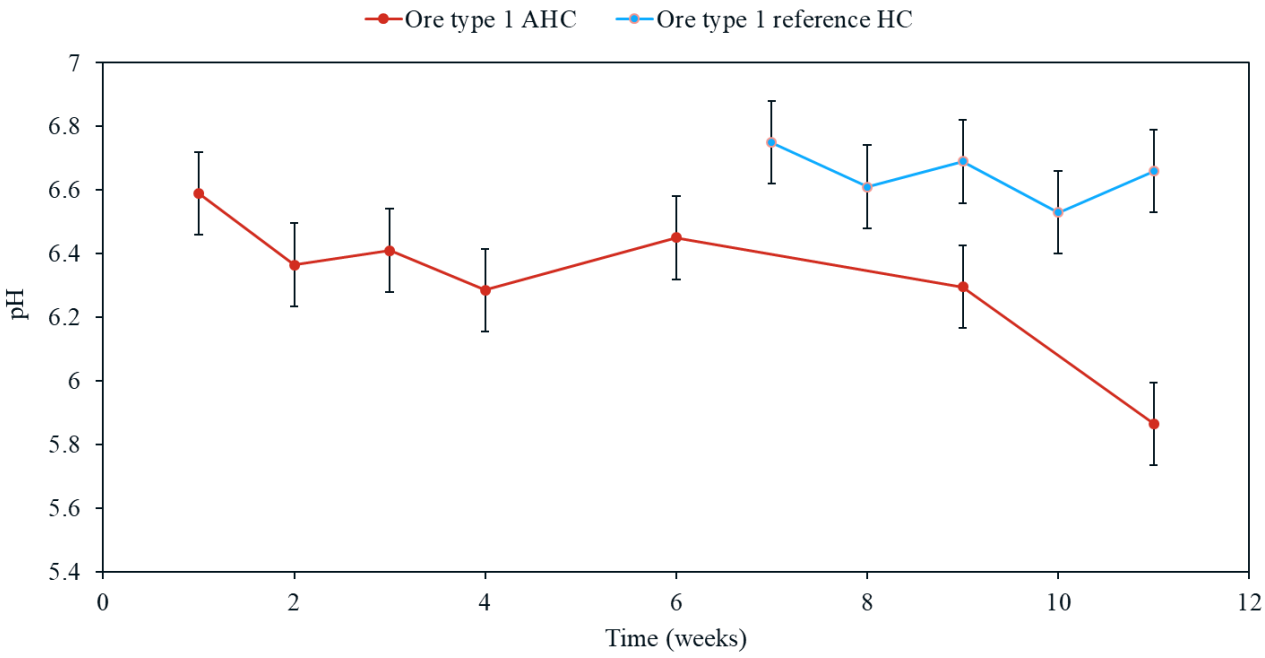

Figure 5.3: Leachate pH of Accelerated Humidity Cell (AHC) vs Reference Humidity Cell (HC) for Ore type 1

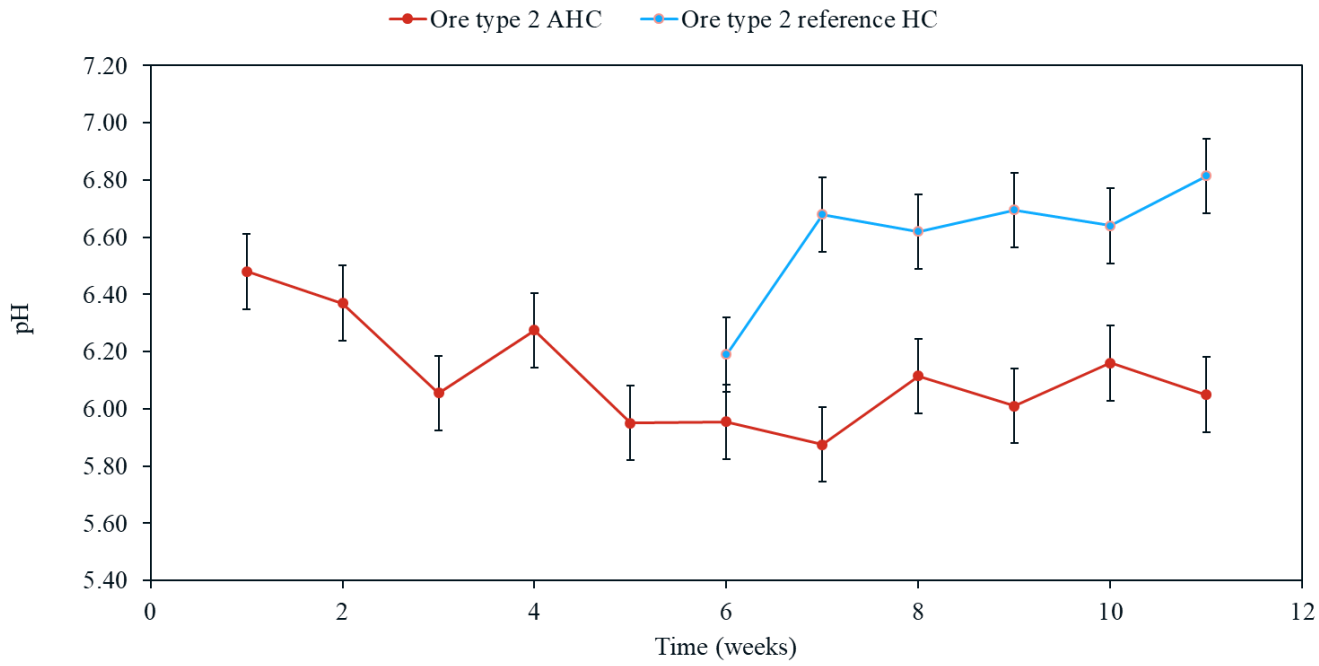

Figure 5.4: Leachate PH of Accelerated Humidity Cell (AHC) vs Reference Humidity Cell (HC) for Ore type 2

Similar to the studies by Erguler and Erguler (2020), and García *et al.* (2005), the SO_4^- ions are considered as the main product of the sulfide minerals oxidation reaction in this study also, and their concentration in the leachate was considered as an indication of the extent/rate of the reaction i.e. acid formation.

The associated cumulative acid (SO_4) concentration found in the leachates of ore type 1 and ore type 2 HC and AHC tests are given in Figure 5.5 and Figure 5.6. Note that in both figures, the acid concentration trends are higher for AHC as compared to HC. This is a similar response to the observed pH response above i.e. this was used to confirm the observed pH response.

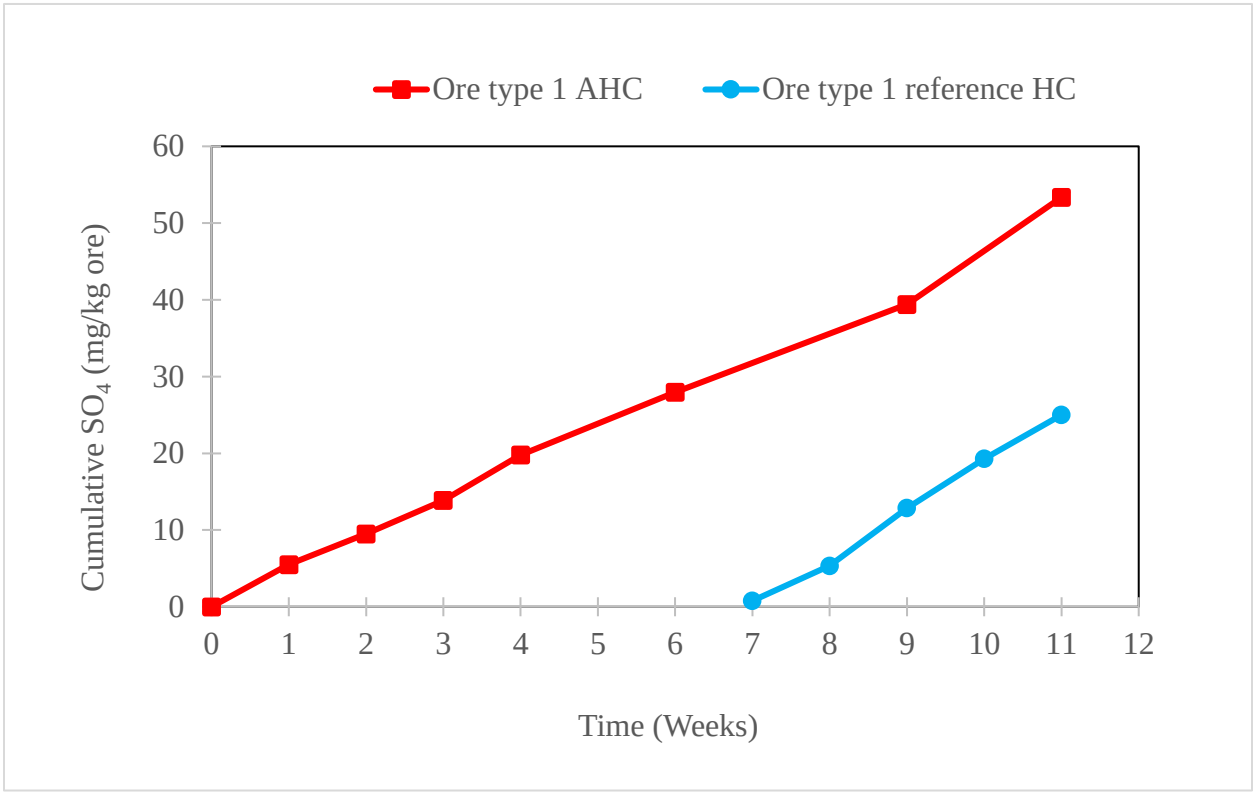

Figure 5.5: Cumulative SO_4 concentration in ore type 1 HC and AHC leachates

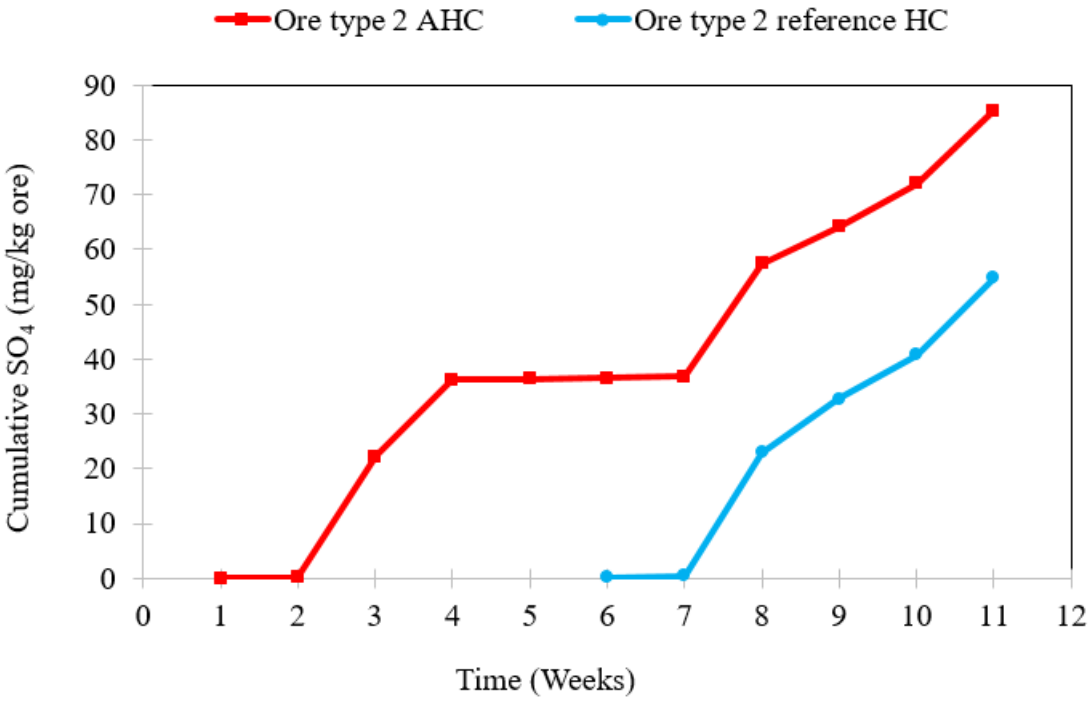

Figure 5.6: Cumulative SO_4 concentration in ore type 2 HC and AHC leachates

5.2. Simulation Results

Note that using a D50 in this study can also be equated to using a static equally spaced mesh cell size. In this document, the D50 results represent the literature model (equations given in Section 2.2.3) while the model with multiple particle sizes includes the proposed additions to the literature model (Section CHAPTER 3.).

The cumulative leachate model simulation results for the ore type 1 HC test are given in Figure 5.7. There is a significant error between the actual experimental test results and the model simulations in the first few weeks, especially before week 6 as there was no significant leachate amount obtained from the experimental test. After week 6, it does show that the experimental data does get closer to the predicted cumulative values. It should also be noted that the proposed model

with multiple particle sizes performed the same as the single particle size (D50) model for this experimental test or ore type. The results for ore type 2 are shown in Figure 5.8. It can be noted that the single particle (D50) model performed better for a short period (weeks 1 to 7), while the multiple particles model was better afterwards. Overall, the proposed model with multiple particle input performed better than the model with a single particle size of D50 for ore type 2 because the final cumulative leachate is much closer to the actual leachate over 11 weeks.

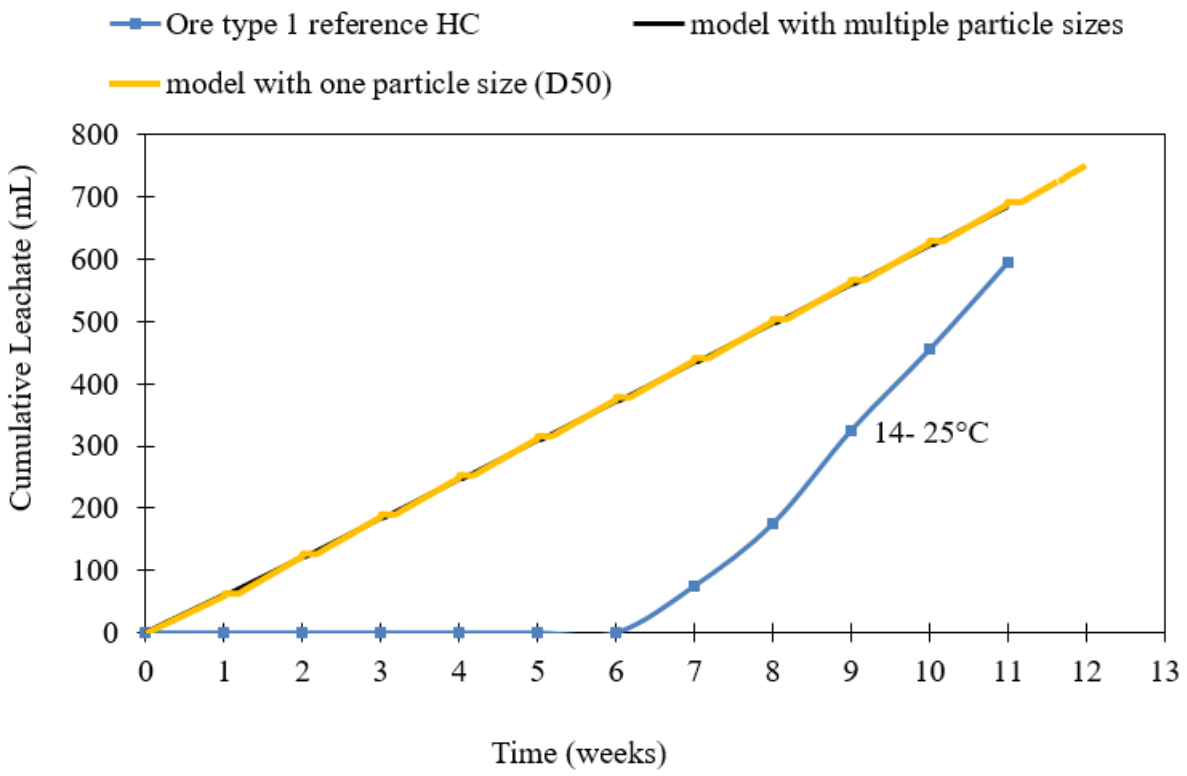

Figure 5.7: Model prediction vs experimental tests – ore type 1 cumulative leachate for HC

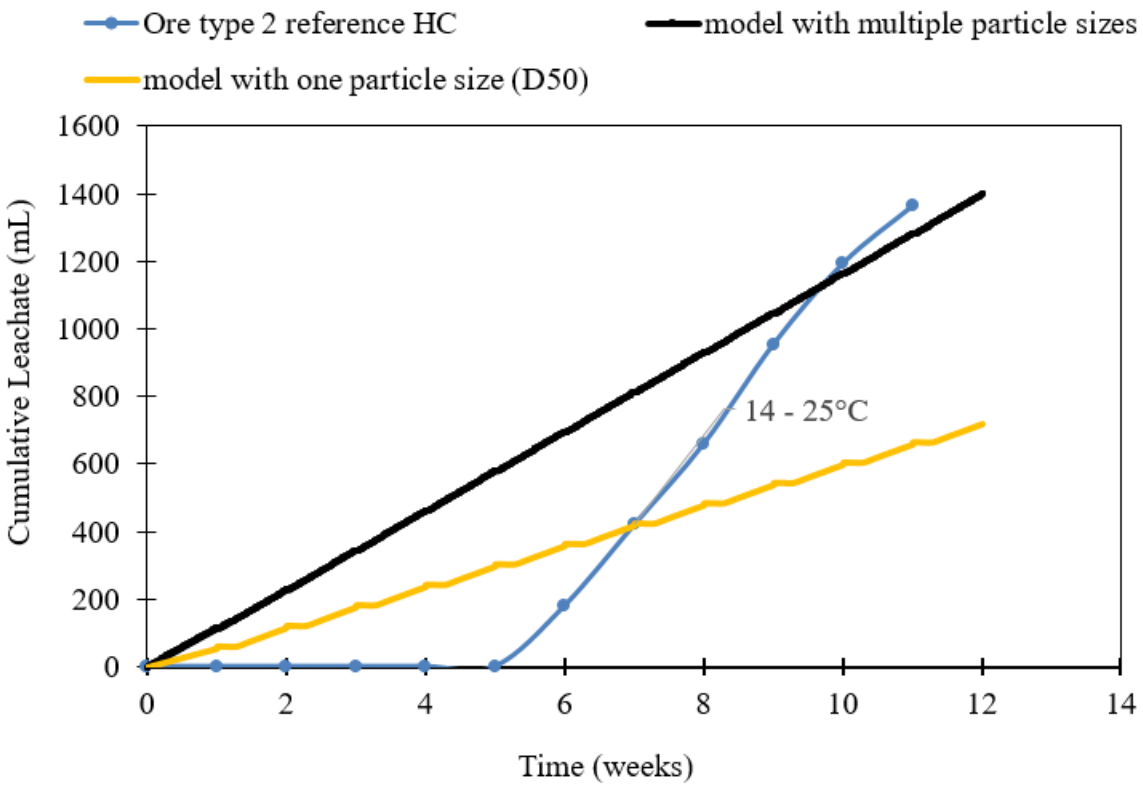

Figure 5.8: Model prediction vs experimental tests – ore type 2 HC cumulative leachate

The AHC leachate model prediction results for ore types 1 and 2 are given in Figure 5.9 and Figure 5.10. Ideally, the effects of temperature change on the infiltration rate should be accounted for using the temperature-based hydraulic conductivity given by Equation 2.8. Section 2.2.3 shows that hydraulic conductivity is the main liquid fluid flow/infiltration parameter directly affected by temperature when compared to the rest of the liquid fluid flow/infiltration equations. However, Braga *et al.* (2007) found that Equation 2.8 did not predict the high infiltration rates of up to 56% observed during their tests. Figure 5.9 below also shows that the predictions were much lower than the actual test results i.e. high temperatures do increase the infiltration rate and, in this figure, it was on average at least 24% higher than what the D50 or the multiple particles input model predicted. For this reason, a leachate temperature correction factor (Equation 5.1) has been proposed in this study.

$$L_T = L\,(1 + \frac{T - T_r}{T_r}) \qquad 5.1$$

Note that (L_T) is the temperature-corrected leachate amount. L, T, and T_r are leachate amounts, temperature, and room temperature, respectively. Any value from 25 °C to 27 °C can be used at room temperature but it is recommended that 27 °C be used as it gave the best fit/correction factor for both ore types used in this study.

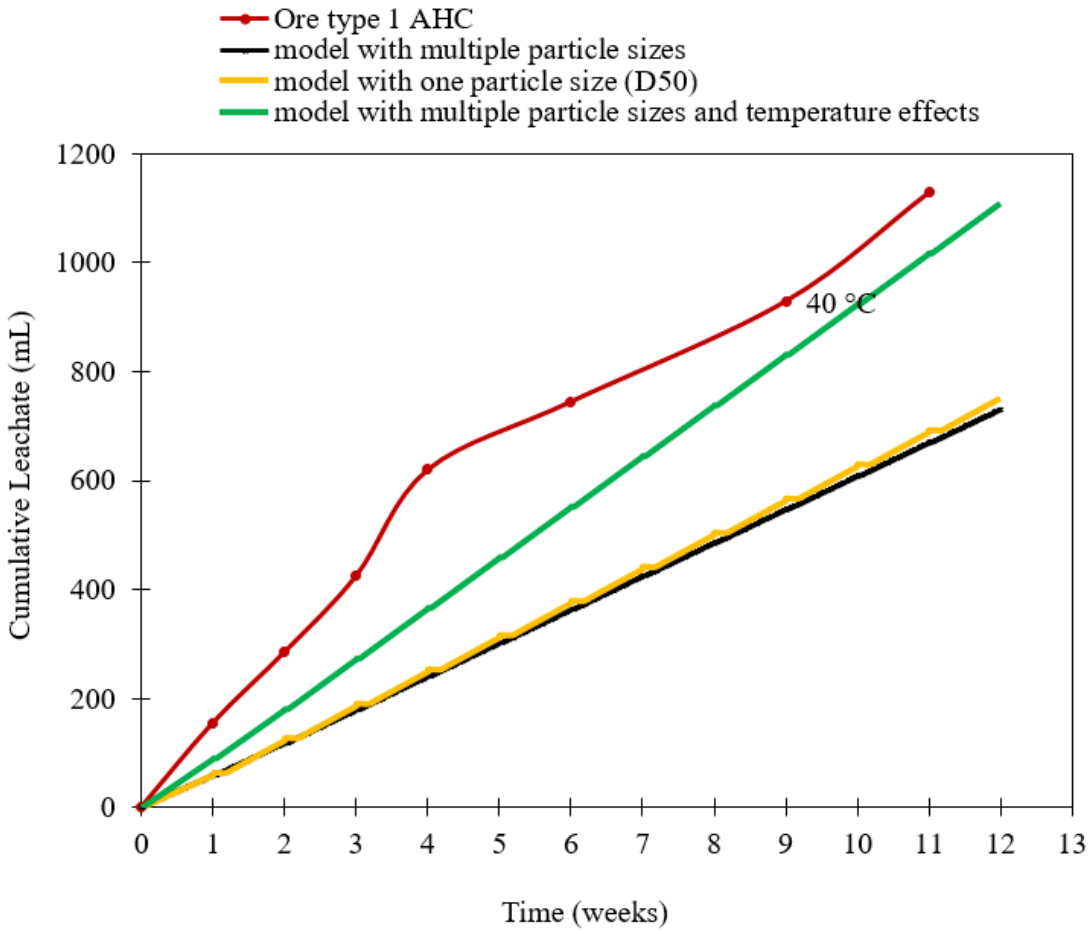

Figure 5.9: Model prediction vs experimental tests – ore type 1 cumulative leachate for AHC

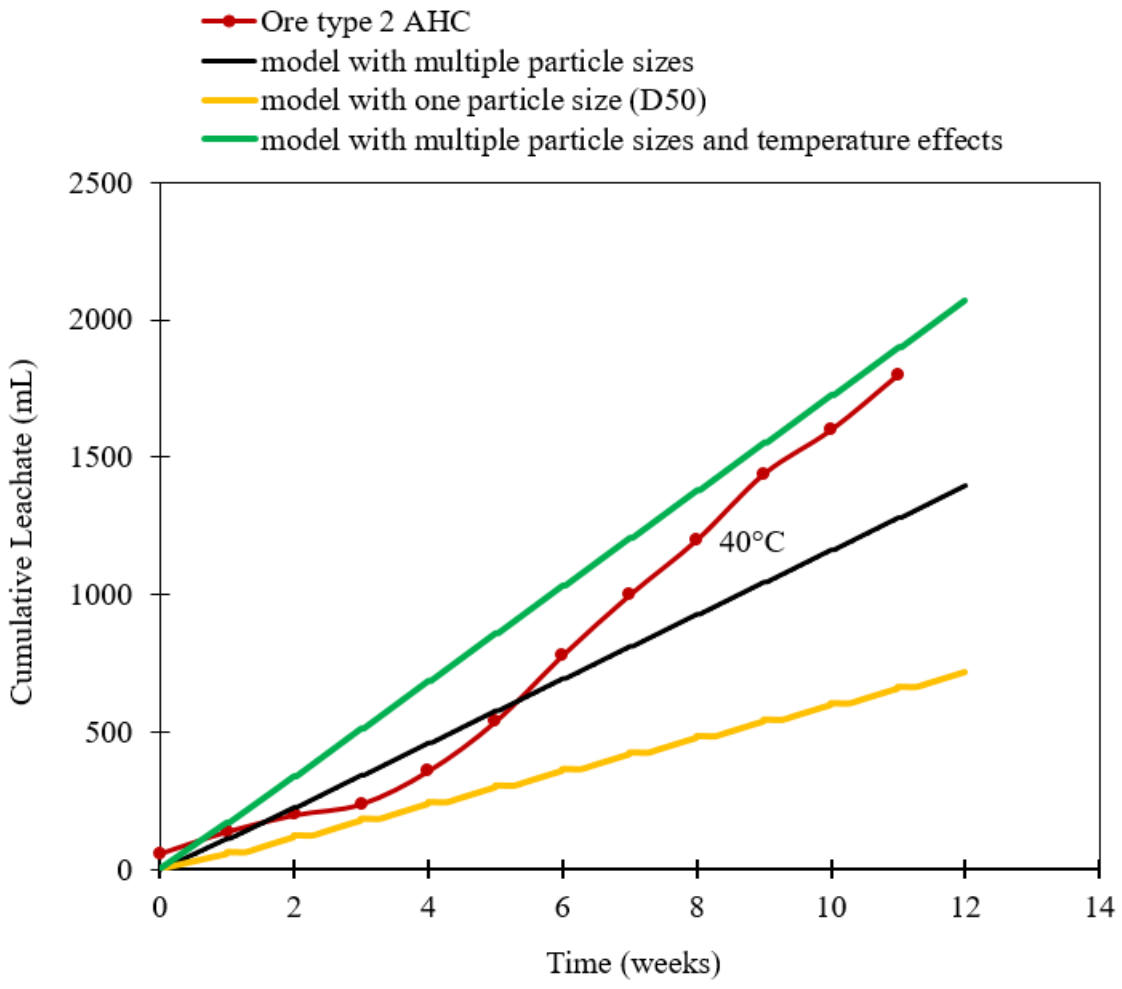

Figure 5.10: Model prediction vs experimental tests – ore type 2 AHC cumulative leachate

Figure 5.11 shows graphs of cumulative acid production for ore type 1 HC from experimental tests and model prediction. Note that a logarithmic scale was used on the y-axis (i.e. cumulative SO_4) because of the significant difference between the initial cumulative amounts of SO_4 produced in the first few weeks compared to the cumulative amount of SO_4 produced during the last weeks of the simulation time. Also, the high difference between the model simulation results and the experimental data in some instances (first and/or last few weeks) is another reason why it was deemed necessary to use the logarithmic scale so that all the profiles can be displayed/compared on a single figure. From Figure 5.11, the single particle size (D50) model was able to predict the

acid production better than the multiple particle size. The same can be observed for ore type 1 AHC tests vs model predictions as shown in Figure 5.12.

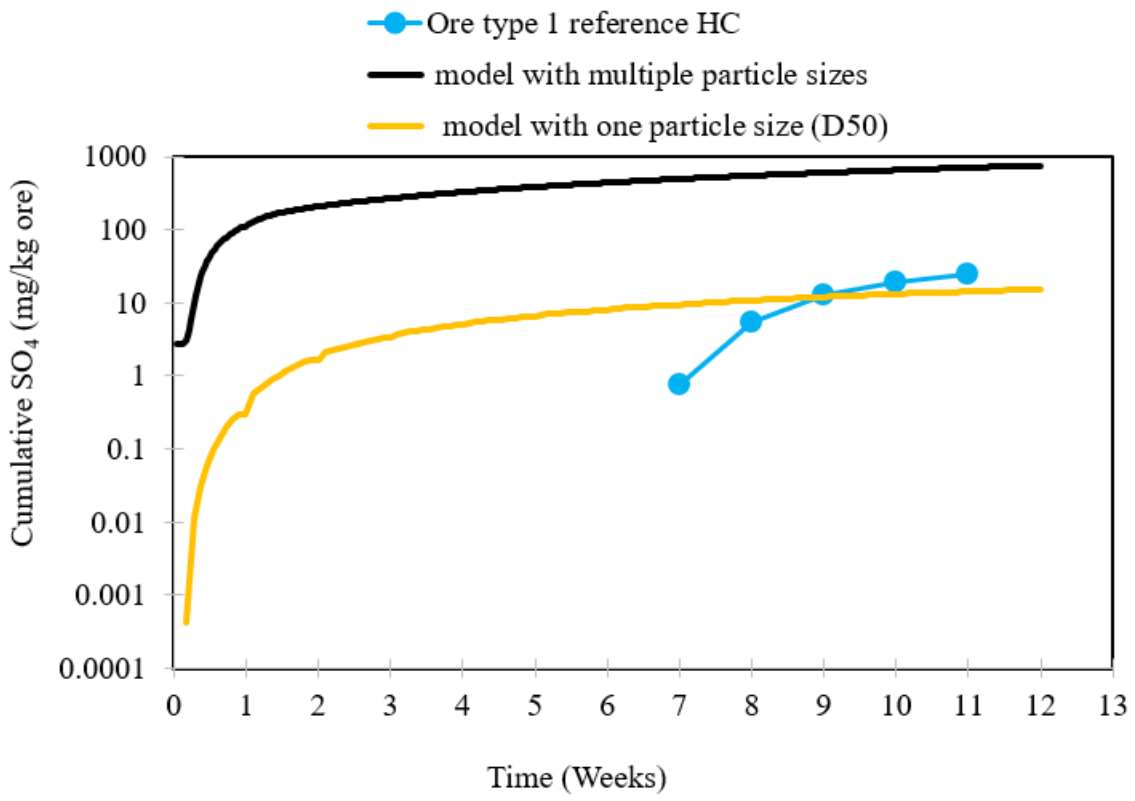

Figure 5.11: Model prediction vs experimental tests – ore type 1 HC cumulative SO_4 in leachate

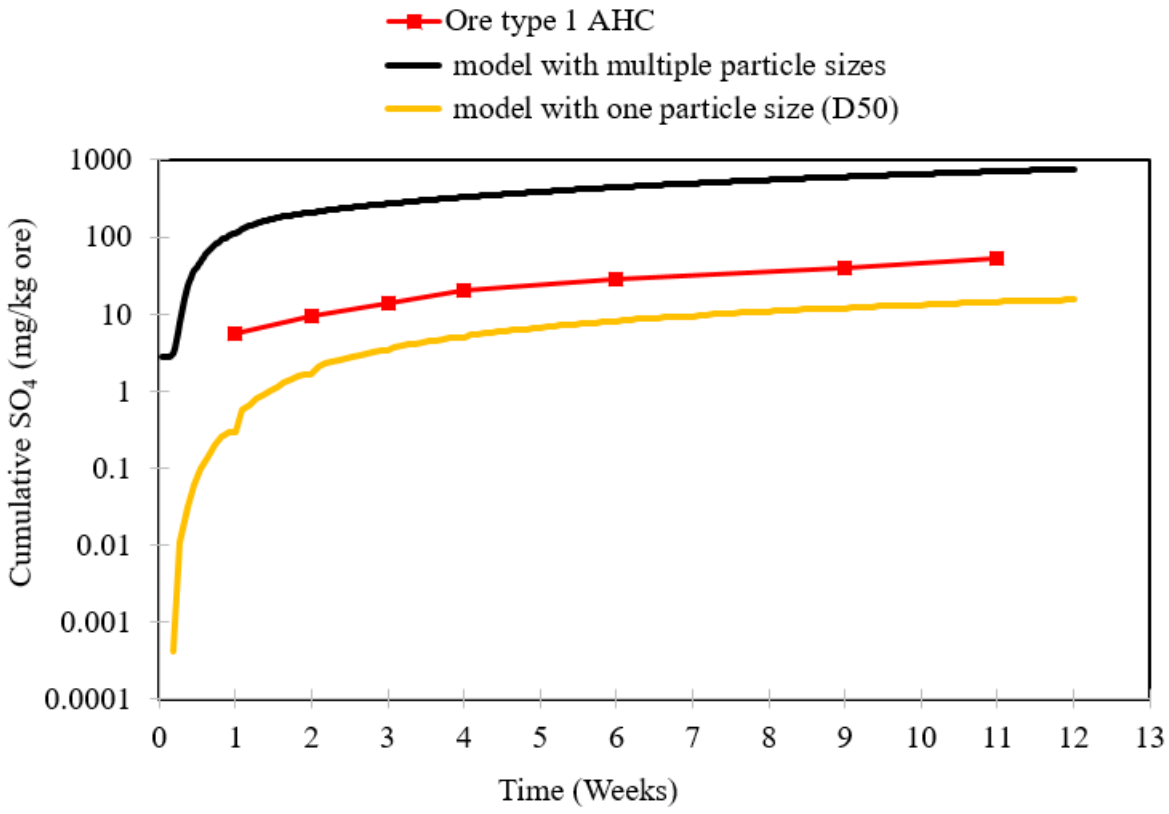

Figure 5.12: Model prediction vs experimental tests – ore type 1 AHC cumulative SO_4 in leachate

The actual measured cumulative acid production from ore type 2 HC experimental tests is compared with the model predictions in Figure 5.13. Although the single particle size (D50) model cumulative acid production prediction was better than that of the multiple particle size model between weeks 6 and 7, overall, the multiple particle size model performed better than the single particle size (D50) model. The single particle size (D50) model predicted much lower than the observed cumulative acid production. The ore type 2 AHC tests comparison between the experimental results and the model predictions is shown in Figure 5.14. It can also be seen from this figure that the single particle size (D50) model gave a better prediction of the cumulative acid production compared to the multiple particle size model in the first 2 weeks, but the multiple particle size model was better afterwards.

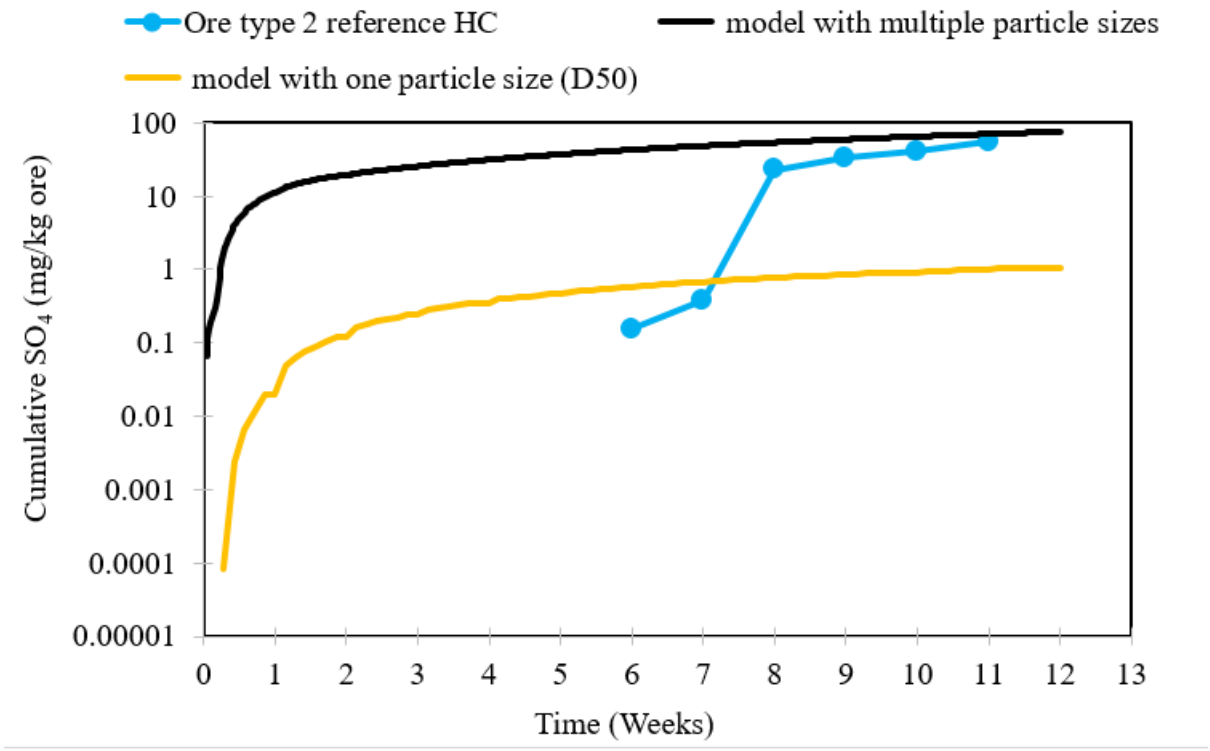

Figure 5.13: Model prediction vs experimental tests – ore type 2 HC cumulative SO_4 in leachate

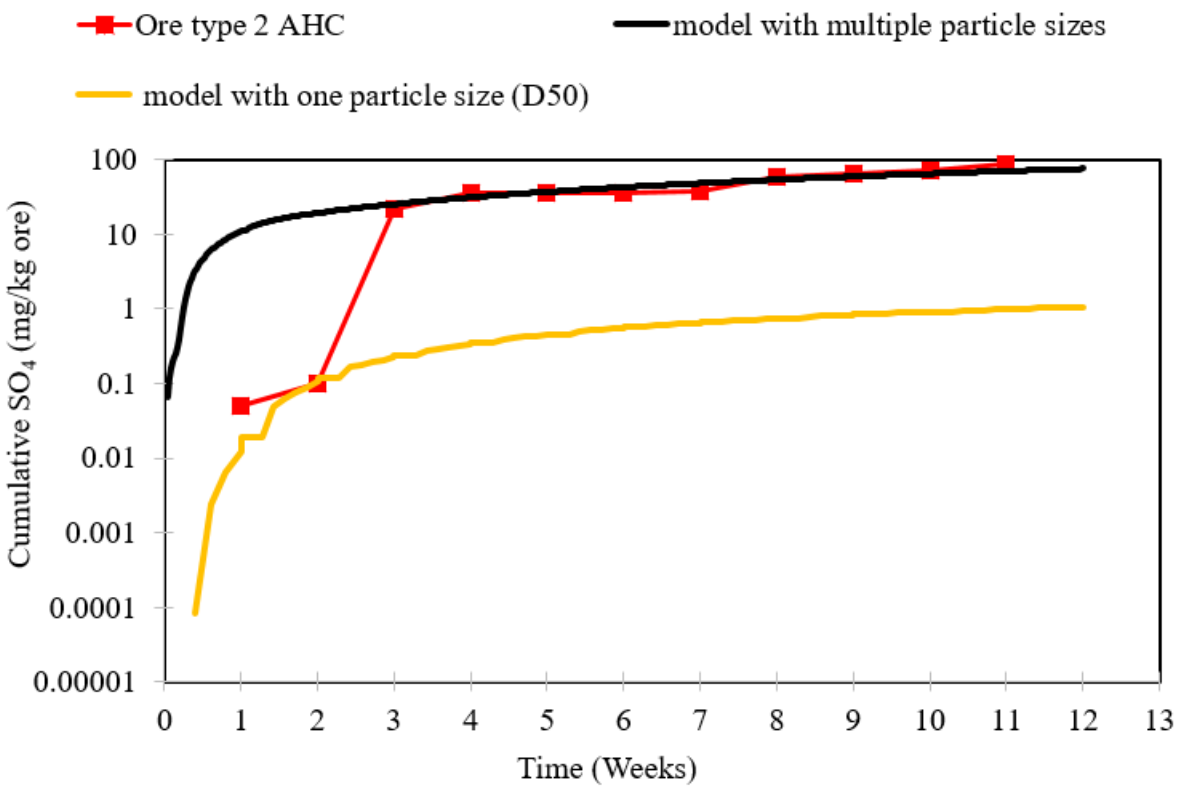

Figure 5.14: Model prediction vs experimental tests – ore type 2 AHC cumulative SO_4 in leachate

Table 5.1 below summarises the model predictions performance with the aid of the 95th percentile of the weekly absolute errors between the model predictions and the experimental cumulative SO_4 in leachate results. It should be noted that the 95th percentile was used in order to discard 5% of the outliers in the data. From Table 5.1, it can be seen that the model with one particle size (D50) performed better (i.e. lower 95th percentile of the weekly absolute errors) than the model with multiple particle sizes for ore type 1 and vice versa for ore type 2. It can also be noted that the 95th percentile of the weekly absolute errors between the model with multiple particle sizes and the experimental results is too high for ore type 1 and low for ore type 2.

From the mineralogical data or the model inputs data (Appendix F Table F. 1), it can be noted that ore type 1 had more sulfide minerals (4.7 %) and lower carbonate minerals (1.04 %) compared to ore type 2 which had 0.53 % sulfide minerals, and 37.4 % carbonate minerals i.e. ore type 1 had high potential to form acid (i.e. SO_4) and very low potential to neutralize it compared to ore type 2. However, the experimental test results shows that the acid produced by ore type 1 was much lower than predicted by the multiple particle sizes. This would either imply that the model was/is over-predicting or there are other minerals not accounted for that neutralized the acid formed.

A literature review with respect to the other minerals present in ore type 1 revealed that besides carbonate minerals, silicate minerals such as albite, biotite, chlorite and muscovite can also neutralize the acid-formed (Wang, 2022; Kollias *et al.* 2021; Madakkaruppan *et al.*, 2019; Brantley, 2008; Palandri and Kharaka, 2004). Because of the significant amount of silicate minerals in ore type 1 (38.14%), it was deemed necessary to include the effects of silicate minerals in the proposed model. The silicate minerals modelling was done similar to the carbonates modelling described in Section 3.2.3. The multiple particle sizes model simulation were then repeated with the silicate minerals contents (see Appendix F Table F. 3 for the multiple particle sizes model simulation inputs with silicate content). The ore type 1 model simulation results with silicate effects are shown in Figure 5.15 and Figure 5.16 for the HC and AHC respectively. From these figures and the 95^{th} Percentile of the weekly absolute errors between the model predictions result and the experimental test results, it can be seen that the multiple particle sizes model prediction has significantly improved with the inclusion of silicate minerals for ore type 1.

Table 5.1: 95th Percentile of the weekly absolute errors between the model predictions and the experimental results (cumulative SO_4 in leachate)

Datasets		**95th Percentile of the weekly Absolute Errors**		
		Model with one particle size (D50)	Model with multiple particle sizes	Model with multiple particle sizes and silicates effects (the graphs are shown in Figure 5.15 to Figure 5.18 below)
Ore Type 1	**HC**	12.4	626.4	70.2
	AHC	36.4	575.4	25.7
Ore Type 2	**HC**	49.7	41.0	25.5
	AHC	88.8	22.5	28.6

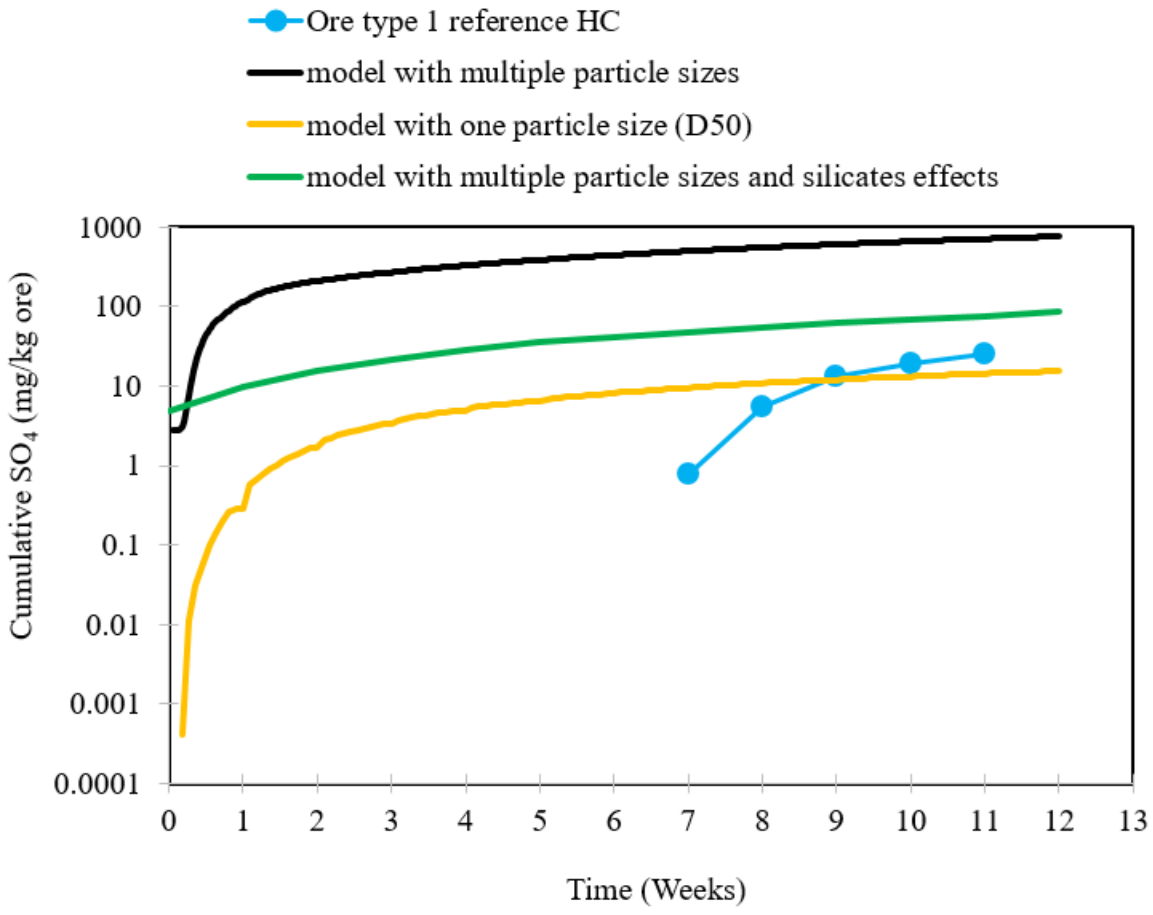

Figure 5.15: Model prediction with silicates effects vs experimental tests – ore type 1 HC cumulative SO4 in leachate

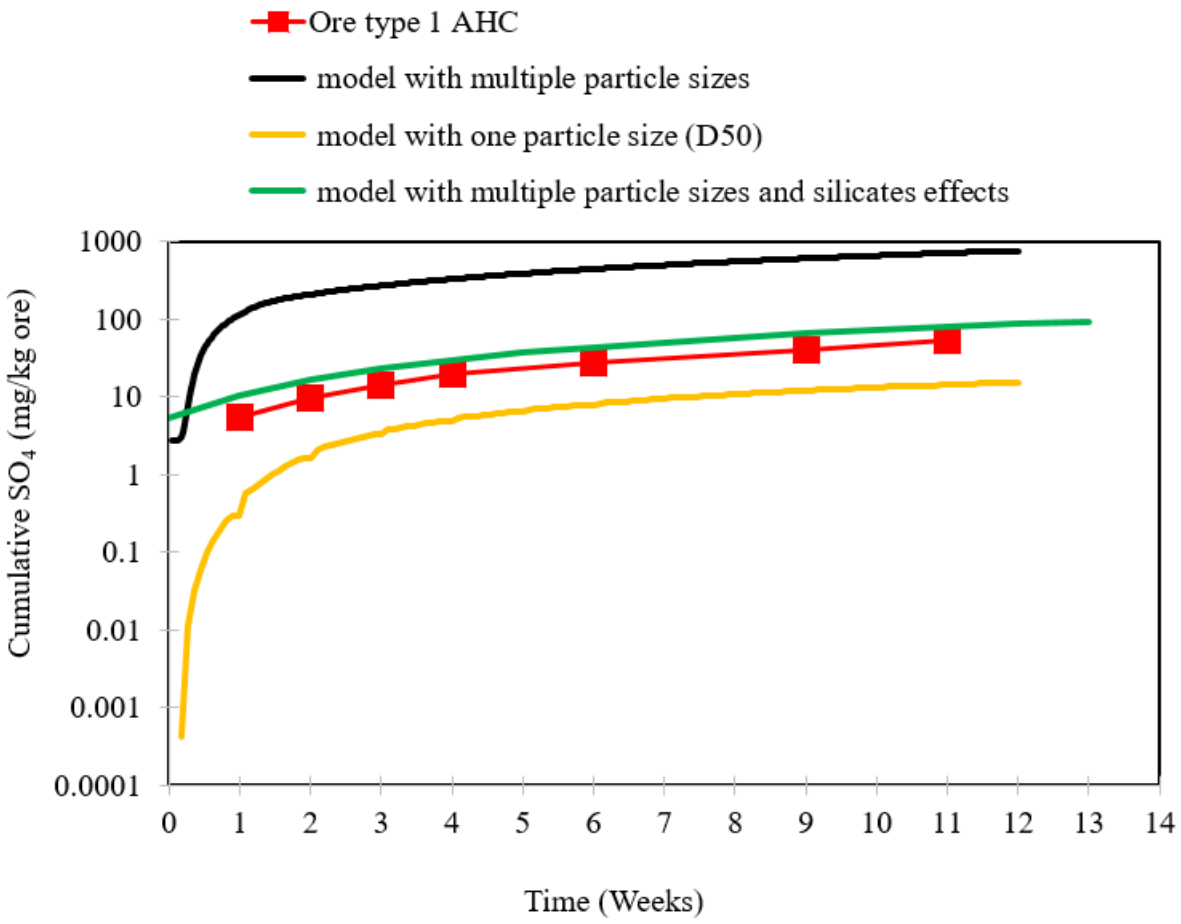

Figure 5.16: Model prediction with silicates effects vs experimental tests – ore type 1 AHC cumulative SO4 in leachate

The simulation results of ore type 2 with silicate effects are shown in Figure 5.17 and Figure 5.18 below for HC and AHC respectively. From these figures and Table 5.1, it can be seen that the impact of silicate minerals is noticeable but not as much as on ore type 1. This is because the silicates were not the main acid-consuming mineral for ore type 2.

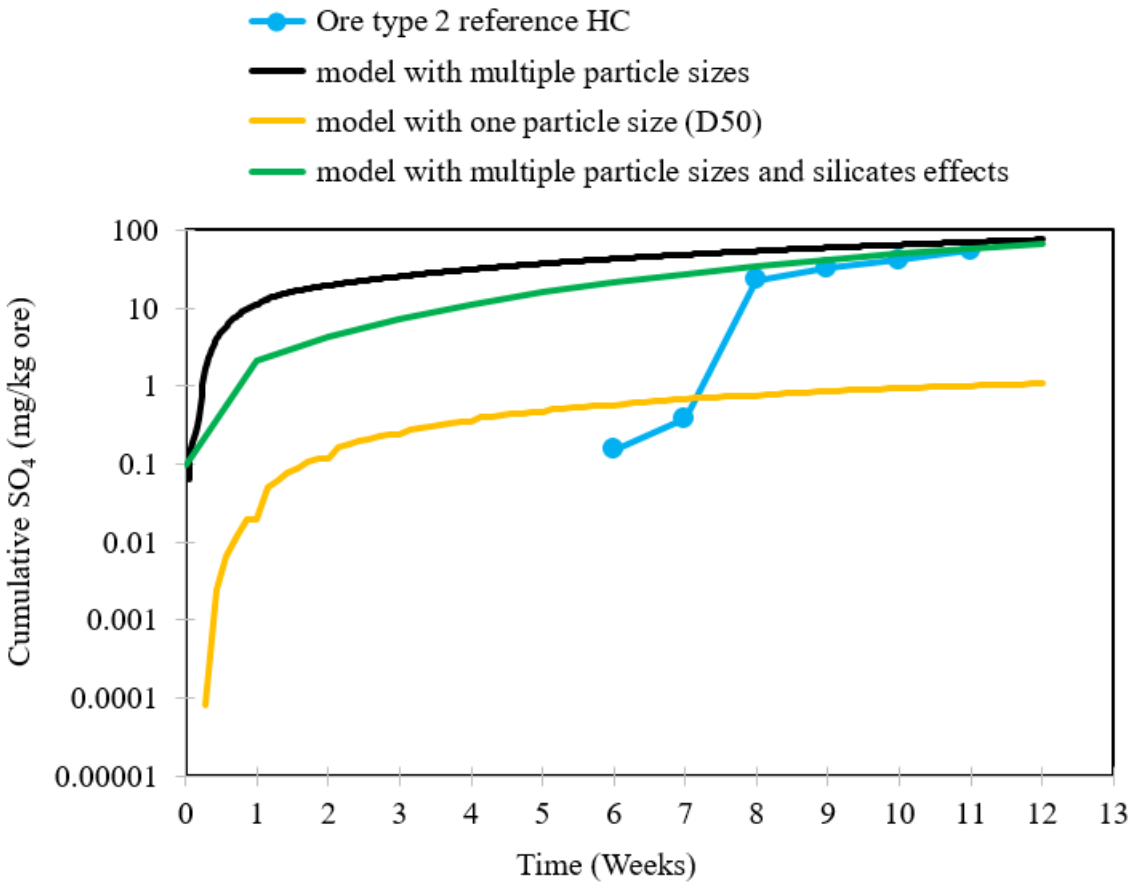

Figure 5.17: Model prediction with silicates effects vs experimental tests – ore type 2 HC cumulative SO4 in leachate

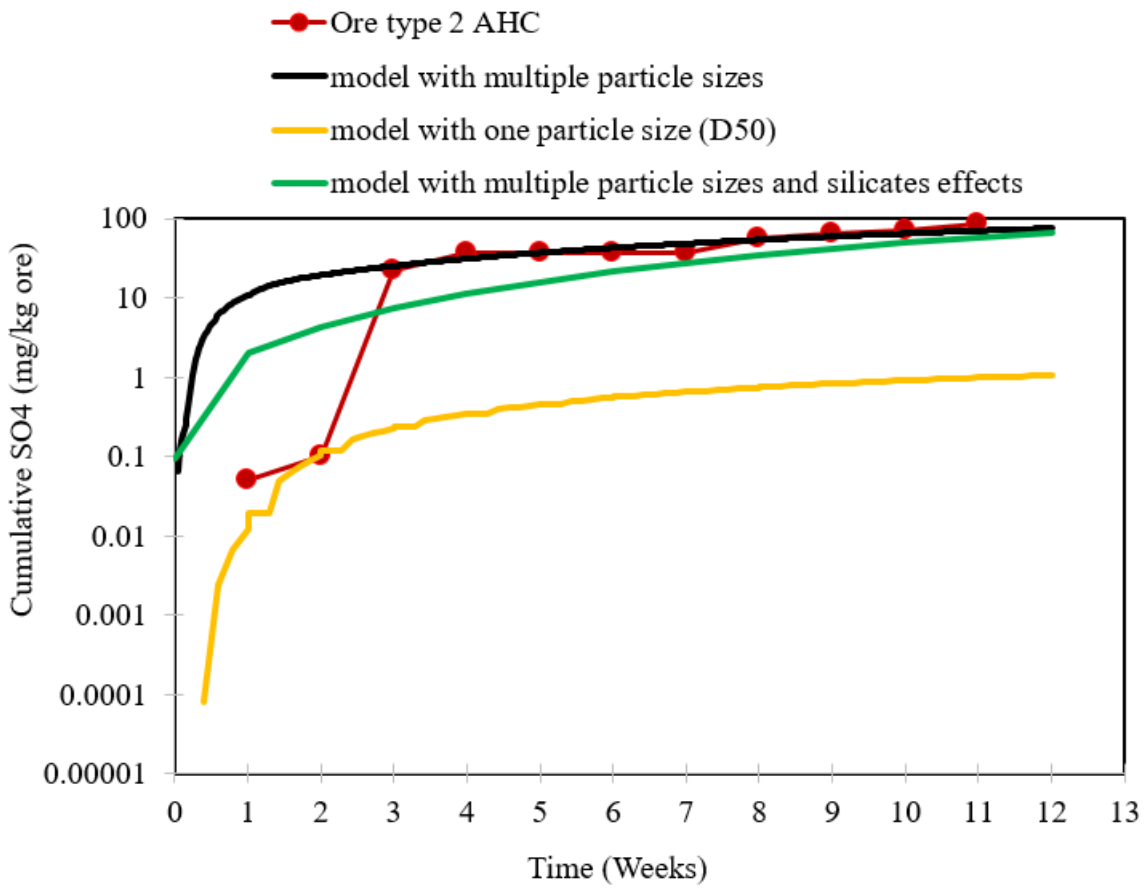

Figure 5.18: Model prediction with silicates effects vs experimental tests – ore type 2 AHC cumulative SO4 in leachate

By mere looking at some of the simulation or experimental test results (especially some of the cumulative leachate profiles) presented in this section, one could wonder why is the model proposed in this study complex and non-linear i.e. why not a simple linear model? As illustrated in Section 3.2, the model proposed in this study is based on typical models used in literature for AMD prediction i.e. non-linear models are typically used for AMD prediction. This is because the actual long-term AMD profiles from actual mine sites are also non-linear (Morin & Hutt, 1997; Ma *et al.*, 2019). AMD formation is complex and non-linear because there are several factors that affect it as shown in Section 2.1.2. However, it is not unusual to get a linear response from the

AMD model simulation or experimental tests conducted over a short period of less than 2 years (similar to this study), as studies by Bradham & Caruccio (1997) and Erguler *et al.*(2020) also showed that these responses are possible. Erguler *et al.* (2020) even proposed empirical linear models for field scale behaviour based on lab kinetic column tests. How well will a linear model predict long-term (more than 2 years) AMD profile is still unclear? Hence, a non-linear model was preferred in this study as they have been shown to have potential to predict AMD profiles for over 10 year period which is usually desired for any AMD model (Morin & Hutt, 1997; Ma *et al.*, 2019).

CHAPTER 6. DISCUSSIONS

6.1. Humidity Cell Design and Experimental Tests

The process control was/is the first phase of automation for the proposed cell. The next would be to make the cell fully automated with no manual sampling of the leachate and the leachate pH, Eh, and conductivity measured online such that the tests could be done with minimal manual labour, and within the planned time even if the person conducting the experiment is not physically available. The problem with weekly manual sampling (and/or analysis) is that it assumes that there will always be someone every week for the duration of the humidity test, which can be at least 20 weeks to a year or more, as reported in the literature (Parbhakar-Fox *et al.*, 2013, Sapsforda *et al.*, 2008; GARD Guide, 2012) - this is not always practical. Adding the instrumentation and control system on the humidity cell to control the temperature, pressure, and humidity eliminates the need to take the humidity cells every week to an enclosure such as recommended in ASTM (2018) and used by Bradham and Caruccio (1997) to study the effects of high temperature on AMD formation.

6.2. Model Predictions and Software

The biggest challenge in this project was trying to balance prediction accuracy and the overall simulation time and equipment (minimum computer specification required). One of the additions to the software to deal with this, especially when solving the 3-D fluid flow infiltration model or Richards equation, is that the extent of the iterative method (trial and error) is automatically adjusted based on the fluid content between the discrete layers. Higher difference means more iterations because the error is or could be significant and low difference means fewer iterations.

Matlab was preferred in this study and most of the algorithms were developed in Matlab because the main researcher in this study i.e. the MSc student or author of this document, is more familiar with Matlab. However, aspects that were running very slow in Matlab (e.g. 3D fluid flow model solvers), were moved to C++ and integrated with Matlab files using MATLAB MEX files and console applications files. This improved the processing time significantly and in some instances, more than 3 hours of simulation time was saved.

CHAPTER 7. CONCLUSIONS AND RECOMMENDATIONS

The first objective of this project was to develop a methodology that can be used to accelerate the kinetic humidity cell tests. For this purpose, an Accelerated Humidity Cell (AHC) was proposed, designed, built, and tested against the reference/normal humidity cell (HC). A control system was added to the AHC so that it can be operated at constant or varying temperature, pressure, and relative humidity to simulate the expected/desired environmental conditions. When compared to the HC experimental test results, it has been shown in this study that the AHC tests:

- Accelerated the leachate production rate by at least 24% – higher infiltration rate
- Accelerated the acid formation – observed from lower pH profiles also

The second objective was to investigate the feasibility of incorporating the full particle size distribution into the AMD prediction i.e. developing a mineral particles-based kinetic AMD prediction tool. This investigation focused on the fluid flow model for now. The literature models were used as the basis and an algorithm to incorporate the full PSD was added to the model. The model was developed and tested with the experimental test data from the HC and AHC tests. The model is promising but also showed that the current literature models used as the basis cannot be used to accurately predict the infiltration rate with relatively higher temperatures e.g. temperature such as 40°C which was used in this study. For this reason, a temperature correction factor has been proposed in this study and it improved the overall model prediction of the actual experimental test results. In terms of the actual acid production rate prediction, the proposed model was able to predict the acid production rate much better than the single particles model for ore type 2 for both HC and AHC tests. However, the single particle model performed better for ore type 1 tests. Overall, the proposed model is promising but it still needs further improvement.

The software has been designed such that it can be run from multiple computers on the same network with a central location (or computer) designated to store the intermediate simulation progress results for all instances. If configured in this manner, the software automatically selects the main PC based on which started the process/simulation first and gives it the title “Main

Instance", and the others would then have their instance names as 2,3,4… etc., depending on which started first. A watchdog has been implemented to track the health of each instance. Each PC i.e. "Instance" will need to report the progress within three cycles at least. A cycle is a period after all the instances have stored their intermediate results on the main progress database (SimulationProgress.db). A cycle time depend on the sample or simulation size, it could be as small as 1 minute if the sample size is small and the computer(s) have decent processing speed. If the "Main Instance" fails, the next in line takes over as the main instance, and the rest of the computers or instances on the same computer then interact with it, i.e. send and receive data from the main instance or PC. This data includes the changes in temperature, additional water to the surface, etc. The software has also been designed such that the simulation can be stopped and started later, i.e. continue from where it ended. It can do this because it saves the simulation progress in a database file. During the trial or testing, a minimum PC RAM of 16 GB was used, but more RAM could be used.

Based on the findings from this study, it is recommended that AHC tests be used with kinetic AMD models for AMD prediction, as this will help reduce the time it takes to get meaningful experimental kinetic test results. The accelerated humidity cell tests can be done in parallel with at least one reference humidity cell at standard temperature and pressure if required to check how much the accelerated test (AHC) speeds.

It is recommended that mineralogical data such as particle minerals association and particle minerals surface liberation be incorporated in the proposed AMD prediction model/software. It is also recommended to test this model further with other different ore types and, if possible, with an actual mine site tails dump i.e. simulating the actual full-size mine tails dump and comparing it with leachate samples collected from the same mine tails dump.

REFERENCES

Amos, R.T., Blowes, D.W., Baily, B.L. and Sego, D., 2014, "Waste-Rock Hydrogeology and Geochemistry", *Applied Geochemistry* 57.

Ayora, C., Macias, F., Torres, E. and Nieto, J.M., 2015, "Rare Earth Elements in Acid Mine Drainage" *Meeting of the Spanish Mineralogy Society* (35), Huelva June 30 to July 3, 2015.

ASTM, 2018, "Standard Test Method for Laboratory Weathering of Solid Materials Using a Humidity Cell", ASTM D5744 -18

Becker, M., Dyantyi, N., Broadhurst, J., Harrison, S.T.L. and Franzidis, J.P., 2015, "Application of quantitative mineralogy in the interpretation of laboratory scale acid rock drainage prediction tests: A gold case study, Minerals to Metals Initiative", Department of Chemical Engineering, University of Cape Town, South Africa.

Benzaazoua, M., Bussière, B., Dagenais, A.-M. and Archambault, M., 2004, "Kinetic tests comparison and interpretation for prediction of the Joutel tailings acid generation potential". Environmental Geology, 46, 1086–1101

Bernardes de Souza, C.M. and Mansur, M. B., 2011, "Modelling of acid mine drainage (AMD) in columns", *Brazilian Journal of Chemical Engineering* 28(3), 425 – 432.

Bonan, G., 2019, *Climate change and Terrestrial Ecosystem Modeling*, Cambridge University Press, Online ISBN 9781107339217, https://doi.org/10.1017/9781107339217

Botros, F.E., Onsoy, Y.S., Ginn, T.R. and Harter, T., 2012, "Richards Equation–Based Modeling to Estimate Flow and Nitrate Transport in a Deep Alluvial Vadose Zone" Special Section: Model-Data Fusion in the Vadose Zone, *Vadose Zone Journal*, doi:10.2136/vzj2011.0145

Bouzahzah, H., Benzaazoua, M., Plante, B. and Bussiere, B., 2015, "A quantitative approach for the estimation of the "fizz rating" parameter in the acid-base accounting tests: A new adaptations of the Sobek test", *Journal of Geochemical Exploration* 153, 53 – 65.

Bradham, W.S., Caruccio, F.T., 1997, "Sensitivity analysis of acid mine drainage prediction leaching tests", *America Society of Mining and Reclamation*, 410 – 423

Braga, A., Horst, M. and Traver, R., 2007, "Temperature Effects on the Infiltration Rate through an Infiltration Basin BMP", *Journal of Irrigation and Drainage Engineering*, 133 (6)

Brantley, S.L, 2008, "Kinetics of Mineral Dissolution", in S.L. Brantley, J.D. Kubicki and A.F. White (eds), *Kinetics of Water-Rock Interaction*, pp. 151 – 210, Springer, New York, https://link.springer.com/chapter/10.1007/978-0-387-73563-4_5

Chetty, D., Bazhko, O., Govender, V. and Ramatsoma, S., 2020, "The prediction of acid mine drainage potential using mineralogy", in E. FossoKankeu, C. Wolkersdorfer and J. Burgess (eds), *Recovery of byproducts from acid mine drainage treatment*, pp. 49 – 71, Scrivener Publishing LLC, Beverly

Coastech Research Inc., 2008, "A manual of chemical evaluation procedures for the prediction of acid generation from mine wastes", prepared for CANMET-MSL Division, Department of Energy, Mines and Resources, Canada, https://mend-nedem.org/wp-content/uploads/2013/01/1.16.1b.pdf

de Mello, J.W.V., Dias, L.E., Daniel, A.M., Abrahao, W.A.P., Deschamps, E. and Schaefer C.E.G.R., 2006, "Preliminary evaluation of acid mine drainage in minas gerais state, brazil" R. Bras. Ci. Solo, 30:365-375.

Deng, B. and Wand, J., 2017, "Saturated-unsaturated groundwater modeling using 3D Richards equation with a coordinate transform of nonorthogonal grids" *Applied Mathematical Modelling*,

Department of Water Affairs (DWA), 2010, *Mine* water management in the Witwatersrand Gold Fields with special emphasis on acid mine drainage. Report to the Inter-Ministerial Committee on Acid Mine Drainage, pp. 146, Pretoria: Department of Water Affairs. Available at: http://www.DWA.co.za.

Dold, B., 2014, "Evolution of Acid Mine Drainage Formation in Sulphidic Mine Tailings", *Minerals 2014*, 4, 621-641.

Dold, B., 2017, "Acid rock drainage prediction: A critical review", *Journal of Geochemical Exploration* 172, 120-132.

Edraki, M., Baumgartl, T., Manlapig, E. and Bradshaw, D., 2014, “Designing mine tailings for better environmental, social and economic outcomes: a review of alternative approaches”, *Journal of Cleaner Production* 84, 411-420.

Elghali, A., Benzaazoua, M., Taha, Y., Amar, H., Ait-kouia, Y., Bouzahzah, H. and Hakkou, R., 2023, “Prediction of acid mine drainage: Where we are” Earth-Science Reviews 241.

Erguler, G.K. and Erguler, Z.A., 2020, “The evaluation of acid mine drainage by kinetic procedures and empirical models for field scale behavior” *Arabian Journal of Geosciences*, 13, https://doi.org/10.1007/s12517-020-05372-0

Erguler, G., Erguler, Z.A., Akcakoca, H. and Ucar, A., 2014, “The effect of column dimensions and particle size on the results of kinetic column test used for acid mine drainage (AMD) prediction”. *Minerals Engineering*, 55, 18–29

Farthing, M.W. and Ogden, F.L., 2017, “Numerical Solution of Richards' Equation: A Review of Advances and Challenges” *Soil Science Society of America Journal*, 81(6), 1257-1269. https://doi.org/10.2136/sssaj2017.02.0058

Fernandes, H.M., Franklin, M.R., 2001, “Assessment of acid rock drainage pollutants release in the uranium mining site of Poços de Caldas — Brazil”, *Journal of Environmental Radioactivity* 54, 5-25.

Fusi, L., Monti, A. and Primicerio, M., 2012, “Determining calcium carbonate neutralization kinetics from experimental laboratory data” *Journal of Mathematical Chemistry* 50(9)

Fusi, L., Primicerio, M., and Monti, A. 2015, “A model for calcium carbonate neutralization in the presence of armoring” Applied Mathematical Modelling, 39 (1), 348-362

García, C., Ballester, A., González, F. and Blázquez, M.L., 2005, “Pyrite behaviour in a tailings pond”, *Hydrometallurgy*, 76, 25–36

GARD (Global Acid Rock Drainage) Guide, 2012, “INAP: The International Network for Acid Prevention: Chapter 5 (5.4.12 Laboratory Kinetic Tests)”, viewed 15 May 2020, http://www.gardguide.com/index.php?title=Chapter_5b#5.4.12_Laboratory_Kinetic_Tests

Garland, R., 2011, “Acid mine drainage – the chemistry” Quest 7(2)

Geochemic, 2022, “Humidity Cell Testing”, viewed 15 June 2021, http://www.geochemic.co.uk/humidity-cell-testing_2.html

Guseva, O.; Opitz, A. K. B.; Broadhurst, J.L.; Harrison, S.T. L.; Bradshaw, D.J.; Becker, M., 2018, “Fe-Sulfide Liberation and Association as a Proxy for the Interpretation of Acid Rock Drainage (ARD) Test Results”. In: Ch. Wolkersdorfer, L. Sartz, A. Weber, J. Burgess & and G. Tremblay (eds), *Mine Water*, 11th ICARD, IMWA, MWD Conference – “Risk to Opportunity”, 345 – 351, viewed on 20 June 2020, https://www.imwa.info/docs/imwa_2018/IMWA2018_Guseva_345.pdf

Herrera, P., Uchiyama, H., Igarashi, T., Asakura, K., Ochi, Y., Iyatomi, N. and Nagae, S., 2007, “Treatment of acid mine drainage through a ferrite formation process in central Hokkaido, Japan: Evaluation of dissolved silica and aluminium interference in ferrite formation” *Minerals Engineering*, 20(13), 1255-1260

Karlsson, T., Alakangas, L., Kauppila, P. and Räisänen, M.L., 2021, “Test of Two Methods for Waste Rock Drainage Quality Prediction: Aqua Regia Extraction and Single-addition Net-acid Generation Test Leachate Analysis”. *Mine Water Environ* 40, 736–751 2021.

Khorasanipour, M., 2015, “Environmental mineralogy of Cu-porphyry mine tailings, a case study of semiarid climate conditions, Sarcheshmeh mine, SE Iran.” *Journal of Geochemical Exploration* 153, 40–52.

Kollias, K., Godelitsas , A., Astilleros , J.M., Ladas, S., Lagoyannis , A. and Mavromoustakos, T., 2021, “ Dissolution and sorption mechanisms at the aluminosilicate and carbonate mineral-AMD (Acid Mine Drainage) interface” *Applied Geochemistry* 131, 105027.

Kreger, 2004, “Acid Mine Drainage: Chemistry” Exploring the Environment Water Quality, viewed August 2022, http://www.cotf.edu/ete/modules/waterq/wqchemistry.html

Leiva, E., Cayazzo, M., Dávila, L., Torres, M. and Ledezma, C., 2021, “Acid Mine Drainage Dynamics from a Paste Tailing Deposit: Effect of Sulfate Content on the Consistency and Chemical Stability after Storage” Metals, 11, https://doi.org/10.3390/met11060860

Li, X., Li, X., Wu, Y., Wu, L., and Yue, Z., 2022, “Selection criteria of mesh size and time step in FEM analysis of highly nonlinear unsaturated seepage process” Computers and Geotechnics 146

Malmström, M., Banwart, S., Duro, L., Wersin, P. and Bruno, J., 1995, Biotite and chlorite weathering at 25 °C, Swedish Nuclear Fuel and Waste Management Technical Report 95-01.

Mauren, B.C., Kharisma, N.I, and Harto, A.W., 2020, "Determination of reaction rate constant for increasing pH level in geothermal hot spring", *Earth and Environmental Science* 451. doi:10.1088/1755-1315/451/1/012088

Ma, L., Huang, C., Liu, Z., Morin, K.A., Aziz, M. and Meints, C., 2019, "Prediction of acid rock drainage in waste rock piles Part 1: water film model for geochemical reactions and application to a full-scale case study", *Journal of Contaminant Hydrology*, 220, 98-107.

Madakkaruppan, V., Pius, A., Sreenivas, T., and Sunilkumar, T.S, 2019, "Behaviour of Si, Al, Fe and Mg during oxidative sulfuric acid leaching of low grade uranium ore: A kinetic approach", *Journal of Environmental Chemical Engineering*, 7 (3), 103139.

Mine Environment Neutral Drainage (MEND), 2009, Prediction Manual for Drainage Chemistry from Sulphidic Geologic Materials, MEND program (Canada), MEND Report 1.20.1

Micron Technology, inc. 2022, "Crucial: How Much RAM Do You Need For Your Computer Memory?", viewed 07 January 2022, https://www.crucial.com/articles/about-memory/how-much-ram-does-my-computer need#:~:text=How%20much%20RAM%20do%20you%20need%3F,use%20this%20as%20a%20guideline.

Moorberg, C.J. and Crouse, D.A., 2017, "Soils Laboratory Manual" viewed 01 March 2022, https://kstatelibraries.pressbooks.pub/soilslabmanual/chapter/soil-texture-and-structure/

Moreno-Maroto, J.M. and Alonso-Azcárate, J., 2022, "Evaluation of the USDA soil texture triangle through Atterberg limits and an alternative classification system". *Applied Clay Science*, 229.

Morin, K. A. and Hutt, N. M., 1997, *Environmental Geochemistry of Minesite Drainage: Practical Theory and Case Studies*, MDAG Publishing, Vancouver, British Columbia, Canada, ISBN 0-9682039-1-4

Nancucheo, I., Bitencourt, J.A.P., Sahoo, P.K., Alves, J.O., Siqueira, J.O., and Oliveira, G., 2017, "Recent Developments for Remediating Acidic Mine Waters Using Sulfidogenic Bacteria", Bioremediation: An Overview on Current Practices, Advances, and New Perspectives in Environmental Pollution Treatment, viewed 20 August 2020, https://www.hindawi.com/journals/bmri/2017/7256582/

Nicholson, R. V., Rinker, M. J., Acott, G. and Venhuis, M. A., 2003, "Integration of field data and a geochemical transport model to assess mitigation strategies for an acid-generating mine rock pile at a uranium mine". *In: Proc. of the Sudbury 2003: Mining and the Environment*, Canada.

Özçelik, G.A.S. 2007, "Prediction techniques of acid mine drainage: a case study of a new poly-metallic mine development in erzincan-iliç, Turkey", PhD Thesis, Middle East Technical University, Ankara

Parbhakar-Fox, A., Lottermoser, B. and Bradshaw, D., 2013, "Evaluating waste rock mineralogy and microtexture during kinetic testing for improved acid rock drainage prediction", *Minerals Engineering* 52, 111 – 124

Sánchez-Andrea, I., Sanza, J., Bijmans, J. M. F. M., Stams, A. J. M., Hazard, J., 2014, "Sulfate reduction at low pH to remediate acid mine drainage". *Journal of Hazardous Materials 269, 30, 98-109*

Sangita, K., Udayabhanu, G. and Prasad, B., 2010, "Studies on environmental impact of acid mine drainage generation and its treatment: an appraisal." *Indian Journal of Environmental Protection*, 30 (11). pp. 953-967. ISSN 0253-7141

Sapsford, D.J. Bowell, R.J., Dey, M. and Williams, K.P., 2009, "Humidity cell tests for the prediction of acid rock drainage", *Minerals Engineering* 22(1), 25 – 36

Sibarani, L. and Damayanti R. 2006, "Prediction of mine drainage quality by kinetic tests" *Indonesian Mining Journal* 9(6)

Simate, G. S. and Ndlovu, S., 2014, "Acid mine drainage: Challenges and opportunities". *Journal of Environmental Chemical Engineering* 2, 1785–1803.

Softusvista, 2022, "Volume of Solids given Porosity Calculator", viewed 22 March 2022, https://www.calculatoratoz.com/en/volume-of-solids-given-poroseny-calculator/Calc-7939

South African Auditor General, 2009, Report of the Auditor-General to Parliament on a performance audit of the rehabilitation of abandoned mines at the Department of Minerals and Energy", viewed 12 June 2019, https://cer.org.za/wp-content/uploads/2011/10/AG_Report_on_abandoned_mines-Oct-2009.pdf

Therriault, S., Diedrich, T. and Day S., 2015, "Evaluation of humidity cell test precision from an Ongoing geochemical characterisation program" Internal Conference on Acid Rock Drainage & IMWA Annual Conference, 21-24 April 2015, Santiago, Chile.

United States Department of Agriculture (US DA), 2008, Natural resources conservation services: Soil quality indicators, viewed 20 July 2024, https://www.nrcs.usda.gov/sites/default/files/2022-10/nrcs142p2_051590.pdf

United States Environmental Protection Agency (US EPA), 1994, Acid mine drainage prediction, Technical document: EPA 530-R-94-036, NTIS PB94-201829, viewed 23 May 2020, https://www.epa.gov/sites/default/files/2015-09/documents/amd.pdf

United States Environmental Protection Agency, 2011, Method 1627: Kinetic Test Method for the Prediction of Mine Drainage Quality, EPA-821-R-09-002

Palandri, J.L. and Kharaka, Y.K., 2004, A compilation of rate parameters of water-mineral interaction kinetics for application to geochemical modeling, United States Geological Survey Open File Report 2004-1068

Wang, Z., Xu, Y., Zhang, Z., and Zhang, Y., 2020, "Review: Acid Mine Drainage (AMD) in Abandoned Coal Mines of Shanxi, China" Water 2021, 13, 8, https://dx.doi.org/10.3390/w13010008

Wang, J., 2022, "Chemical weathering mechanism of Albite-rich rocks in Grottoes under an acidic environment: An atomistic view from ReaxFF simulation". *Computational Materials Science*, 211, 111498

Weber, P.A., Hughes, J.B., Conner, L.B., Lindsay, P., and Smart, R.C, 2006, "Short-term acid rock drainage characteristics determined by paste pH and kinetic nag testing: cypress prospect, new Zealand" Paper presented at the 7th International Conference on Acid Rock Drainage (ICARD), March 26-30, St. Louis MO

Weatherspark, n.d,, "Climate and average weather year round in Ndola Zambia", viewed July 2024, https://weatherspark.com/y/95296/Average-Weather-in-Ndola-Zambia-Year-Round#Figures-WindSpeed

Yeheyis, M. B., Shang, J. Q., & Yanful, E. K., 2009, "Long-term evaluation of coal fly ash and mine tailings co-placement: a site-specific study". *Journal of Environmental Management*, 91, 237–244

APPENDICES

APPENDIX A. MAIN HARDWARE COMPONENTS OF THE CUSTOMISED HUMIDITY CELL

The main hardware components of the customized humidity cell without the instruments, tubing, and valves are given in Table A. 1 below.

Table A. 1: Components of the Customised Humidity Cell without the tubing, valves, and instruments

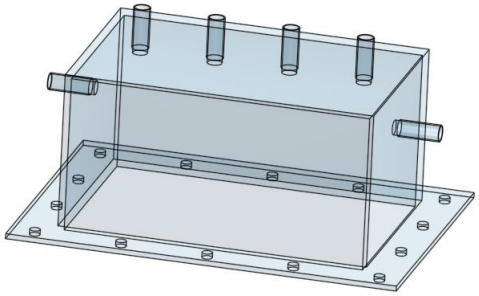 A. Top compartment
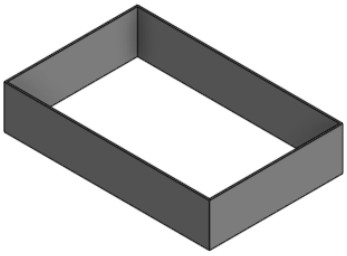 B. Sample Positioner – placed inside the Top compartments(i.e. component A) and on the perforated plate (Component C)

Table A. 1 Continues

A. Perforated plate – Material holder. A filter cloth is placed on top of it. It is mounted between the top and bottom compartment (component D)

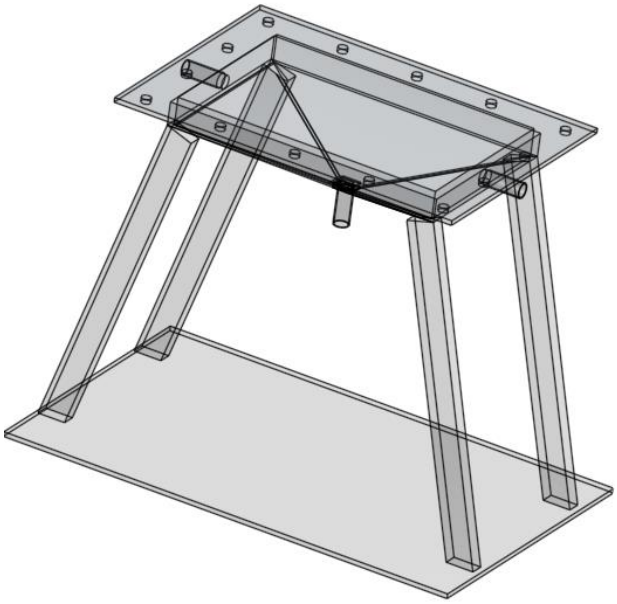

B. Bottom compartment

APPENDIX B. CUSTOMISED HUMIDITY CELL INSTRUMENTS AND CONTROL SYSTEM

Table B. 1 below shows a list of the main sensors and actuators used for the Customized Humidity Cell.

Table B. 1: Customized Humidity Cell main sensors and actuator

Sensors and Actuators used for the Customized Humidity Cell	
Temperature Sensor RS PRO Infrared Temperature Sensor, 0°C to +1000°C. RS stock no.:161-8103; Manufacturer: RS PRO	
Humidity Sensor TE Connectivity Temperature & Humidity Sensor, RS stock no.:893-7373; Mfr. Part No.:HPP809A031 Manufacturer: TE Connectivity	
Pressure sensor Teren PT2321 https://robertec.net/products/pressure-sensor	
Heating Element 200 W, 100 → 240 V ac/dc RS stock no.:No.: HPG-2/22-75X35-100-240 Manufacturer: DBK Enclosures https://za.rs-online.com/web/p/heating-elements/7256528	

Table B. 1 continues

Sensors and Actuators used for the Customized Humidity Cell	
Water Pump, Flow: 2.4 Litres/min. Power: 12VDC, Current draw: 2.1A Dimensions: 150 x 100 x 64mm https://www.makro.co.za/home-garden/lawn-garden/water-storage/water-storage/solar-12-volt-pump---self-priming-water-pump---16-3l-min---max-height-of-24-metres/p/ca53e5d0-a9dc-4425-b3bf-31cb5a0720b6?gad_source=4&gclid=EAIaIQobChMI-qi31rTThAMVfZZQBh1KYgMWEAQYESABEgKqc_D_BwE	

The Mintek StarCS (process control system) custom setup done and used for controlling the AHC is shown in Figure B. 1 and Figure B. 2. For temperature control, the setup was such that the control system was calculating the time that the heater needed to be ON to achieve the desired temperature setpoint which was 40 °C in this study. The PID tuning parameters used are shown in Figure B. 2.

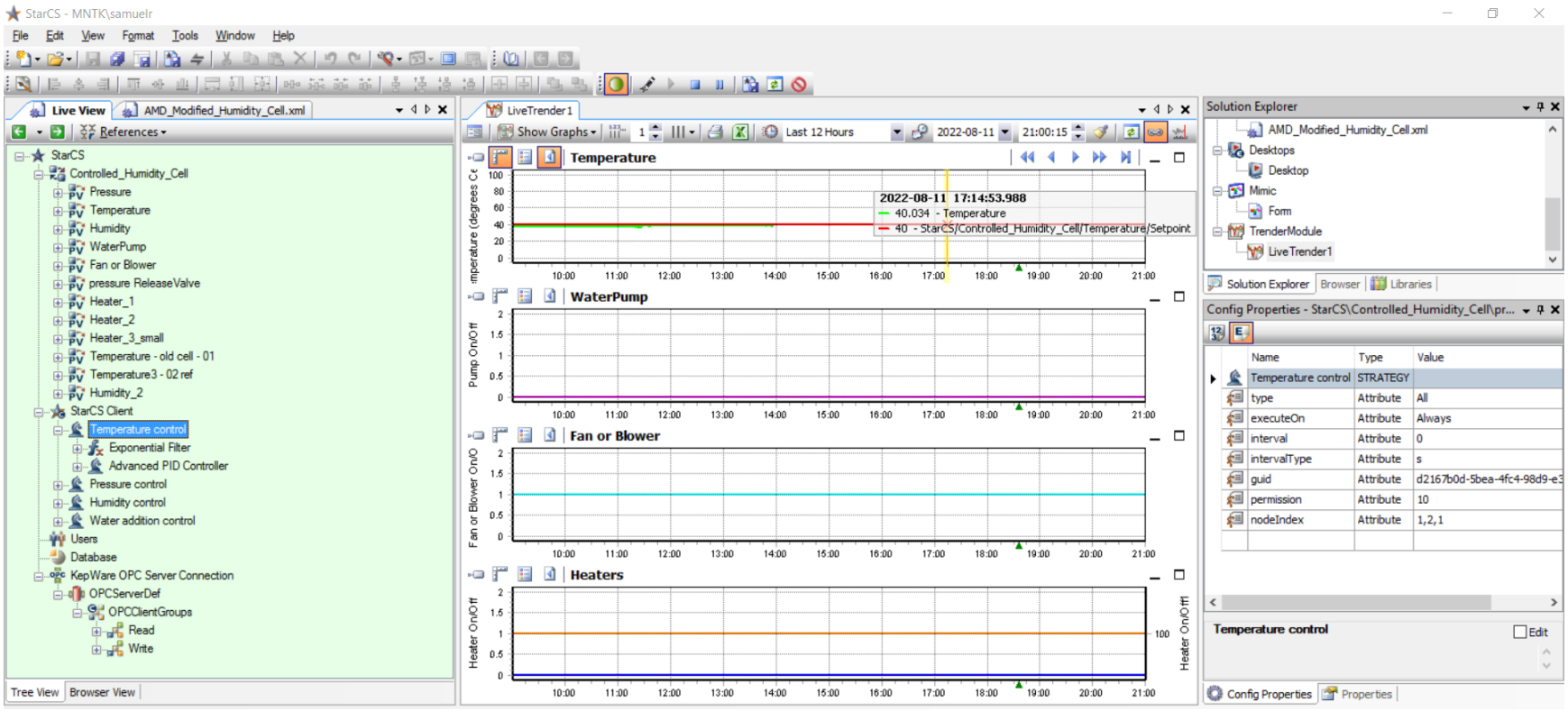

Figure B. 1: Mintek StarCS control system setup used to control the AHC operating conditions

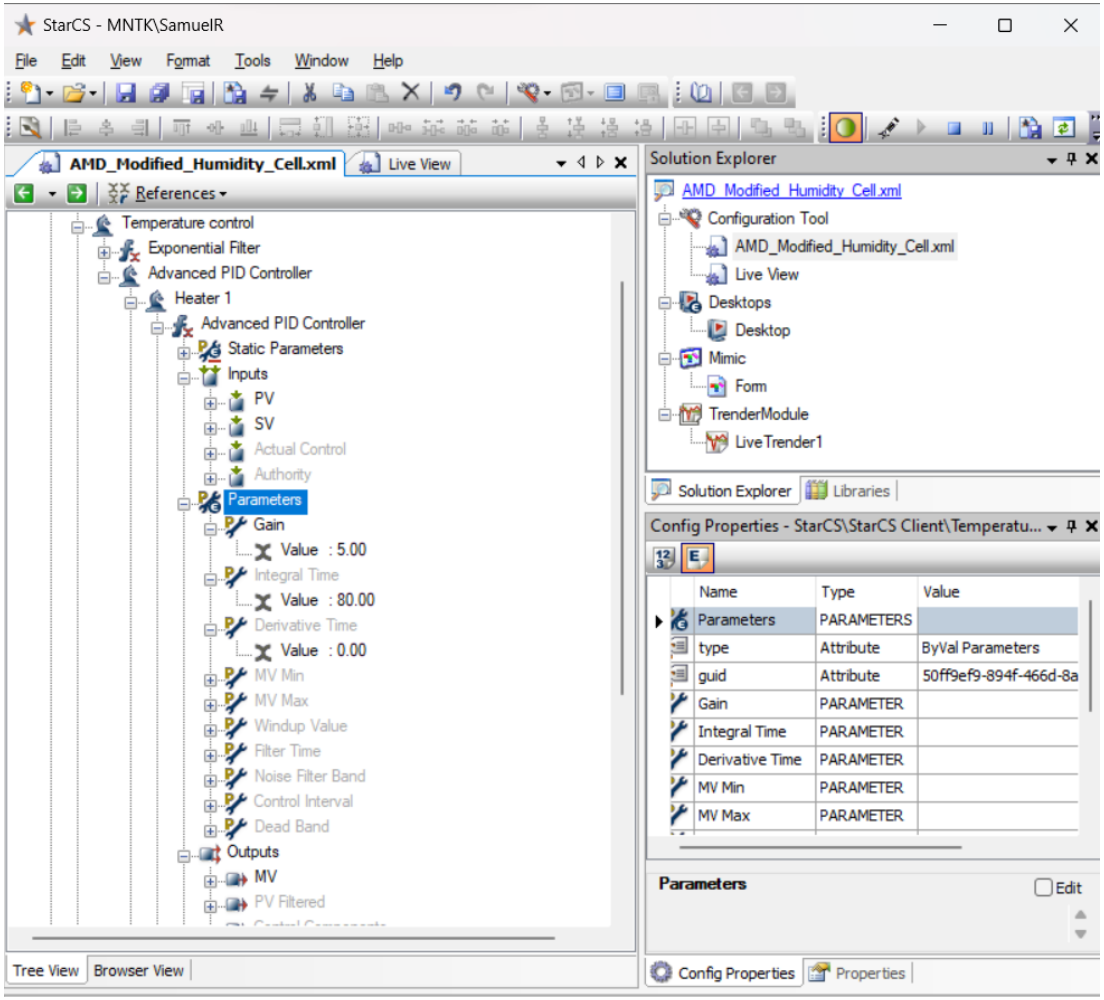

Figure B. 2: Mintek StarCS setup done for AHC temperature control – PID tuning parameters used

APPENDIX C. PARTICLES SIZE DISTRIBUTION DATA OF THE ORE USED

The head ore particle size distributions for both ore types 1 and 2 are given in Table C. 1 and Table C. 2 respectively. The average particle size (D50) was approximately 32 µm and 53 µm for ore type 1 and type 2 respectively.

Table C. 1: Ore Type 1 head sample particle size distribution

Sieve (µm)	Mass (g)	Mass (%)
+300	0	0
+212	6.60	2.17
-212+150	25.10	8.25
-150+106	35.30	11.60
-106+75	32.80	10.78
-75+53	25.50	8.38
-53+38	15.20	5.00
-38+25	26.40	8.68
-25	137.40	45.15
Total	304.30	100

Table C. 2: Ore Type 2 head sample particle size distribution

Sieve size(µm)	mass (g)	mass %
+300	0.00	0.00
+212	90.84	16.27
+150	78.31	14.02
+106	62.99	11.28
+75	48.30	8.65
+53	43.11	7.72
+38	32.12	5.75
-38	202.82	36.32
Total	558.49	100.00

APPENDIX D. MINERALOGICAL DATA OF THE ORE USED

The head ore sample mineralogy for both ore types 1 and 2 are given in Table D. 1 and Table D. 1respectively.

Table D. 1: Ore Type 1 head sample mineralogy

Mineral	**Mass%**
Quartz	33.33
Albite	15.79
Muscovite	14.77
Plagioclase (Ca)	13.02
Biotite	7.42
Orthoclase	4.22
Pyrrhotite	2.89
Chalcopyrite	1.65
Montmorillonite	1.65
Hematite	1.51
Calcite	1.02
Magnetite	0.84
Goethite	0.70
Kaolinite	0.40
Rutile	0.28
Pyrite	0.16
Chlorite	0.16
Sphalerite	0.05
Hornblende	0.04
Covellite	0.03
Dolomite	0.02
Ilmenite	0.01
Galena	0.01
Zircon	0.01
Bornite	0.01
Chalcocite	0.01
Cuprite	0.01
Total	100

Table D. 2: Ore Type 2 head sample mineralogy

Mineral	Mass%
Chalcopyrite	0.49
Bornite	4.07
Chalcocite	0.28
Covellite	0.04
Native_Copper	0.01
Pyrite	0.01
Pyrrhotite	0.03
Galena	0.03
Quartz	27.90
Orthoclase	7.01
Plagioclase	4.57
Hornblende	1.22
Chlorite	0.10
Kaolinite	0.02
Biotite	16.07
Calcite	37.40
Dolomite	0.06
Magnetite	0.16
Goethite	0.24
Hematite	0.03
Zircon	0.05
Rutile	0.20
Monazite-(Ce)	0.01
Total	100.0

APPENDIX E. ORE BED COMPARISON AFTER EXPERIMENTAL TESTS

Figure E. 1 shows the ore bed image comparison between the AHC and HC test for ore type 2 after the 11-week test duration. As expected, the AHC ore bed after the test is drier compared to the HC ore bed because the AHC ore bed was exposed to higher temperatures.

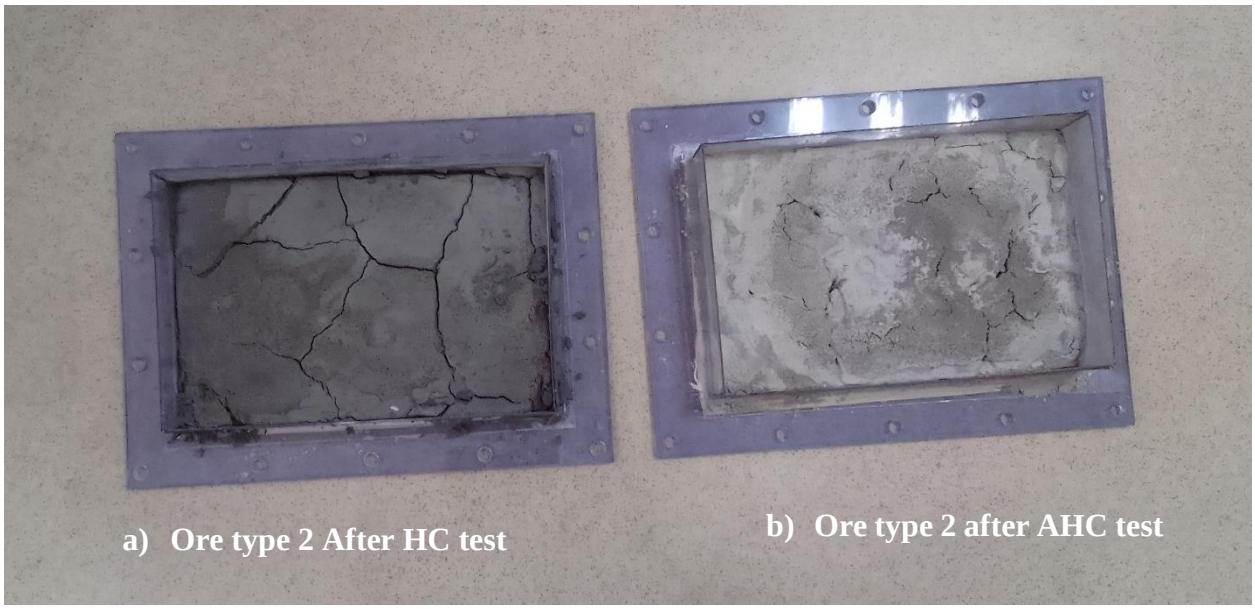

Figure E. 1: Actual ore comparison between AHC and HC after the 11 weeks of tests

APPENDIX F. DEVELOPED SOFTWARE INTERFACE AND INPUTS

The interface of the developed software is shown in Figure F. 1. It is called Mine Dumps Acid Estimator (MiDAE) – trademark registration is in process. Most of the software components e.g. interface, inputs processing, mine dump shape and particle position reconstruction, and matrix operations were developed using Matlab. It can be installed as a standalone application on Windows operating systems 10 and 11. An example of the input Excel file or parameters is shown in Figure F. 2 below. Additional input options can be accessed after clicking the "Advanced" button on the software interface page shown in Figure F. 1. A brief user manual can also be accessed using or after clicking the "Help" button on the interface page.

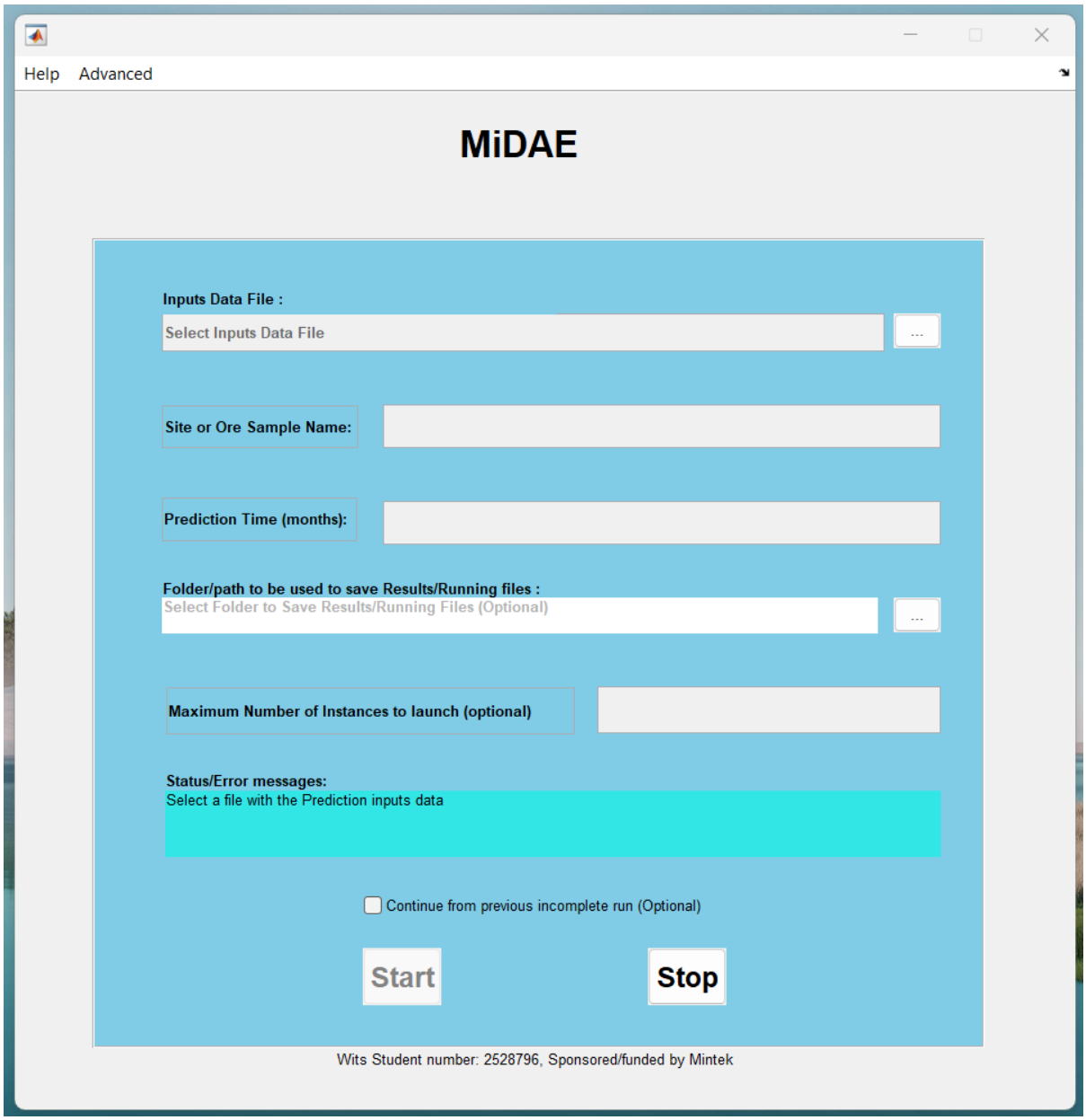

Figure F. 1: Developed software interface

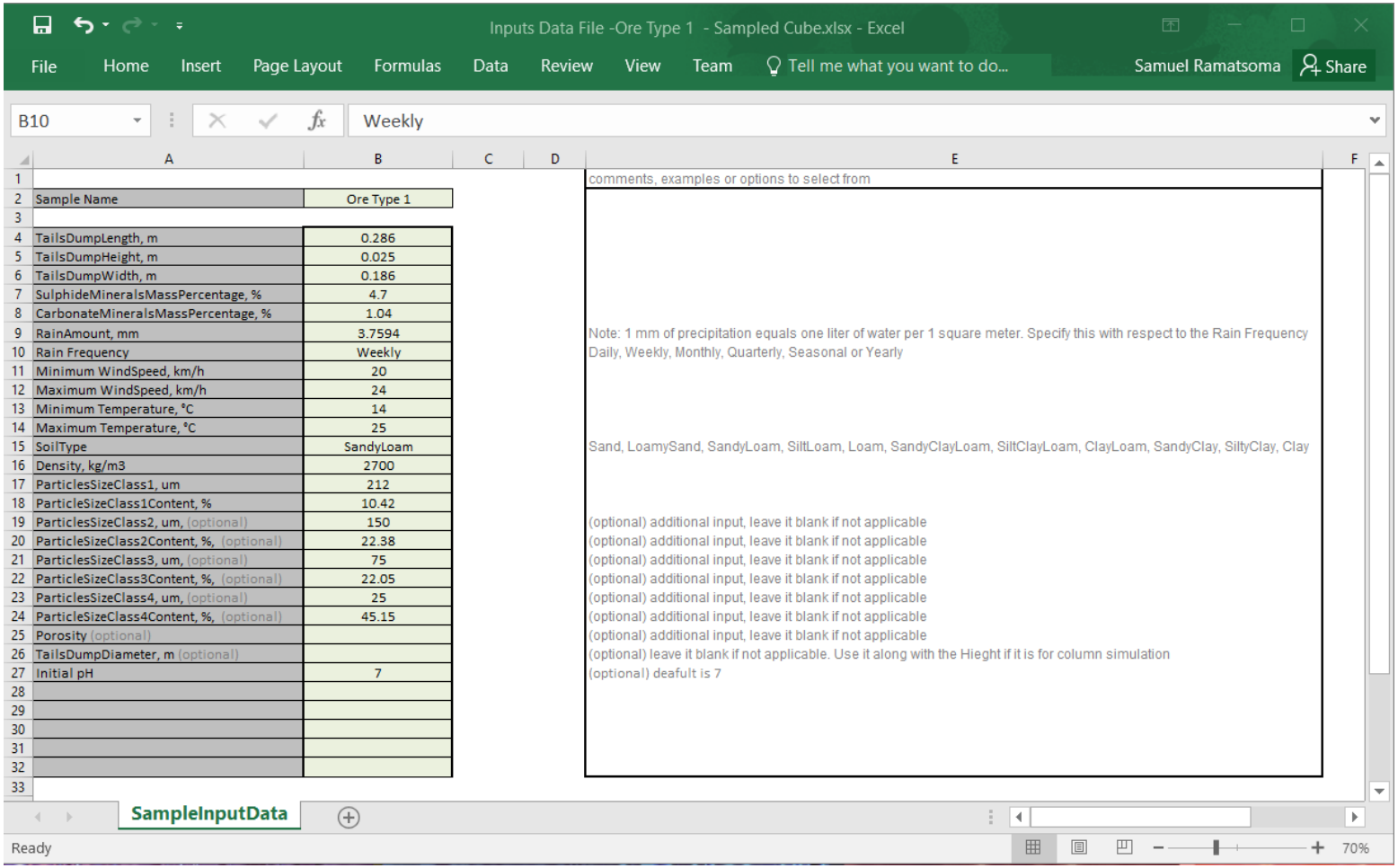

	A	B
2	Sample Name	Ore Type 1
4	TailsDumpLength, m	0.286
5	TailsDumpHeight, m	0.025
6	TailsDumpWidth, m	0.186
7	SulphideMineralsMassPercentage, %	4.7
8	CarbonateMineralsMassPercentage, %	1.04
9	RainAmount, mm	3.7594
10	Rain Frequency	Weekly
11	Minimum WindSpeed, km/h	20
12	Maximum WindSpeed, km/h	24
13	Minimum Temperature, °C	14
14	Maximum Temperature, °C	25
15	SoilType	SandyLoam
16	Density, kg/m3	2700
17	ParticlesSizeClass1, um	212
18	ParticleSizeClass1Content, %	10.42
19	ParticlesSizeClass2, um, (optional)	150
20	ParticleSizeClass2Content, %, (optional)	22.38
21	ParticlesSizeClass3, um, (optional)	75
22	ParticleSizeClass3Content, %, (optional)	22.05
23	ParticlesSizeClass4, um, (optional)	25
24	ParticleSizeClass4Content, %, (optional)	45.15
25	Porosity (optional)	
26	TailsDumpDiameter, m (optional)	
27	Initial pH	7

Figure F. 2: MiDAE software input Excel file example – Sample Input Data

Table F. 1: Multiple particle sizes simulation inputs

Parameters	**Experiments simulated**			
Sample Name	Ore Type 1 AHC	Ore Type 1 HC	Ore Type 2 AHC	Ore Type 2 HC
TailsDumpLength, m	0.286	0.286	0.286	0.286
TailsDumpHeight, m	0.025	0.025	0.025	0.025
TailsDumpWidth, m	0.186	0.186	0.186	0.186
SulphideMineralsMassPercentage, %	4.7	4.7	0.53	0.53
CarbonateMineralsMassPercentage, %	1.04	1.04	37.4	37.4
RainAmount, mm	3.759	3.759	3.759	3.759
Rain Frequency	Weekly	Weekly	Weekly	Weekly
Minimum WindSpeed, km/h	10.8	10.8	10.8	10.8
Maximum WindSpeed, km/h	10.8	10.8	10.8	10.8
Minimum Temperature, °C	40	14	40	14
Maximum Temperature, °C	40	25	40	25
SoilType	SandyLoam	SandyLoam	SandyLoam	SandyLoam
Density, kg/m3	2710	2710	2638	2638
ParticlesSizeClass1, um	212	212	212	212
ParticleSizeClass1Content, %	10.42	10.42	16.27	16.27
ParticlesSizeClass2, um, (optional)	150	150	150	150
ParticleSizeClass2Content, %, (optional)	22.38	22.38	25.3	25.3
ParticlesSizeClass3, um, (optional)	75	75	75	75
ParticleSizeClass3Content, %, (optional)	22.05	22.05	22.11	22.11
ParticlesSizeClass4, um, (optional)	25	25	38	38
ParticleSizeClass4Content, %, (optional)	45.15	45.15	36.32	36.32
Porosity (optional)				
TailsDumpDiameter, m (optional)				
InitialpH (optional)	7	7	7	7

Table F. 2: Single particle size (D50) simulation inputs

Parameters	**Experiments simulated**			
Sample Name	Ore Type 1 AHC	Ore Type 1 HC	Ore Type 2 AHC	Ore Type 2 HC
TailsDumpLength, m	0.286	0.286	0.286	0.286
TailsDumpHeight, m	0.025	0.025	0.025	0.025
TailsDumpWidth, m	0.186	0.186	0.186	0.186
SulphideMineralsMassPercentage, %	4.7	4.7	0.53	0.53
CarbonateMineralsMassPercentage, %	1.04	1.04	37.4	37.4
RainAmount, mm	3.759	3.759	3.759	3.759
Rain Frequency	Weekly	Weekly	Weekly	Weekly
Minimum WindSpeed, km/h	10.8	10.8	10.8	10.8
Maximum WindSpeed, km/h	10.8	10.8	10.8	10.8
Minimum Temperature, °C	40	14	40	14
Maximum Temperature, °C	40	25	40	25
SoilType	SandyLoam	SandyLoam	SandyLoam	SandyLoam
Density, kg/m3	2710	2710	2638	2638
ParticlesSizeClass1, um	32	32	53	53
ParticleSizeClass1Content, %	100	100	100	100
ParticlesSizeClass2, um, (optional)				
ParticleSizeClass2Content, %, (optional)				
ParticlesSizeClass3, um, (optional)				
ParticleSizeClass3Content, %, (optional)				
ParticlesSizeClass4, um, (optional)				
ParticleSizeClass4Content, %, (optional)				
Porosity (optional)				
TailsDumpDiameter, m (optional)				
InitialpH (optional)	7	7	7	7

Table F. 3: Multiple particle sizes simulation inputs with silicate minerals

Parameters	**Experiments simulated**			
Sample Name	Ore Type 1 AHC	Ore Type 1 HC	Ore Type 2 AHC	Ore Type 2 HC
TailsDumpLength, m	0.286	0.286	0.286	0.286
TailsDumpHeight, m	0.025	0.025	0.025	0.025
TailsDumpWidth, m	0.186	0.186	0.186	0.186
SulphideMineralsMassPercentage, %	4.7	4.7	0.53	0.53
CarbonateMineralsMassPercentage, %	1.04	1.04	37.4	37.4
SilicateMineralsMassPercentage, %	38.14	38.14	16.17	16.17
RainAmount, mm	3.759	3.759	3.759	3.759
Rain Frequency	Weekly	Weekly	Weekly	Weekly
Minimum WindSpeed, km/h	10.8	10.8	10.8	10.8
Maximum WindSpeed, km/h	10.8	10.8	10.8	10.8
Minimum Temperature, °C	40	14	40	14
Maximum Temperature, °C	40	25	40	25
SoilType	SandyLoam	SandyLoam	SandyLoam	SandyLoam
Density, kg/m3	2710	2710	2638	2638
ParticlesSizeClass1, um	212	212	212	212
ParticleSizeClass1Content, %	10.42	10.42	16.27	16.27
ParticlesSizeClass2, um, (optional)	150	150	150	150
ParticleSizeClass2Content, %, (optional)	22.38	22.38	25.3	25.3
ParticlesSizeClass3, um, (optional)	75	75	75	75
ParticleSizeClass3Content, %, (optional)	22.05	22.05	22.11	22.11
ParticlesSizeClass4, um, (optional)	25	25	38	38
ParticleSizeClass4Content, %, (optional)	45.15	45.15	36.32	36.32
Porosity (optional)				
InitialpH (optional)	7	7	7	7

APPENDIX G. DEVELOPED SOFTWARE SOURCE CODE

Screenshots of the developed MiDAE software files (source code) are shown in Figure G. 1 to Figure G. 12. The link or interaction between the files is shown in Section 3.2.4, Figure 3.7. Note that the Matlab split document view vertically (top/bottom) was selected so that key lines of the code could be shown in the figures below. The files are summarized as follows:

- ***MainGUI.m*** – source code file created for creating and/or launching the main graphical user interface (Figure G. 1)
- ***ReadInputsFromExcel.m*** – source code file created to read in data from the Inputs Excel file (Figure G. 2)
- ***Predictions.m*** – source code file created for scheduling fluid flow and particle-chemical reaction processes, and to simulate the changes in temperature and airflow (Figure G. 3)
- ***ParticlesCounter.m*** – source code file created for material ore bed reconstruction (Figure G. 4)
- ***FillEmptyArrayWithParticles.m*** – source code file created for material particle placement (Figure G. 5)
- ***ComputerAllowMaxArrayAndMatrixRCsize.m*** – source code file created to ensure that MiDAE software does not try to create arrays or matrices that exceed the maximum possible size for the computer it is running on (Figure G. 6)
- ***FluidFlowWithPCMemoryAndInstancesMex.m*** – source code file created to interact with the Mex file which is created from the C++ file for bulk flow, components mass balance, and chemical reactions (Figure G. 7)
- ***DiffEqnsSolver.m*** – source code file created for solving particles' chemical reactions differential equations (Figure G. 8)
- ***MexFunctionFlow.cpp*** – source code file created for generating the ***MEXFunctionFlow.mexw64*** which is used by *FluidFlowWithPCMemoryAndInstancesMex.m* for solving the 3D fluid flow model and for chemical compounds mass balance (Figure G. 9)
- ***SQLiteDBRunningOrResults.m*** – source code file created for saving results data to the database (Figure G. 10)
- ***SQLiteDBSimProgress.m*** – source code file created for saving simulation progress data to the database (Figure G. 11)
- ***SQLiteDBSimProgressAdd.m*** – source code file created for saving Instances ID and rain/top surface water simulation progress data to the database (Figure G. 12)

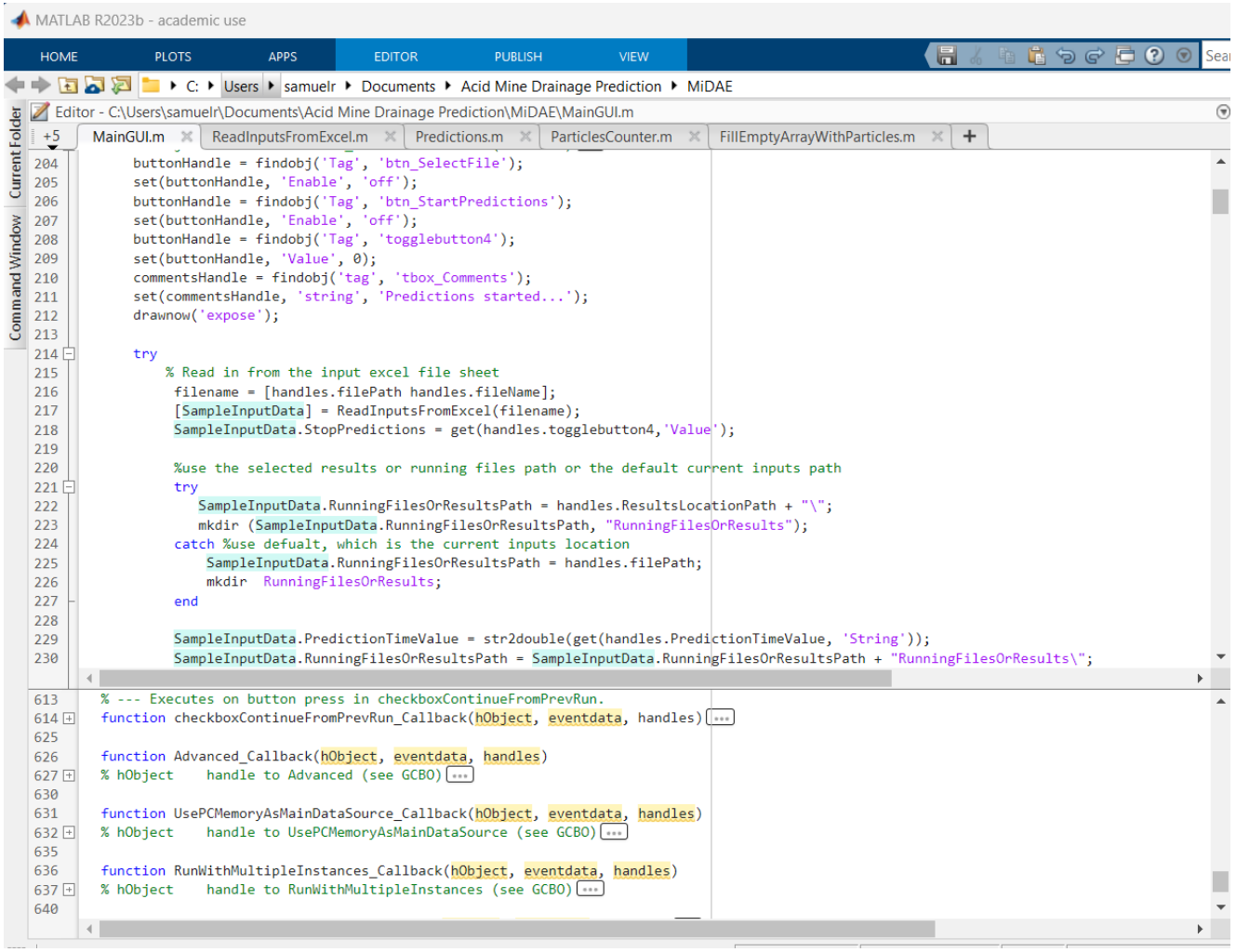

Figure G. 1: Matlab code file created for the main graphical user interface - MainGUI.m

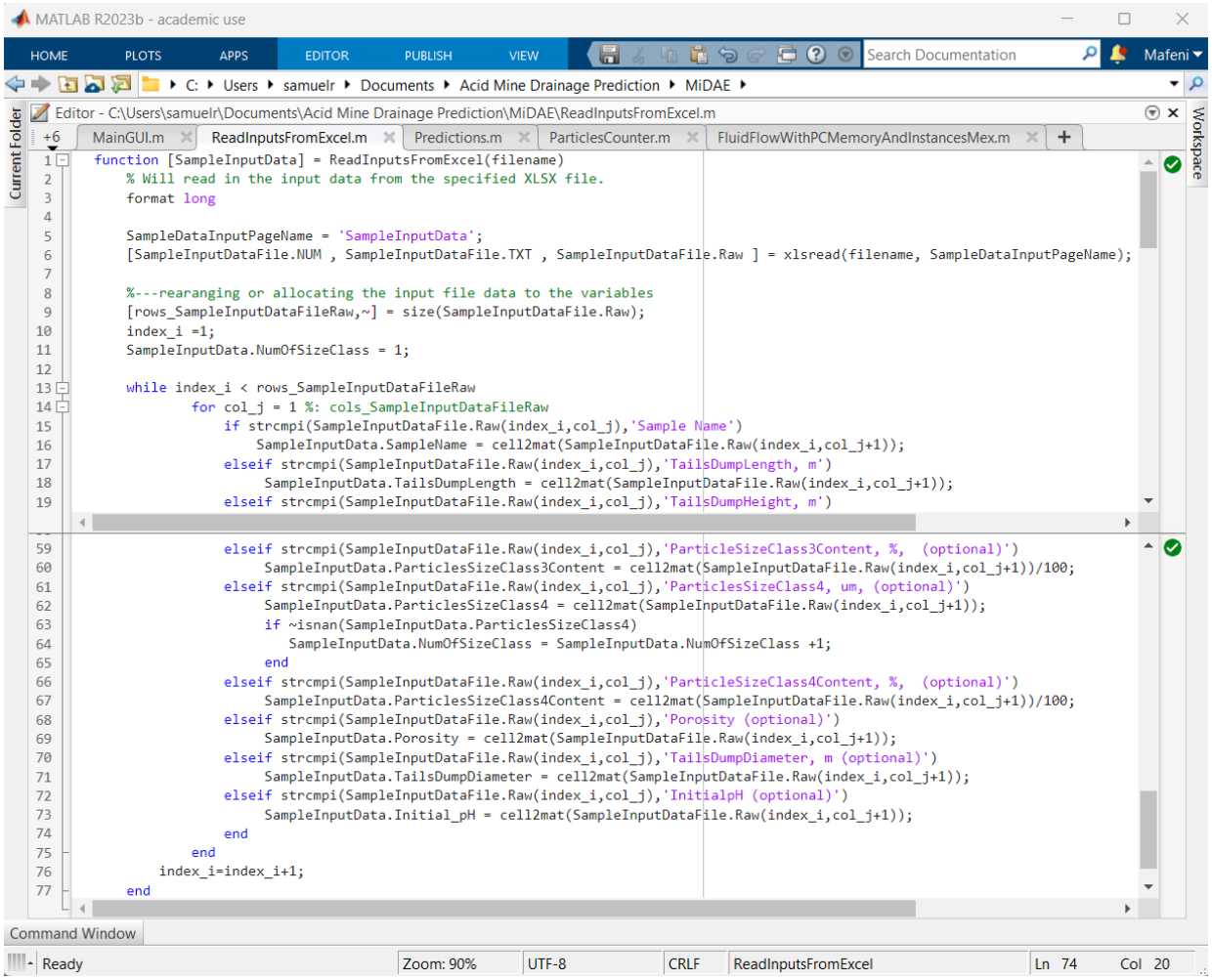

Figure G. 2: Matlab code file created to read in data from the Inputs Excel file – ReadInputsFromExcel.m

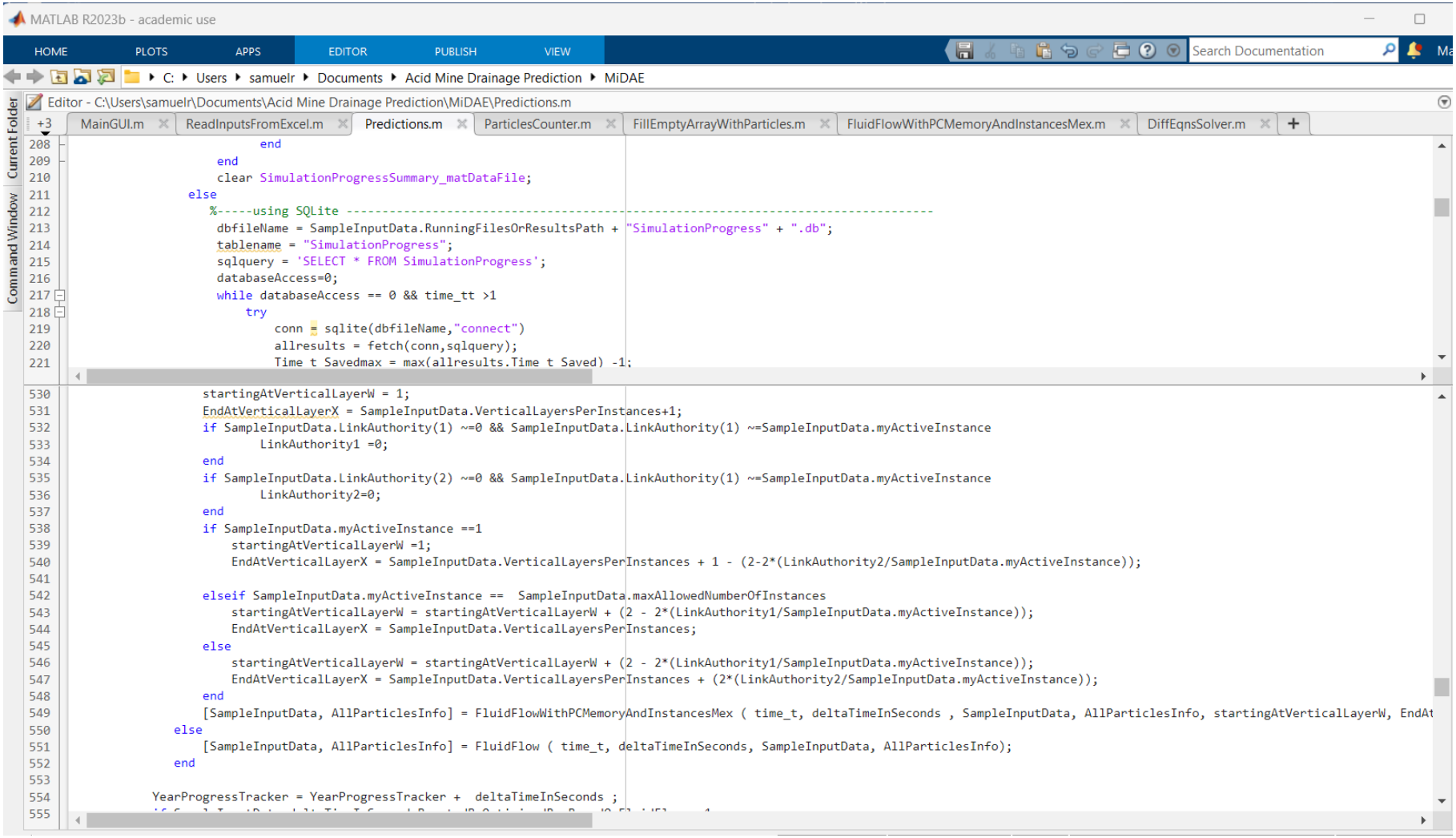

Figure G. 3: Matlab code file created for scheduling processes and to simulate environmental conditions – Predictions.m

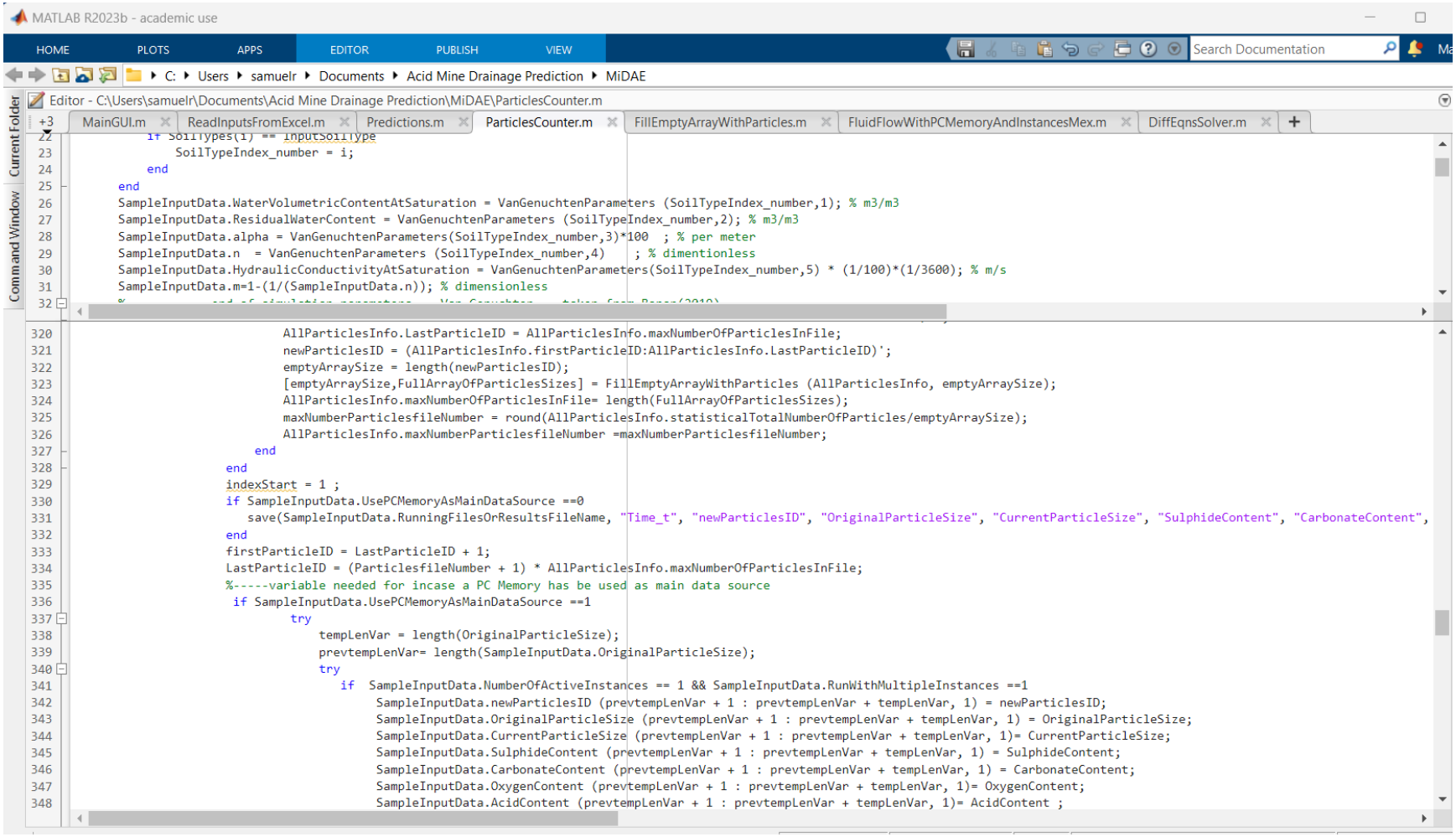

Figure G. 4: Matlab code file created for material ore bed reconstruction –ParticlesCounter.m

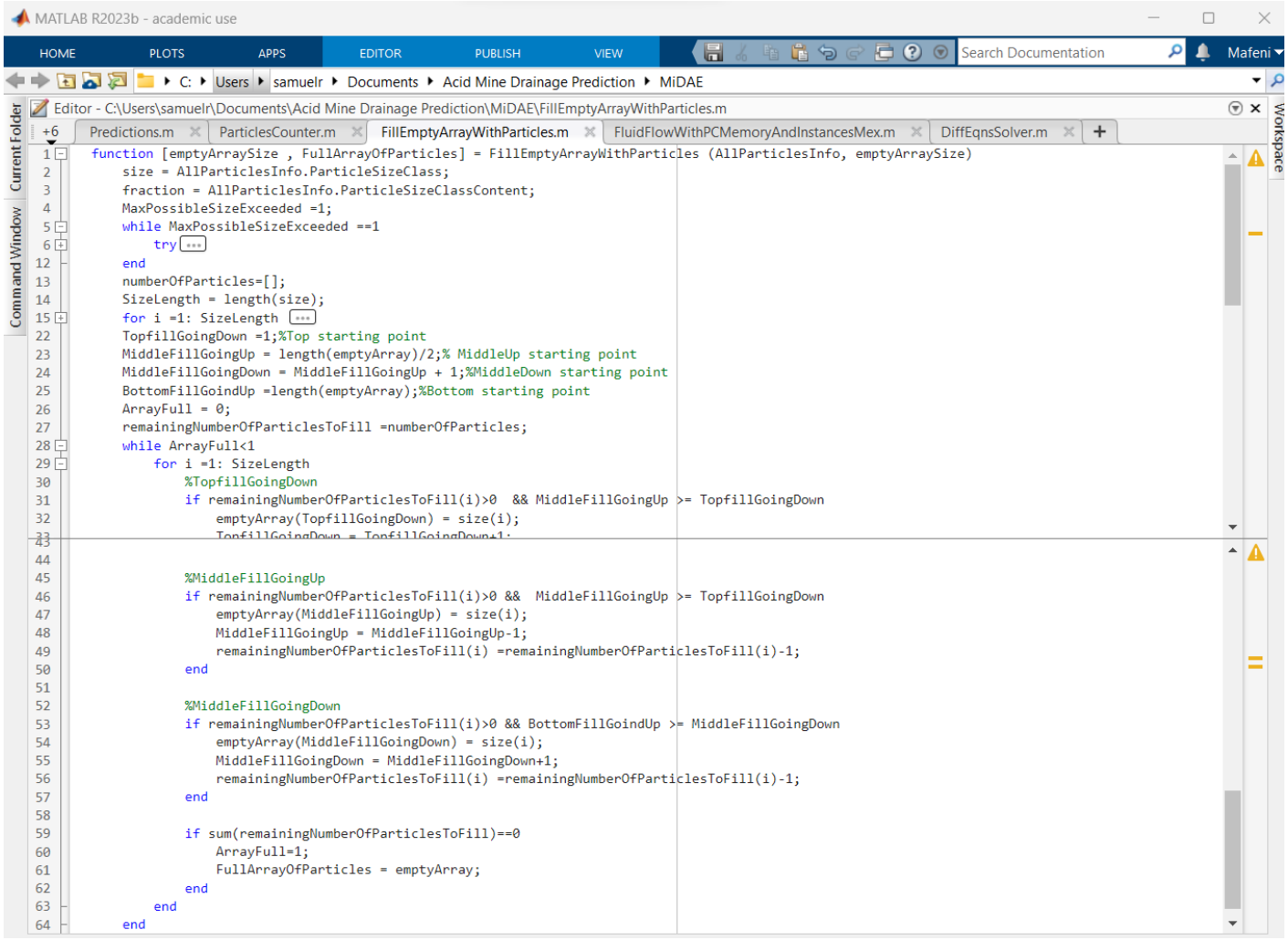

Figure G. 5: Matlab code file created for material particles placement – FillEmptyArrayWithParticles.m

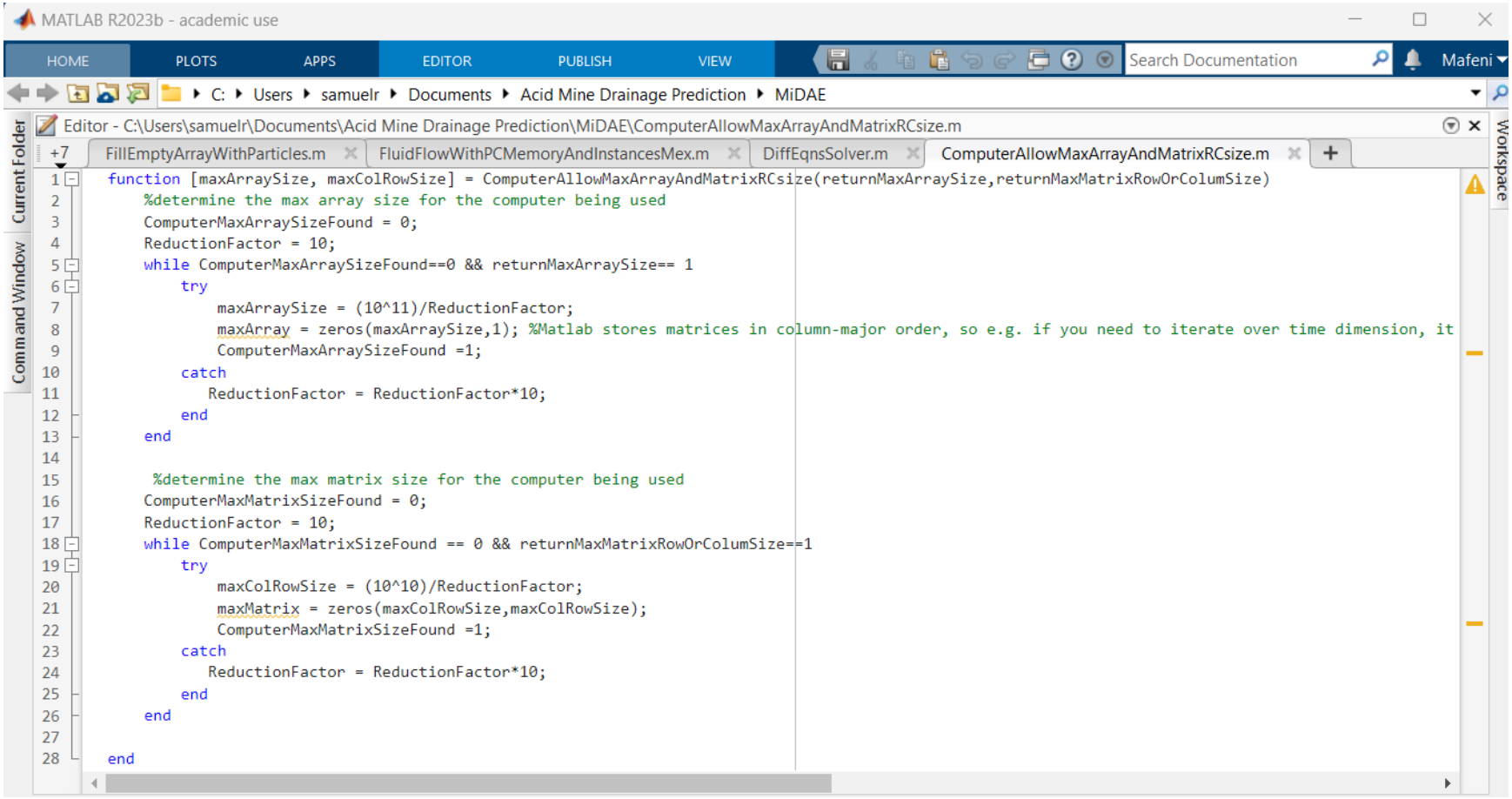

Figure G. 6: Matlab code file created to ensure that arrays or matrices are created within the computer limits – ComputerAllowMaxArrayAndMatrixRCsize.m

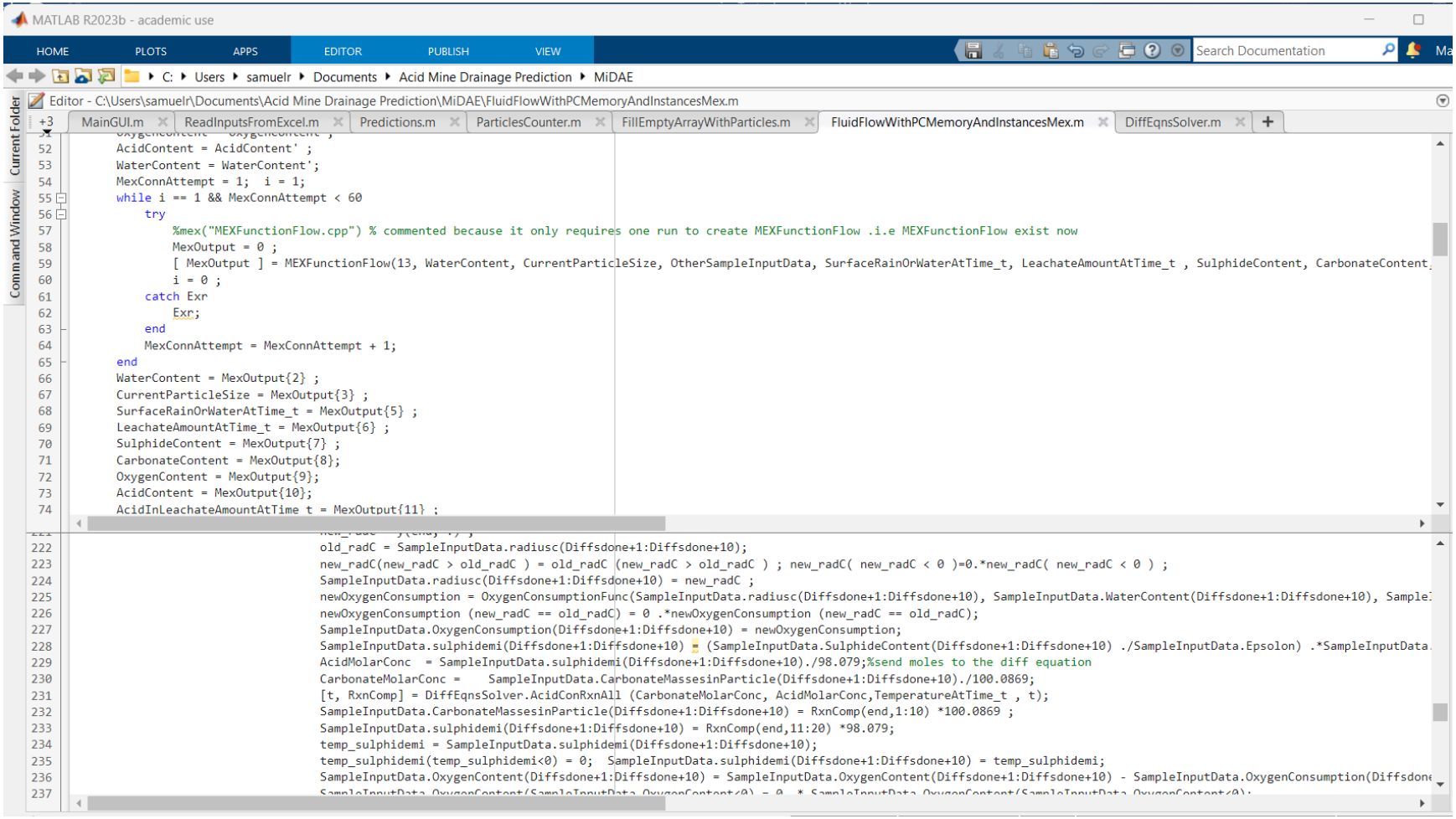

Figure G. 7: Matlab code file created to interact with C++ file for bulk flow, components mass balance, and chemical reactions – FluidFlowWithPCMemoryAndInstancesMex.m

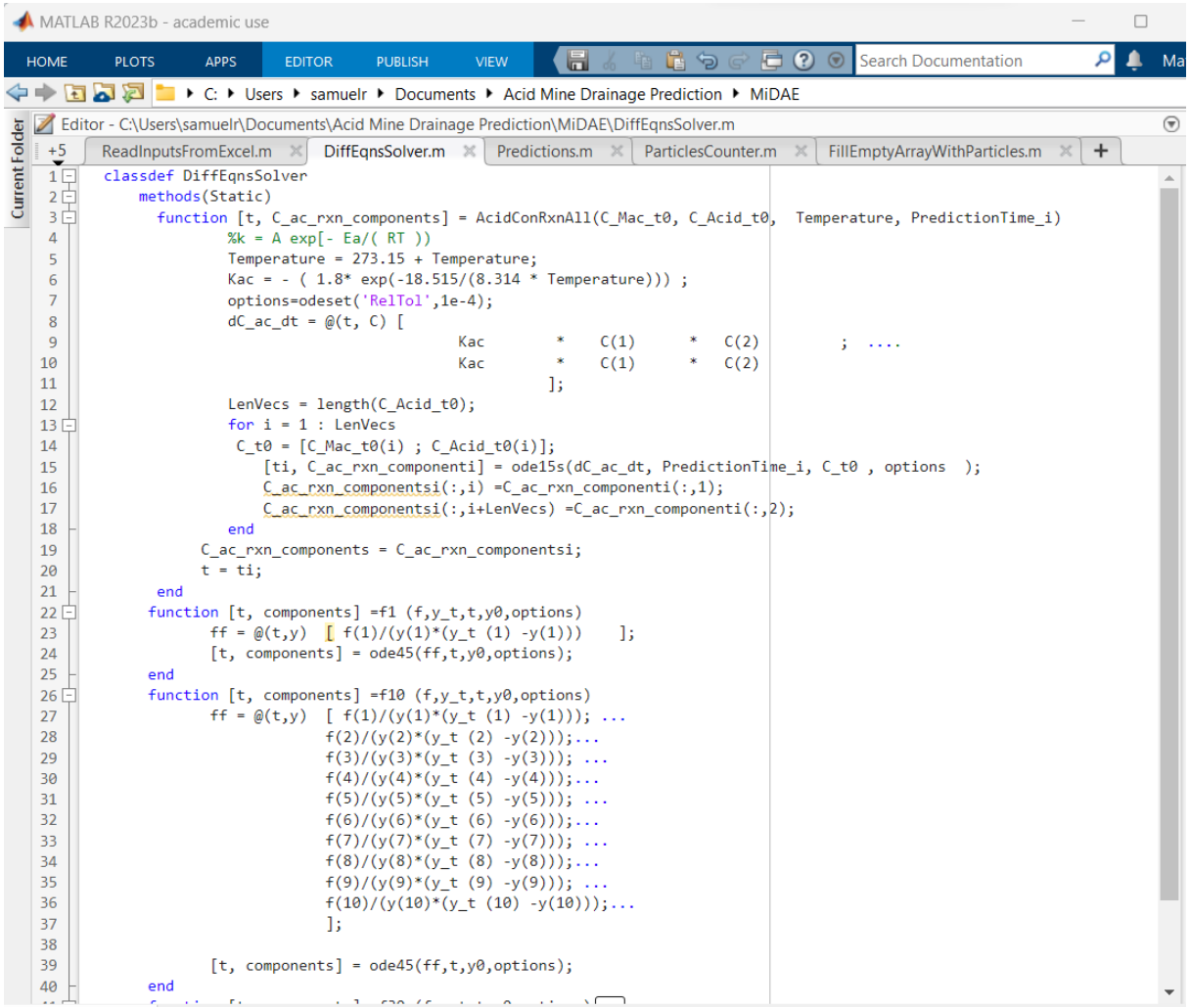

Figure G. 8: Matlab code file created for solving particles' chemical reactions differential equations – DiffEqnsSolver.m

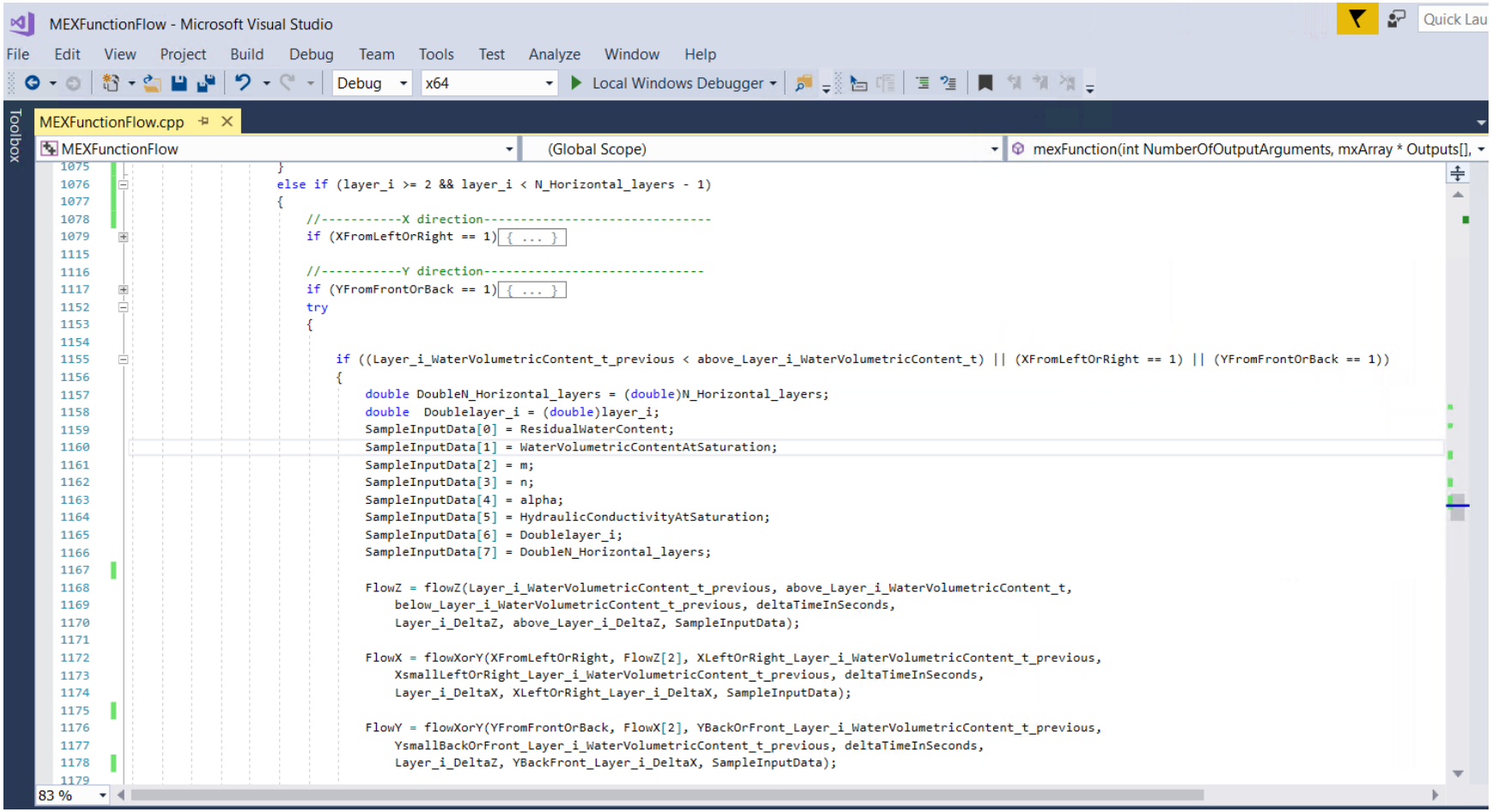

Figure G. 9: C++ code file created for solving the 3D fluid flow model and for chemical compounds mass balance– MexFunctionFlow.cpp which is used to create MEXFunctionFlow.mexw64

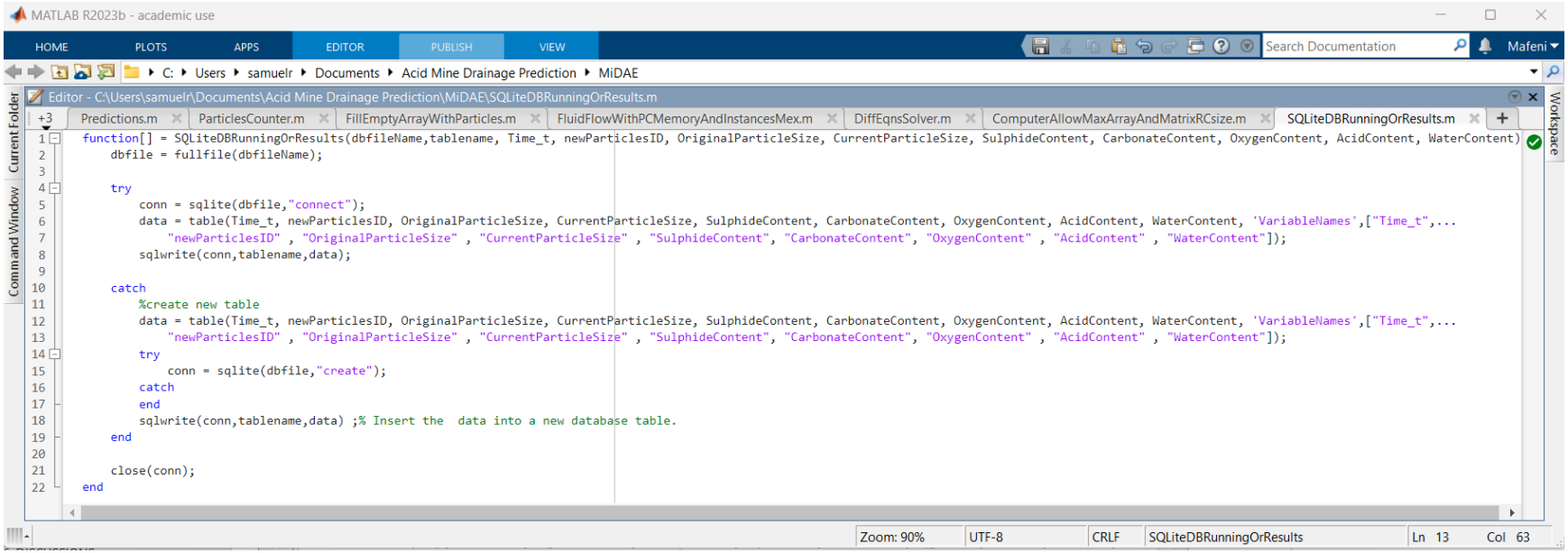

Figure G. 10: Matlab code file created for saving results data to the database – SQLiteDBRunningOrResults.m

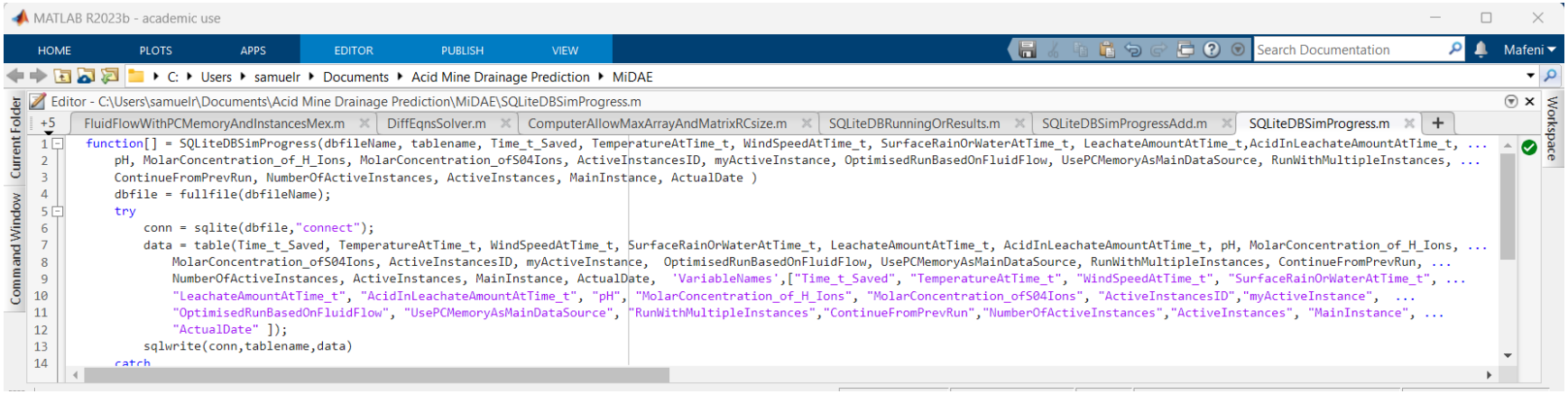

Figure G. 11: Matlab code file created for saving simulation progress data to the database – SQLiteDBSimProgress.m

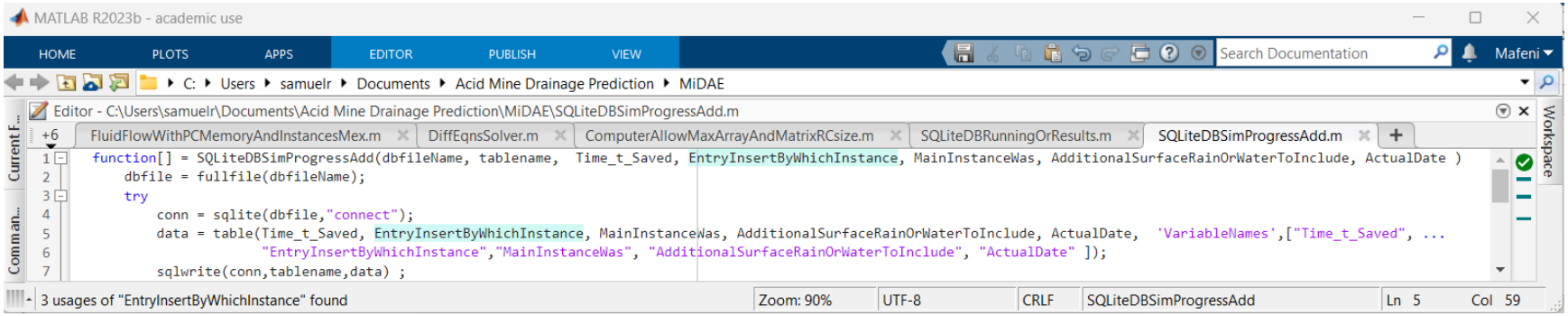

Figure G. 12: Matlab code file created for saving simulation Instances water addition simulation progress data to the database – SQLiteDBSimProgressAdd.m

APPENDIX H. USING THE DEVELOPED SOFTWARE WITH MULTIPLE INSTANCES

The following steps are a quick guide to using the developed acid mine drainage predictor (MiDAE) with multiple instances on the same computer and two different computers on the same network. Four MiDAE Instances are used in this example:

Step 1: Populate the input data file as shown in Figure F. 2. The template/example is also available from the MiDAE Help menu as shown in the next figure. The file can be saved anywhere on the computer.

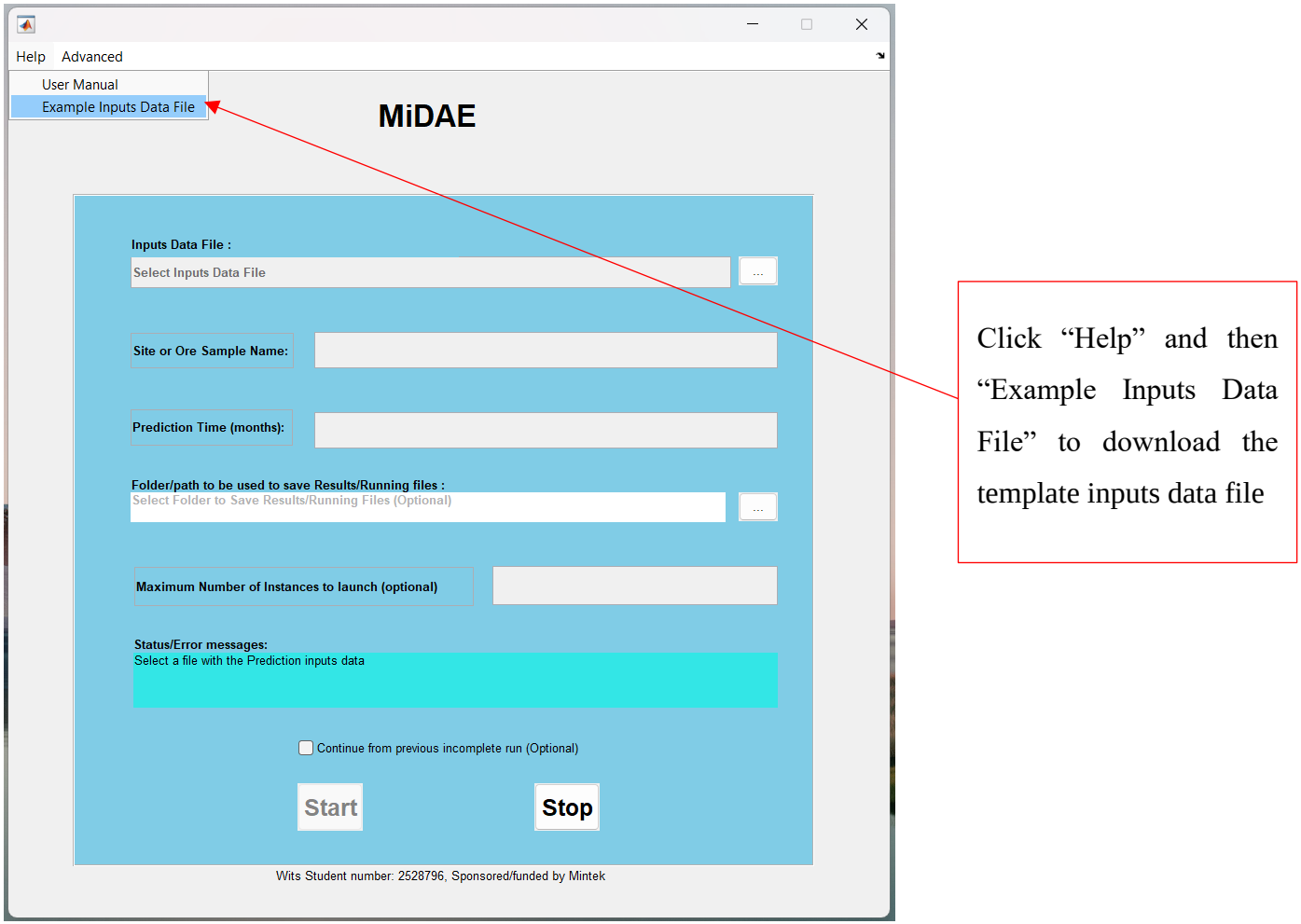

Figure H. 1: How to download the Inputs Data file template from the MiDAE App interface

Step 2: On the MiDAE interface, click the “three-dot menu” to browse to the location where the input data file populated in Step 1 is saved as shown in the following figure.

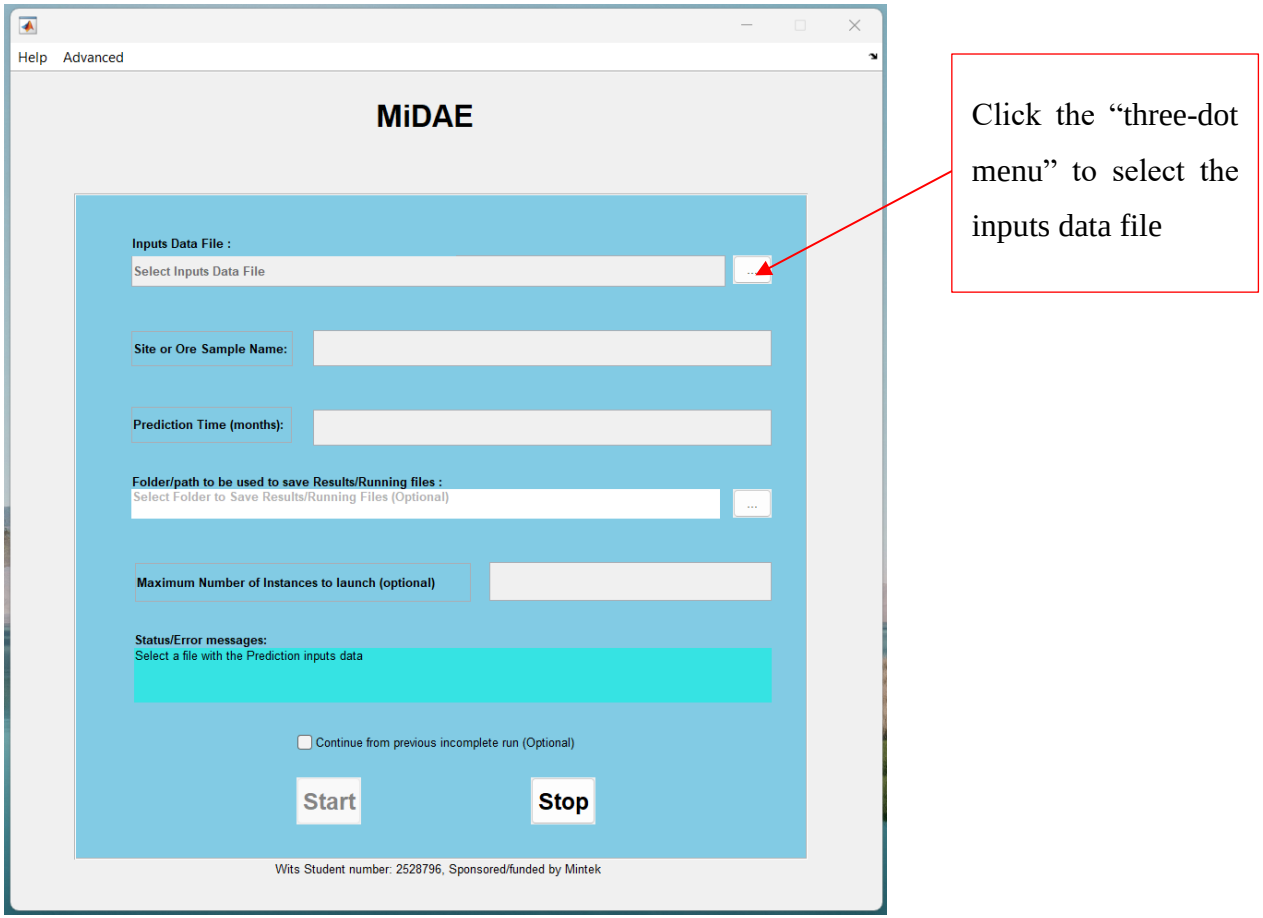

Figure H. 2: Browse to the input data file location

Step 3: Go to the inputs data file location and select it – click open afterward or double-click it as shown in the following figure.

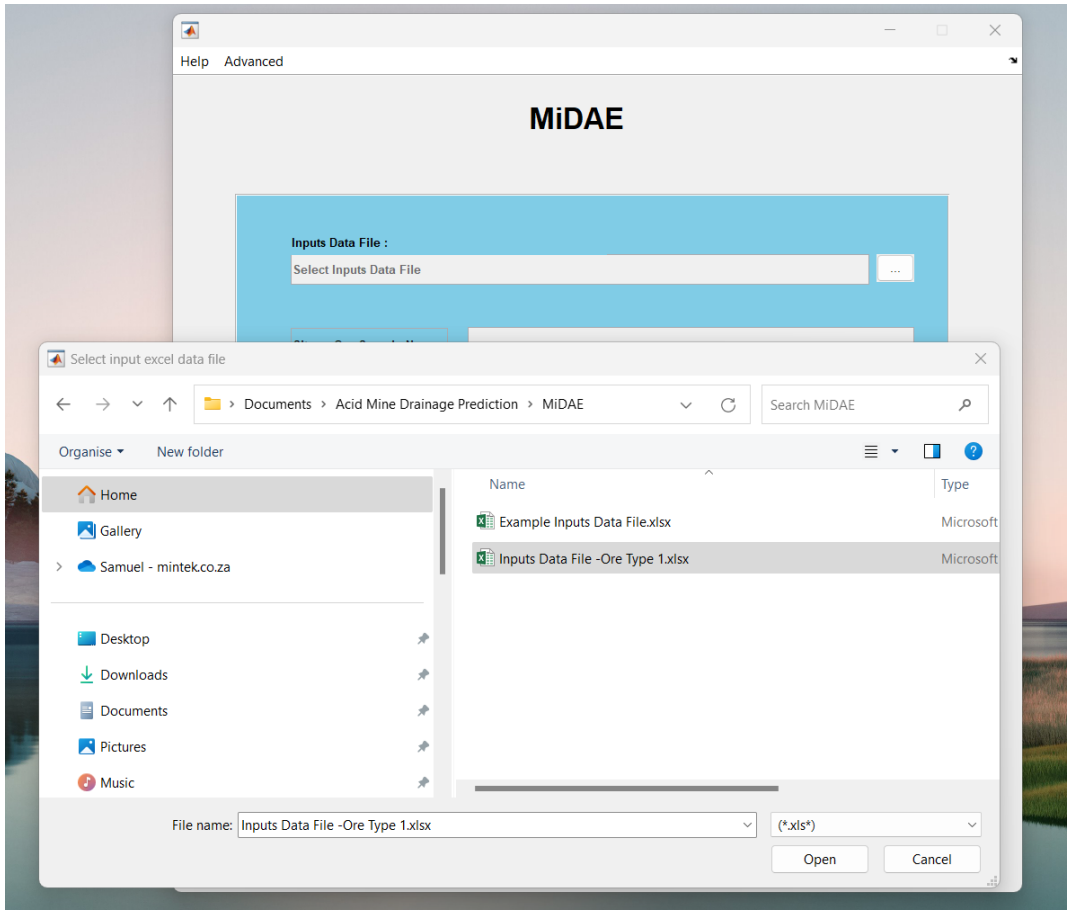

Figure H. 3: Selecting an input file location

Note that the prediction time box is now white i.e. after step 3, it becomes an available input option. Enter the prediction time (see Figure H. 4).

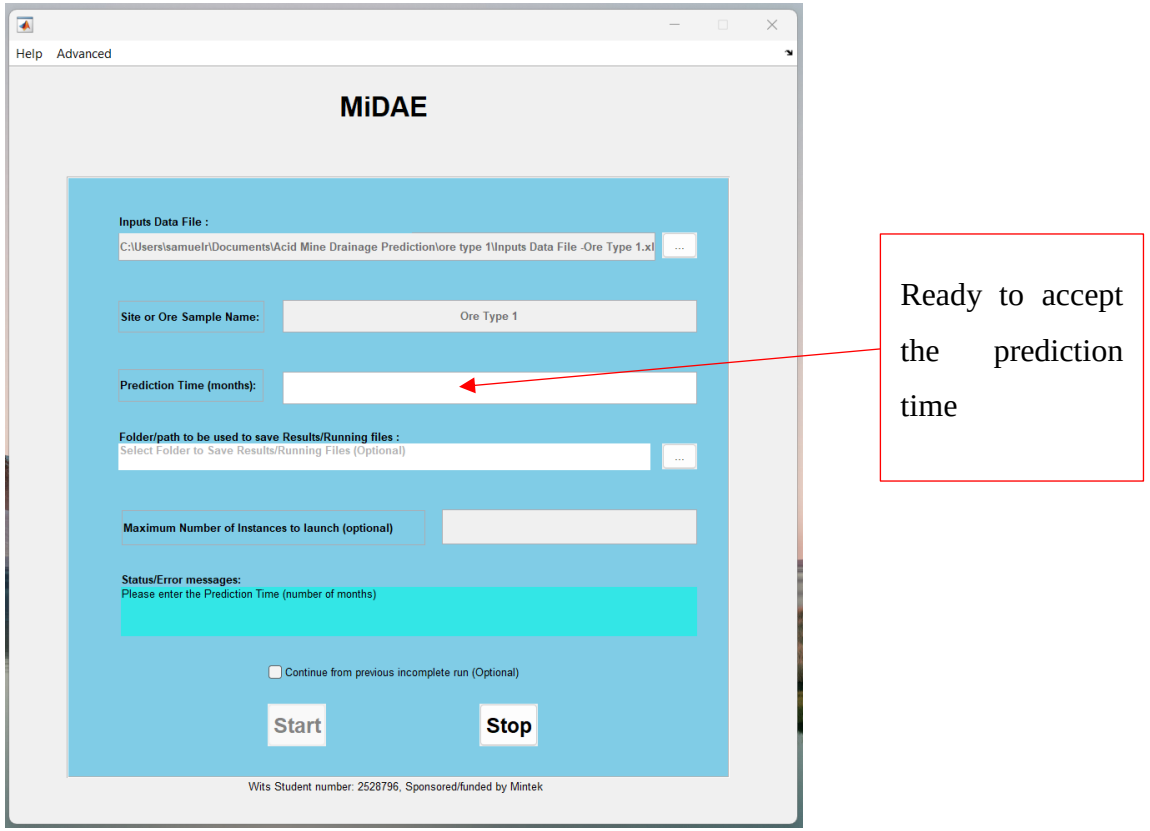

Figure H. 4: Inputs file selected and prediction time box enabled

After entering the minimum required inputs – the start button becomes green as shown in the following figure.

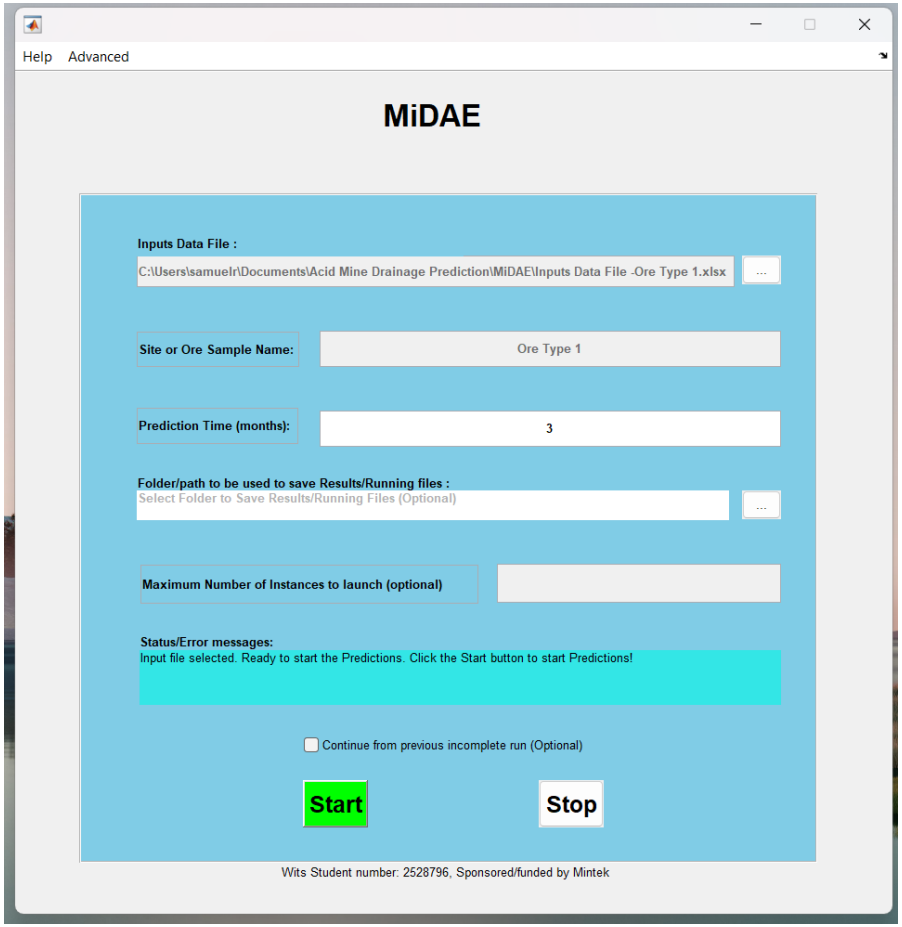

Figure H. 5: The start button becomes green after entering the minimum required inputs

Step 4: The optional inputs can be added at any time before pressing the “Start” button, examples are given in this step:

- Selecting a folder where the running/results files and the database will be saved; Figure H. 6 to Figure H. 8 below shows how to select the desired location for saving the simulation running/results database files.

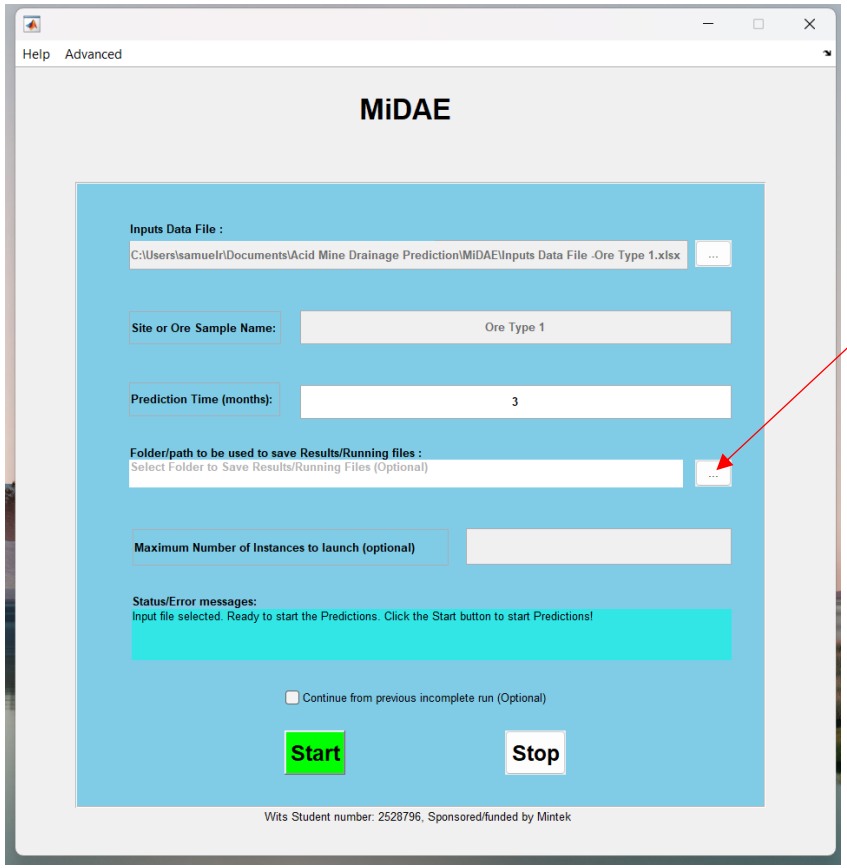

Click the “three-dot menu” to browse to the location/folder where the running/results database files will be saved.

Figure H. 6: Option to select the location where the simulation progress and results database files should be saved

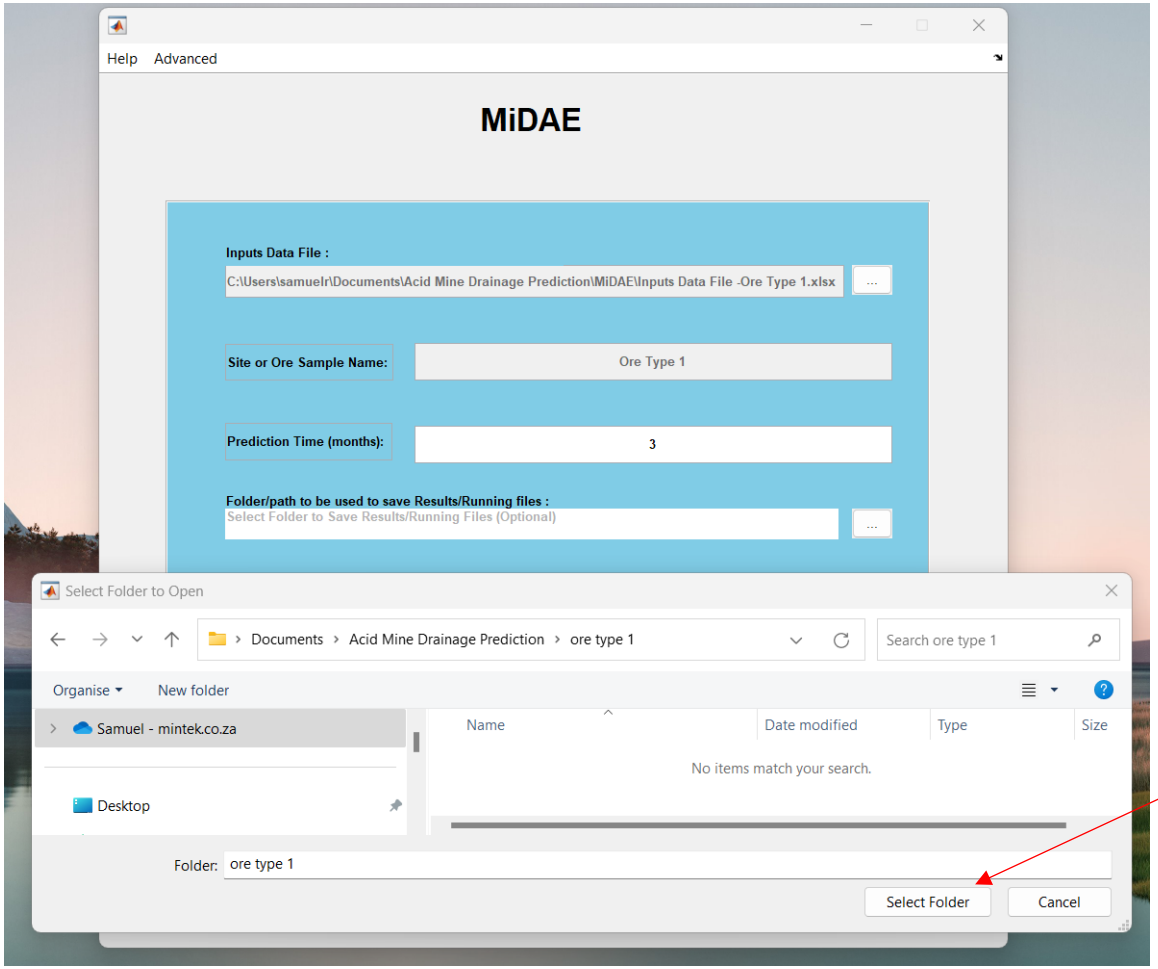

Click the "Select Folder" to select the location/folder where the running/results database files will be saved.

Figure H. 7: Select the location where the progress and results database should be saved

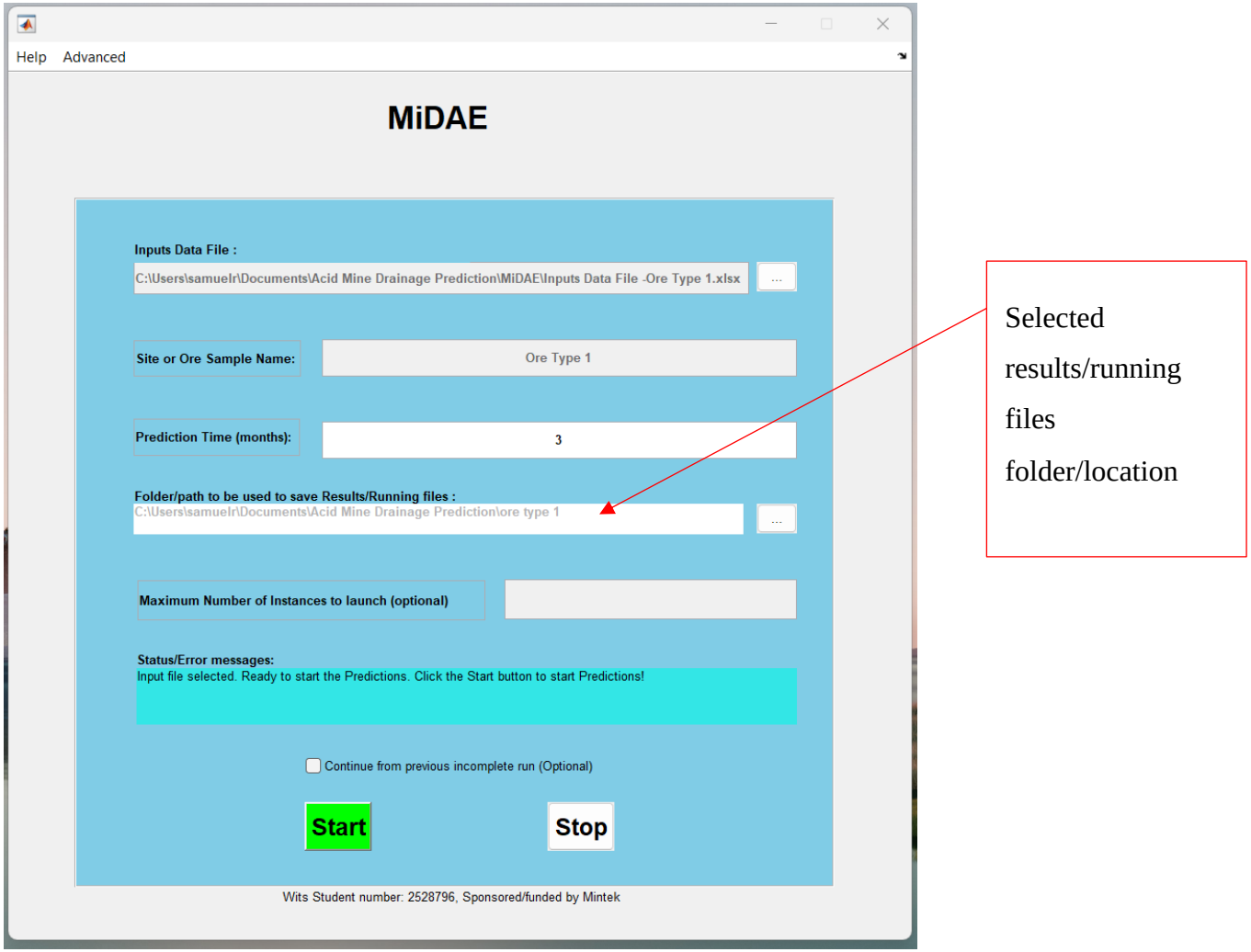

Figure H. 8: After selecting the results/running files location

Step 5: Selecting optional inputs from the "Advanced" menu:

- "UsePCMemoryAsMainDataSource" – this option gives the application (MiDAE) authority to use the full capacity of the PC memory (RAM) as the main data source for intermediate storage for fast processing/simulation. For large systems that require more RAM than what the computer has, it is recommended to use this option with "RunWithMultipleInstances" so that the ore bed/heap can be divided into multiple small instances that the computer RAM can handle. The other instance can be launched from a separate computer on the same network. With few instances or no additional instances specified, it is not recommended to select this option and it will not work if the simulated mine dump is large such that the computer memory (RAM) is not enough to store intermediate results or properties for all particles. For this case (i.e. large ore bed or mine dump), it will create Matlab and database files to store intermediate results and properties but it will run slower.
- "RunWithMultipleInstances" – An instance is a single launch of a MiDAE application. When the "RunWithMultipleInstances" is selected, the ore bed or mine dump simulation is then divided into a specified number of instances provided the final ore bed segments (vertical layers) are at least 2 for each instance. These instances communicate with each other via the instance link file. If too many instances are requested such that the resultant vertical layers are less than two per instance, the software automatically adjusts the number of instances such that the final number of instances is at least two. This should be done only on the first (original) instance that starts the overall simulation. These instances can then be run from different computers for as long as they are on the same network and can access the central data location specified on the first/original instance interface. All the instances will then have to reference this central data storage point. The central data storage point can be on the network or the first computer drive/folder. After selecting this option, the "Maximum number of instances to launch" input box becomes active (white background), enter the number in the box. If this input box is enabled after selecting "RunWithMultipleInstances" but left blank, a default of 10 instances is then assumed by the app. See Figure H. 9 to Figure H. 11 for the demonstration. Note that the "Maximum number of instances to launch" is 4 in this example.
- "OptimisedRunBasedOnFluidFlow" – this option is added to assist with speeding up the simulation time. It monitors the top layer (surface) water content, rainfall/water addition, and the leachate amount rate. If the water addition is zero, surface water is at the minimum or zero and the leachate amount is also zero for more than 3 cycles, it then changes or increases the simulation time increment for the next cycle to run such that it can reach the next water addition time faster.

This feature has been added as part of the findings/suggestion from Farthing and Ogden (2017) that the adaption of space and time produces benefits in terms of balancing between processing speed and accuracy.

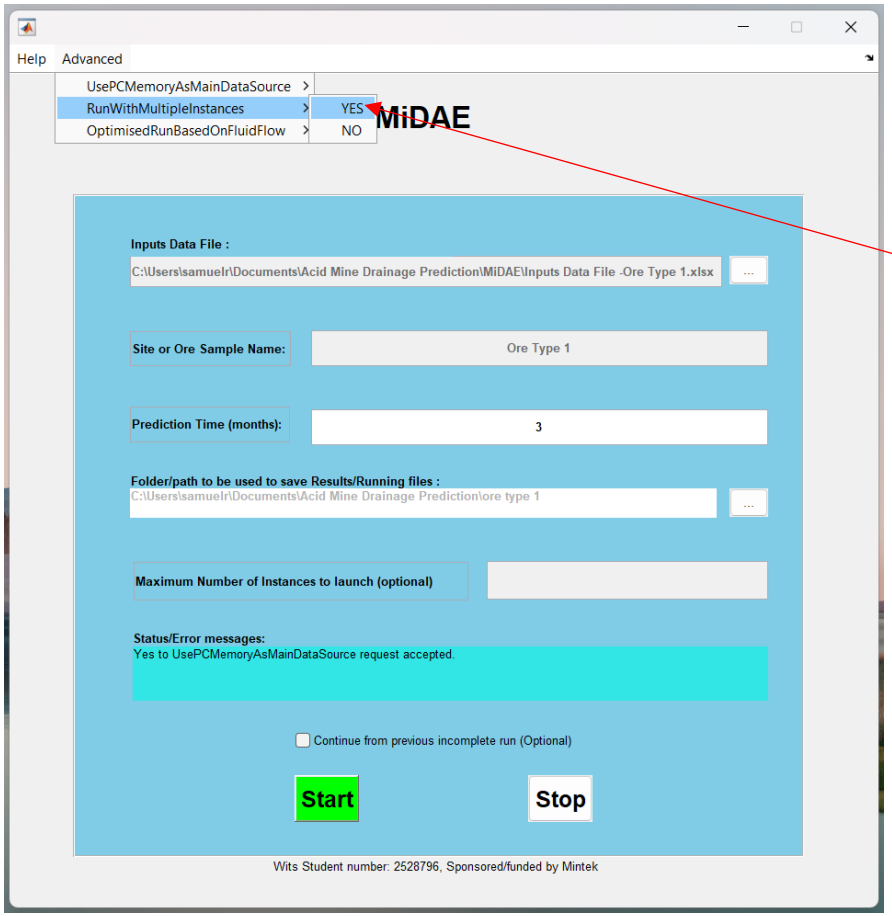

Click “Advanced”, “RunWithMultipleInstances”, and then “Yes” for simulation with multiple instance and/or computers.

Figure H. 9: Option to run with multiple instances

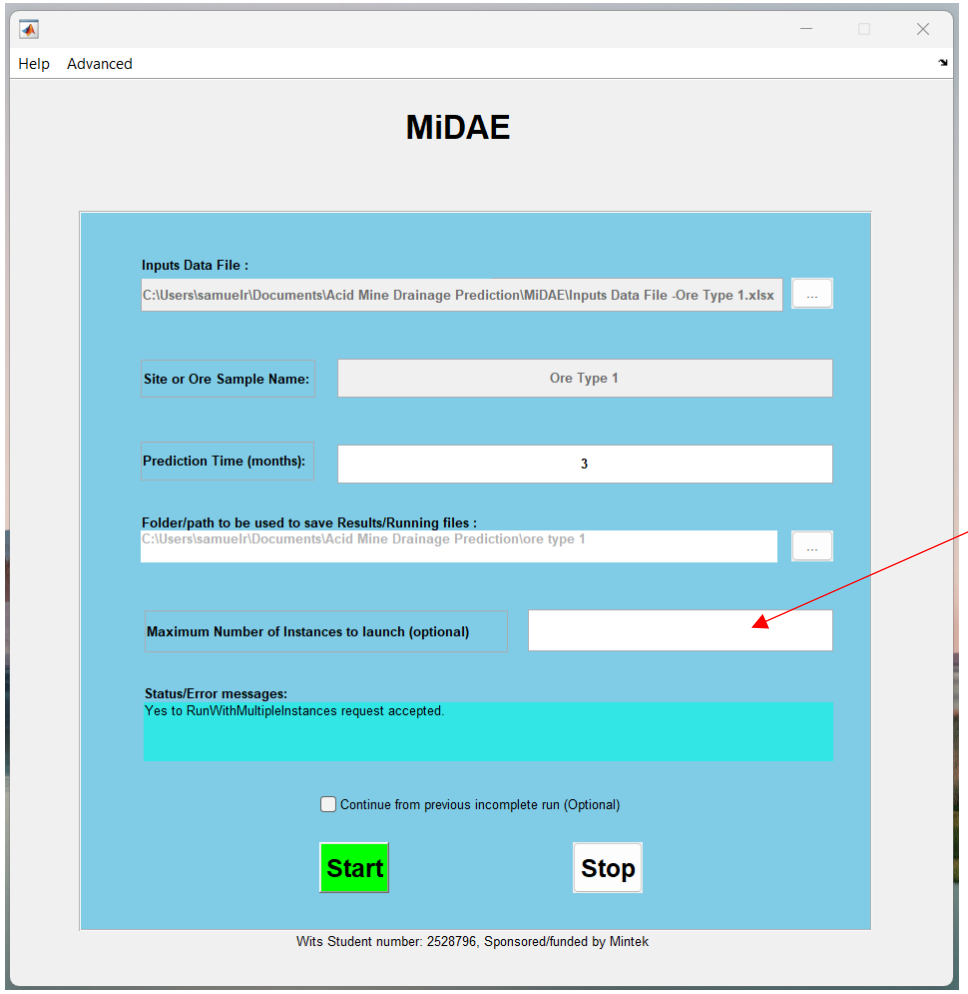

Enter the Maximum number of instances and/or computers to be launched including this one. If activated by selecting "Yes" to "RunWithMultipleInstances", but the Maximum Number of Instances to launch is left blank, the default of 10 is assumed.

Figure H. 10: Maximum number of instances

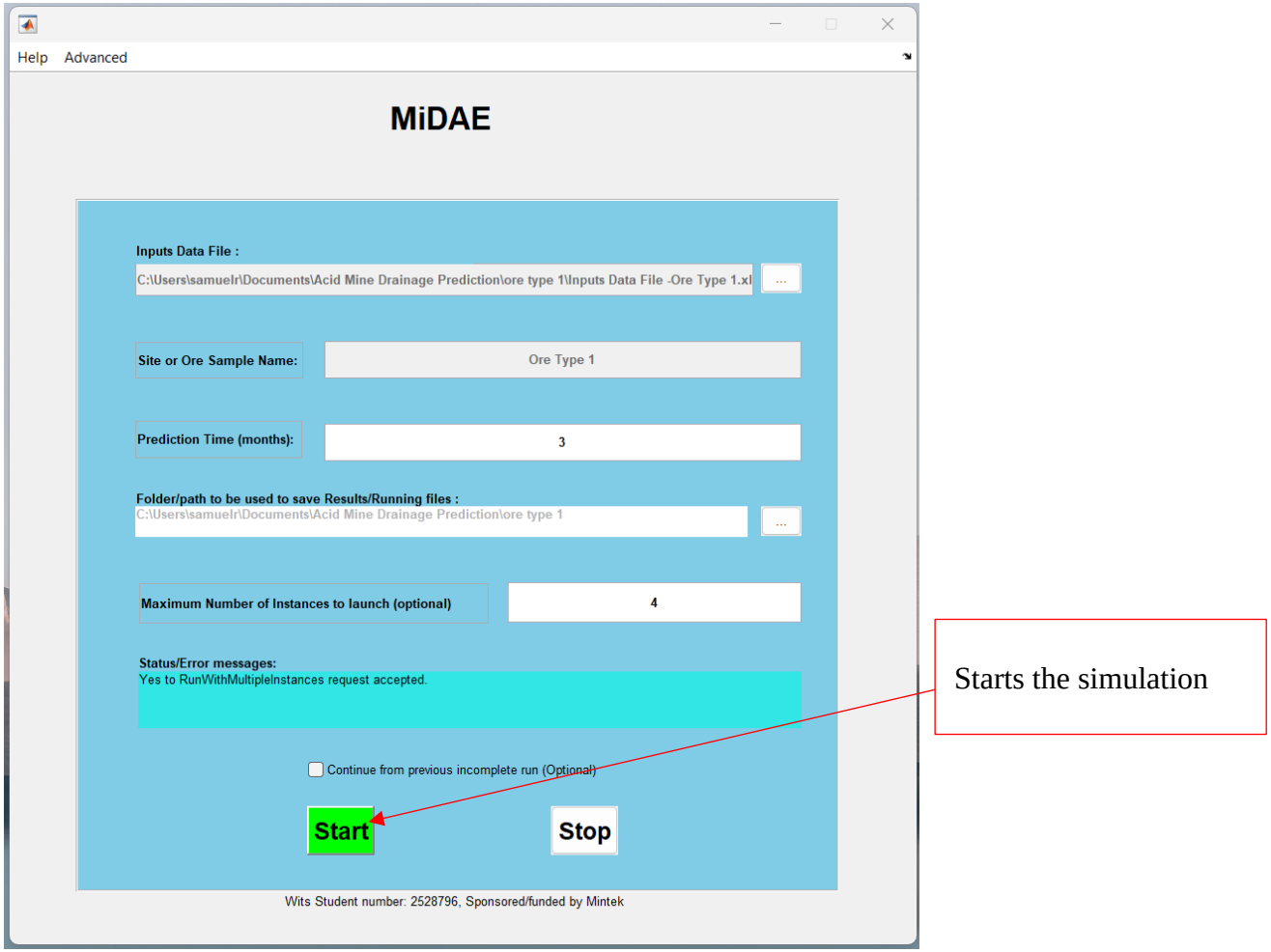

Figure H. 11: Click the Start button to start the simulation after entering the inputs

Step 6: Click the "Start" button to start the predictions. A status message (i.e. "Predictions started… Running/Simulation instance Number 1") as shown in Figure H. 12 should appear if the instance is running correctly. The running and/or results files (.csv, .mat, and .db) shown in Figure H. 13 to Figure H. 16 will also be generated once the first instance has started predictions.

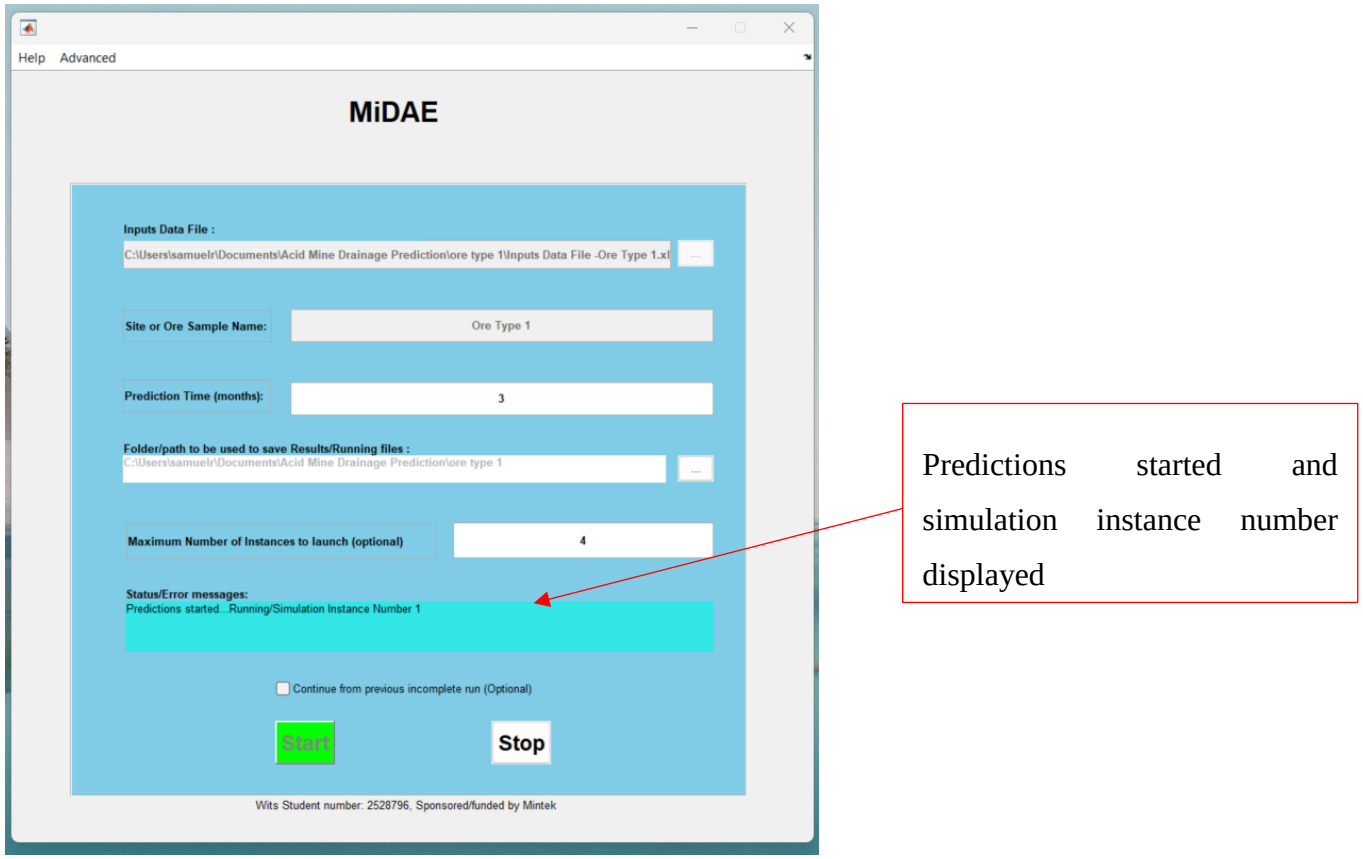

Figure H. 12: Predictions started for Simulation Instance Number 1

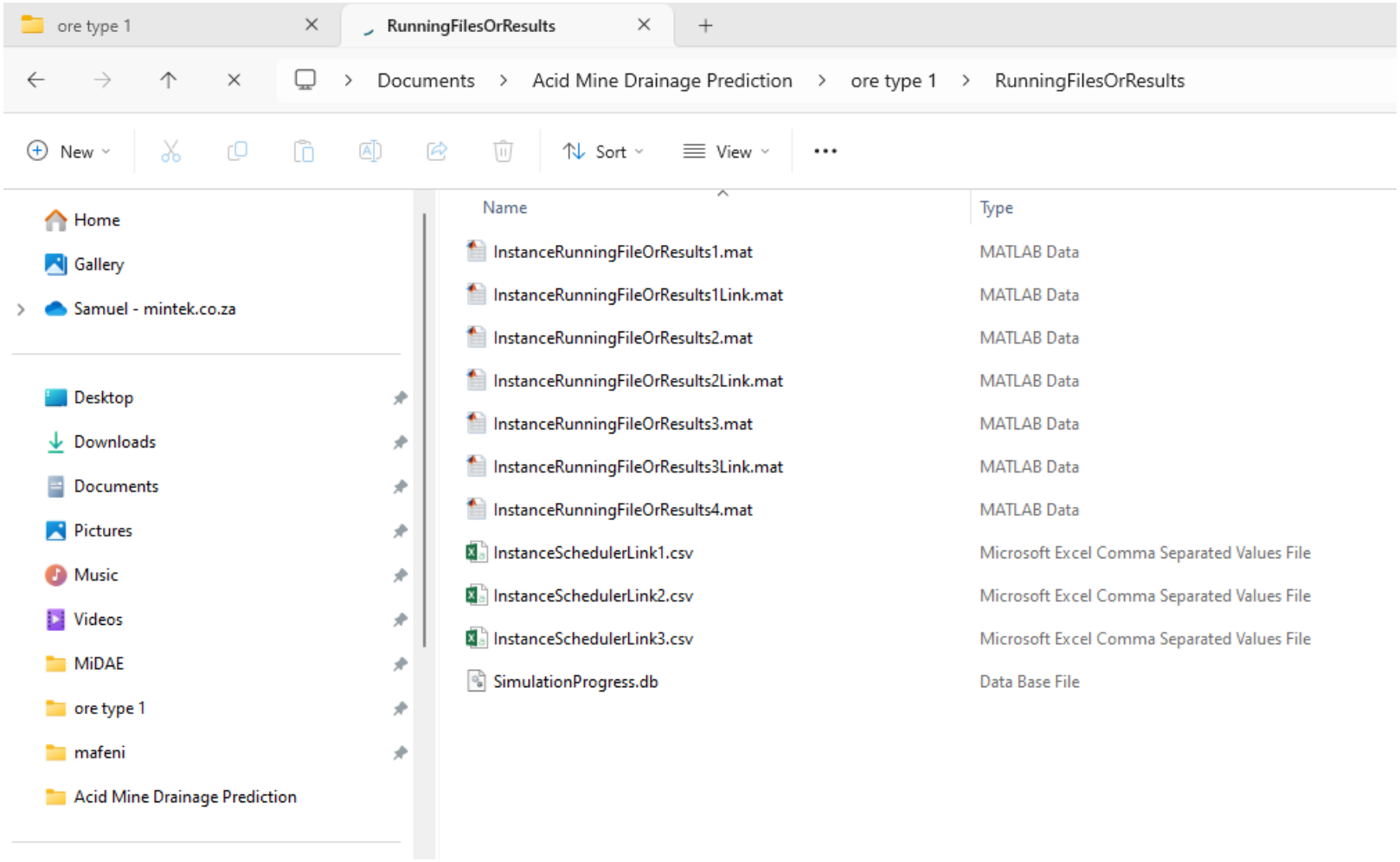

Figure H. 13: MiDAE instance running or results files and simulation progress database files

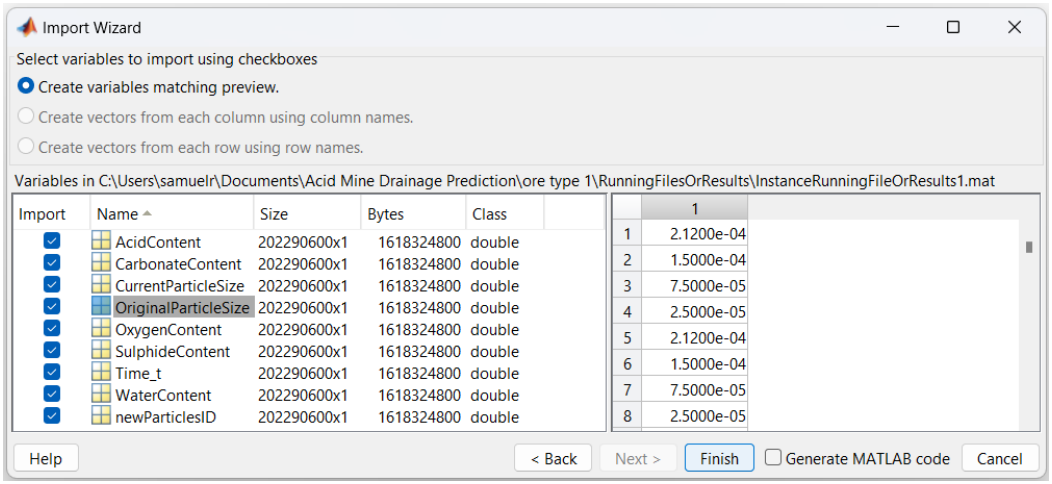

Figure H. 14: An Instance 1 running/results file

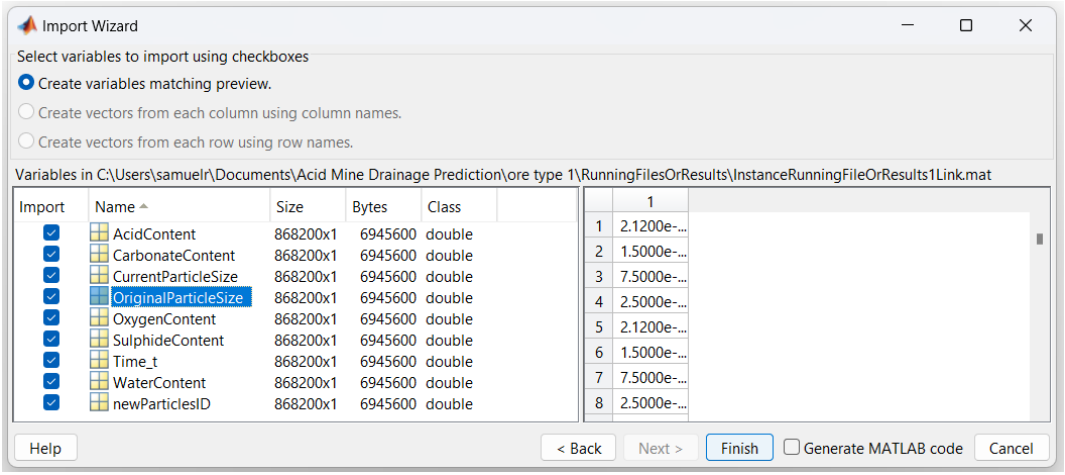

Figure H. 15: An Instance Link1 file

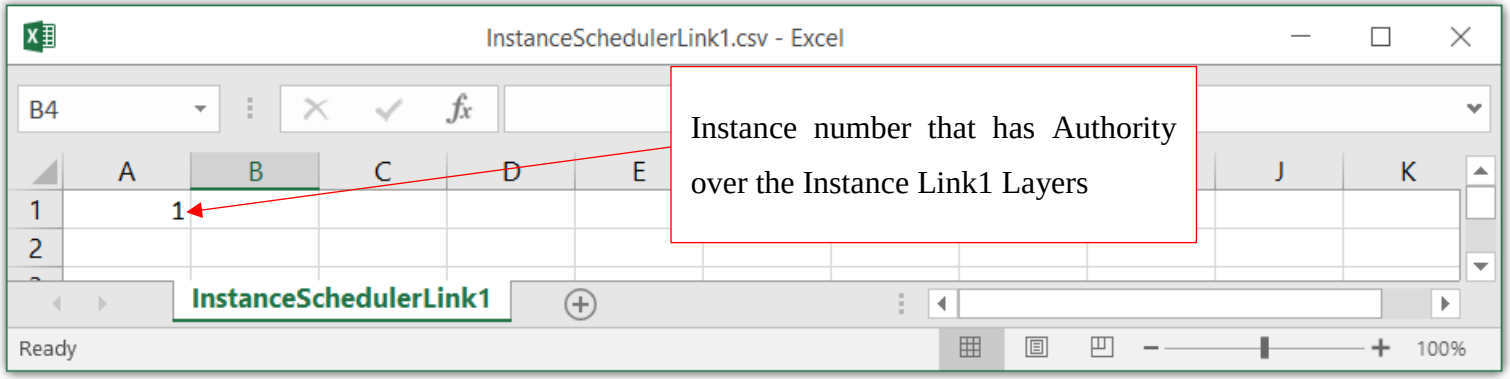

Figure H. 16: An Instance Link1 Scheduler – an instance association scheduling file

It should be noted that it was and/or is possible to combine all the instance running/results files, link files, and/or the link scheduler file into one file or database. However, this was not chosen as the trial of it resulted in the overall simulation running too slow because of file access traffic i.e. the instance simulations were too slow as the file was locked by other instances. Hence, it was decided to separate them.

The rest of the simulation parameters such as Time and the corresponding temperature, wind speed, surface rain or water, leachate amount, acid in the leachate, pH, etc. are stored in the *SimulationProgress.db* database file using SQLite (see Figure G. 10 to Figure G. 12 for more information on how it is done). Figure H. 17 shows how to view or query the data from the *SimulationProgress.db* database file using Matlab. It should be noted that any other program that can query data from the SQLite database can be used.

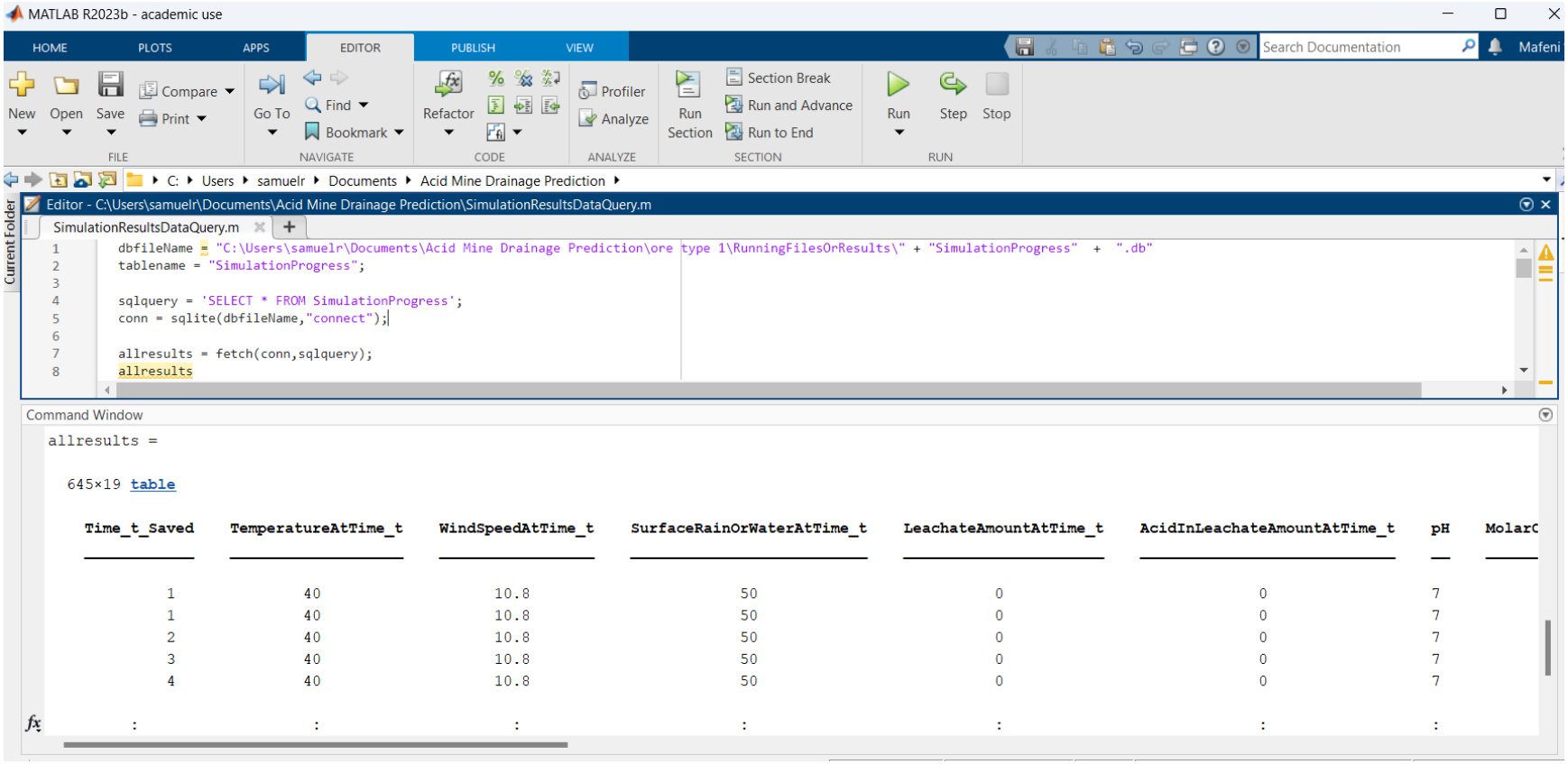

Figure H. 17: To access the results data from SimulationProgress.db

Step 7: To start the other instances, repeat steps 2, 3, and 4 but before pressing the "Start" button, click on the "continue from previous incomplete run (optional)" tick box as shown in Figure H. 18 so that the MiDAE software can know that it does not need to create new databases but either continue creating new instances as per the specified number of instances or reactivate an instance which stopped prematurely. Then click the "Start" button to start the next simulation instance (See Figure H. 19 for the response). Multiple instances imply parallel processing for everything and as a result, a faster processing time can be expected.

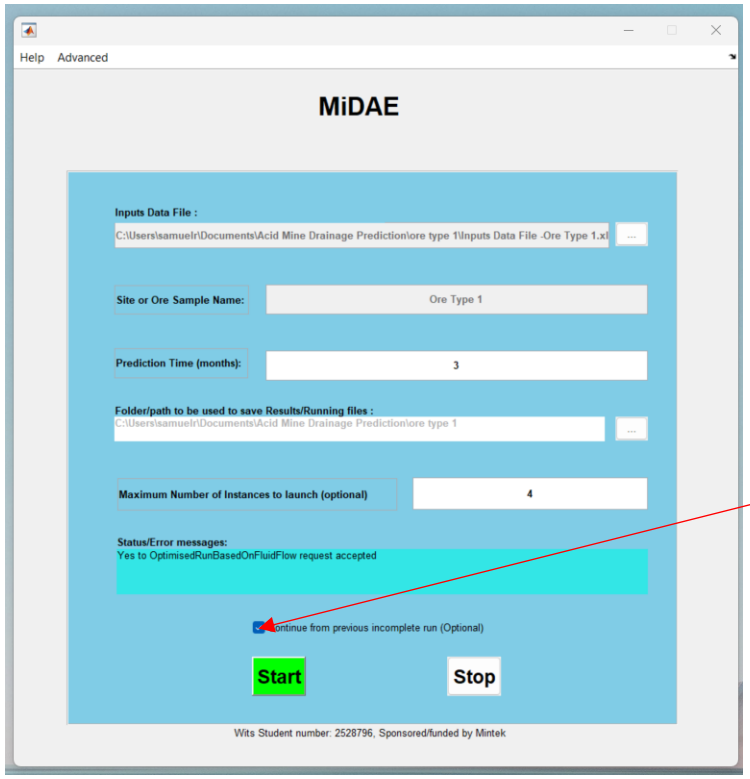

Click on the "continue from previous incomplete run (optional)" tick box to create new instance or reactive an old inactive instance.

Figure H. 18: Continue from the previous incomplete run is also used to create a new instance that has not started yet

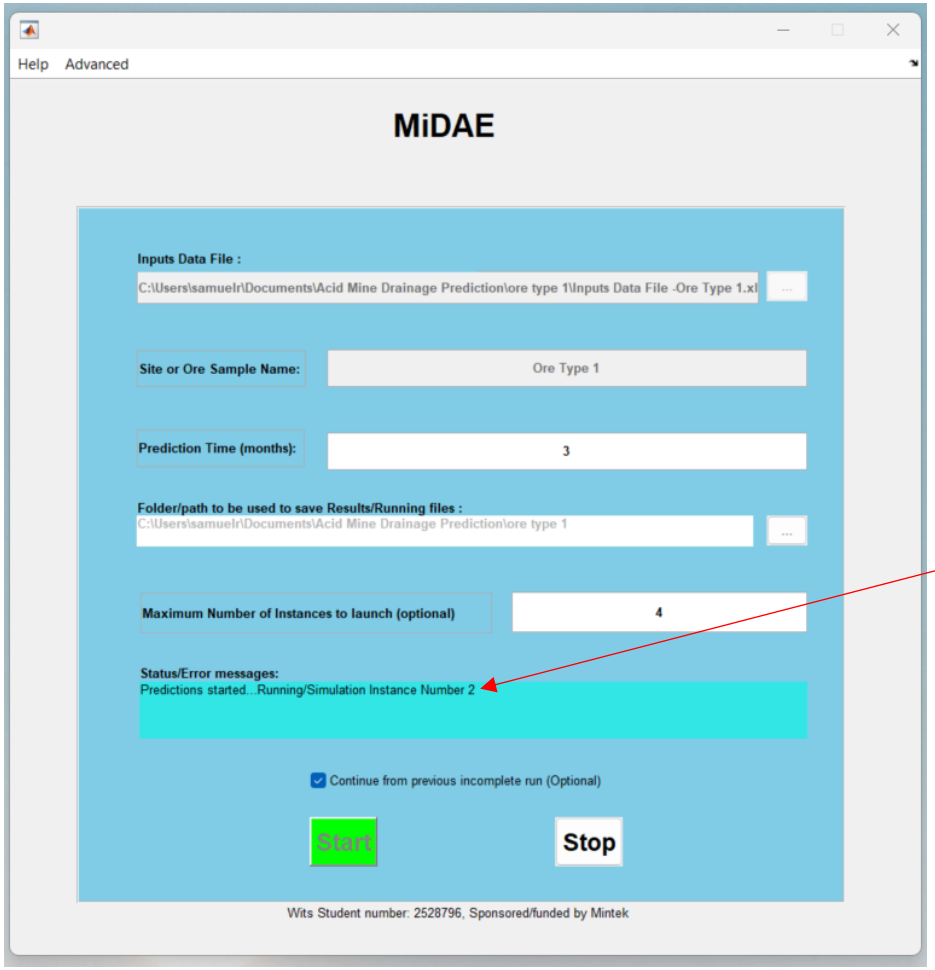

Figure H. 19: Simulation Instance 2 started

Figure H. 20 below shows an example of four instances running on the same computer. Figure H. 21 shows the same setup but with the 4th instance running on a different computer which is on the same network.

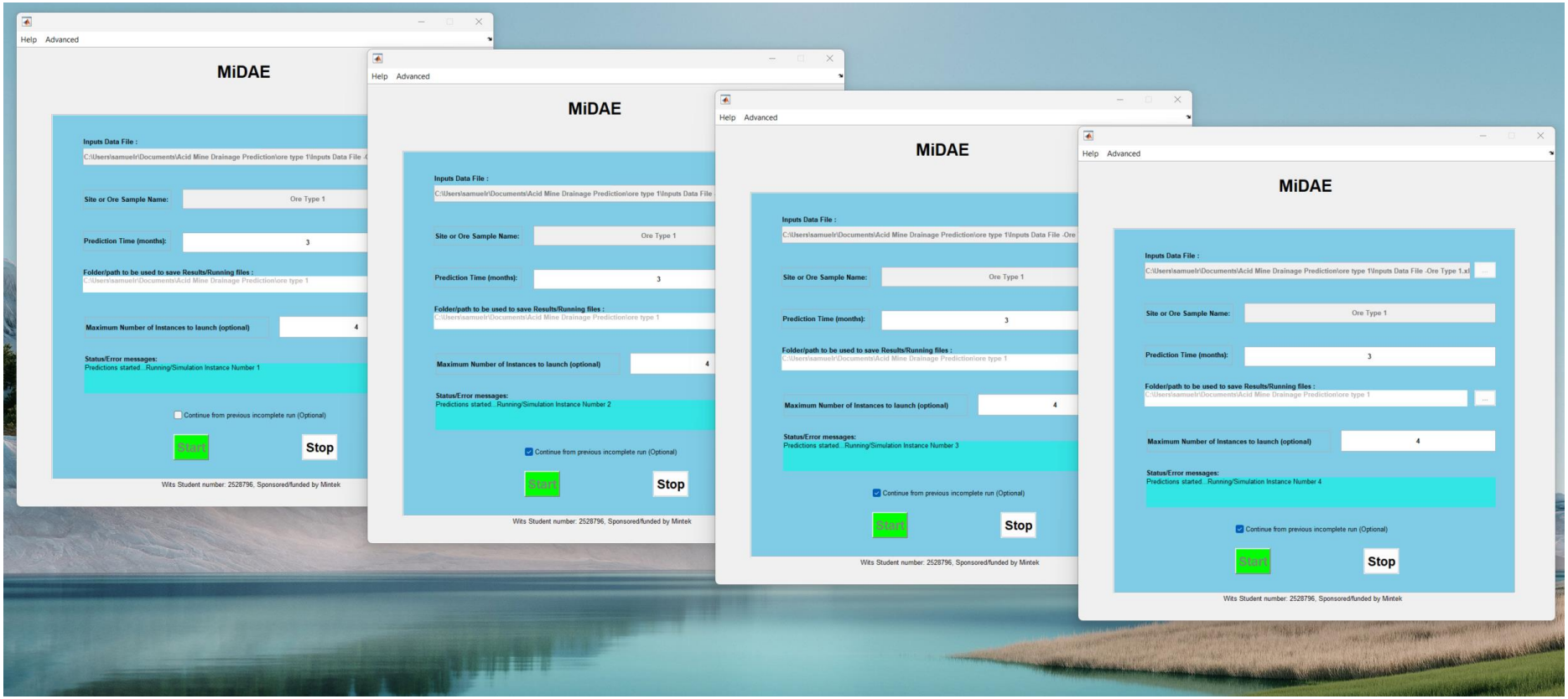

Figure H. 20: MiDAE running with 4 simulation instances on the same computer

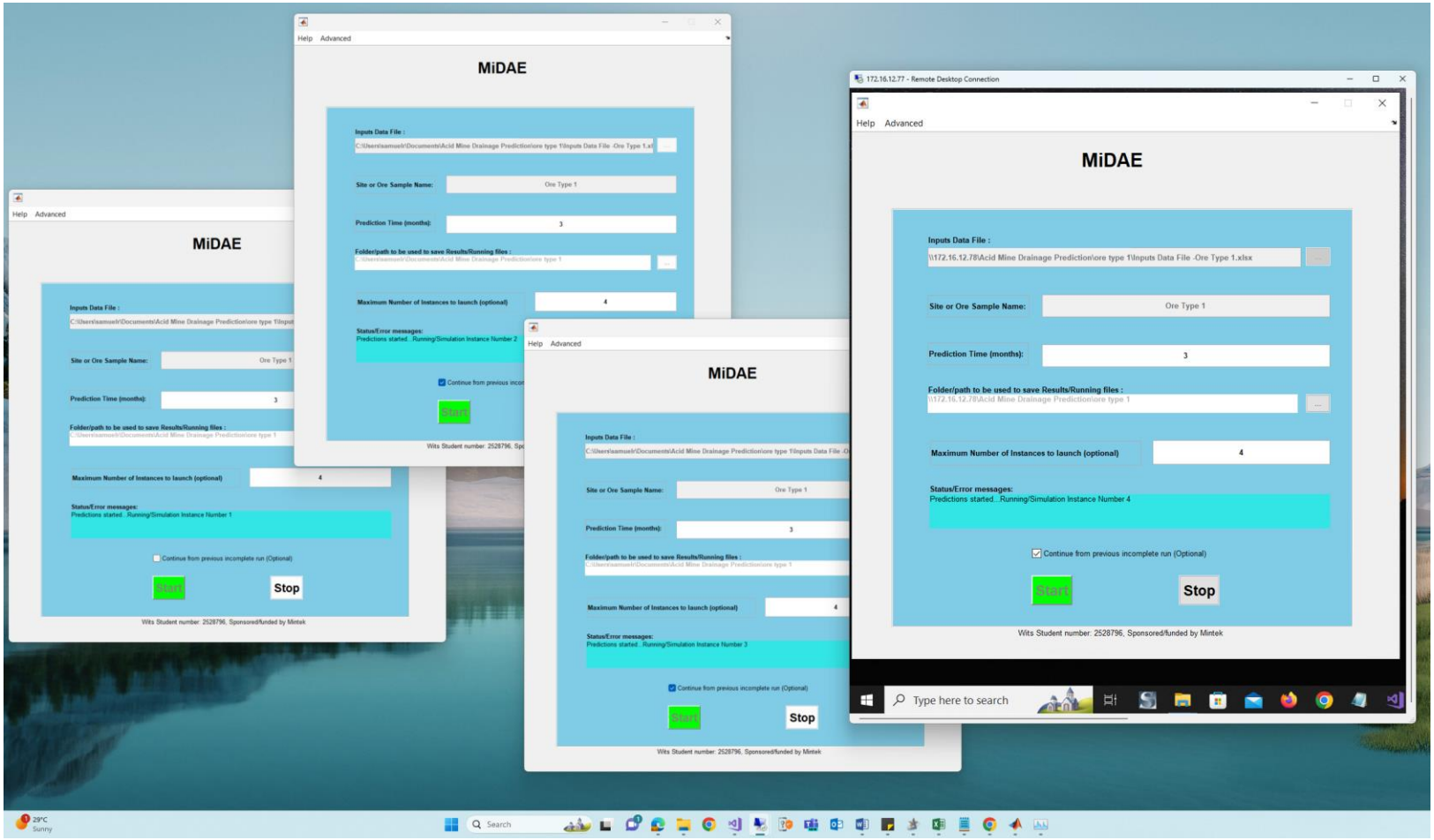

Figure H. 21: MiDAE running with 4 simulation instances and the 4th instance on a separate PC on the same network

When the simulation is complete, the user interface will display a message saying “Predictions complete and results saved to disk. Check the results folder” as shown in the figure below. The results from all the simulation Instances are saved in the selected folder. The results data can be accessed from the results folder using Matlab or any other program that can access the SQLite database as illustrated in Step 6:

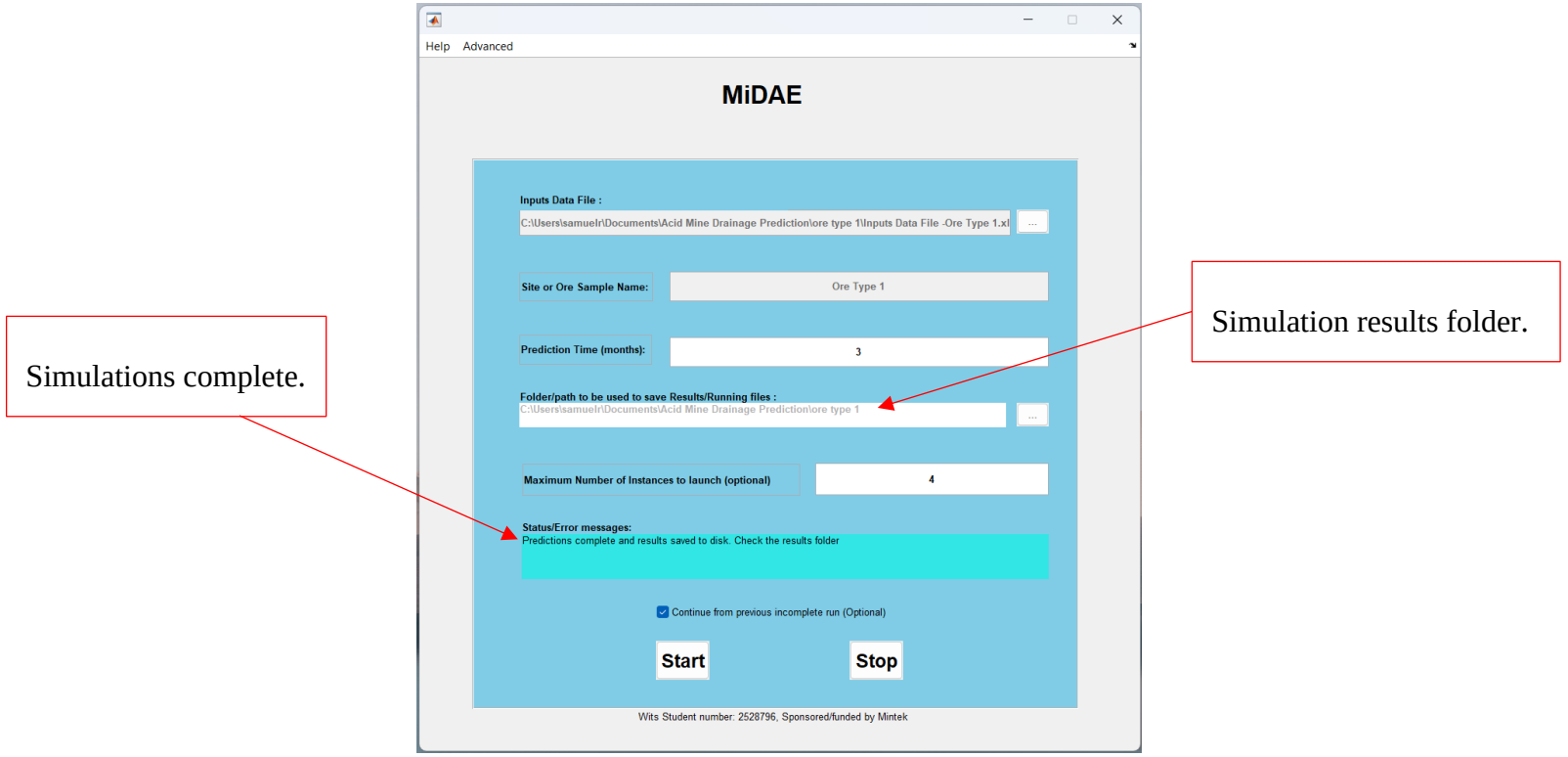

Figure H. 22: MiDAE status message when the predictions are complete

As an example, a full year simulation was done with the environmental weather conditions given in Table H. 1 below for both ore type 1 and ore type 2. The rest of the software input parameters were kept the same as in Table F. 3. The simulations profile obtained is shown in Figure H. 23.

Table H. 1: Typical full year weather conditions at the mine site of ore type 1 and type 2 (Weatherspark, n.d.)

		Jan.	**Feb.**	**Mar.**	**Apr.**	**May**	**June**	**July**	**Aug.**	**Sept.**	**Oct.**	**Nov.**	**Dec.**
Rainfall (mm)		243	220	108	25	3	0	0	0	0	15	85	213
Wind Speed (km/h)	minimum	3	3	5	8	10	10	10	11	11	10	6	5
	maximum	16	16	16	19	19	19	23	24	26	24	19	16
Temperature (°C)	minimum	17	17	17	14	12	9	9	12	15	18	18	17
	maximum	26	26	26	26	26	25	26	28	32	34	31	27

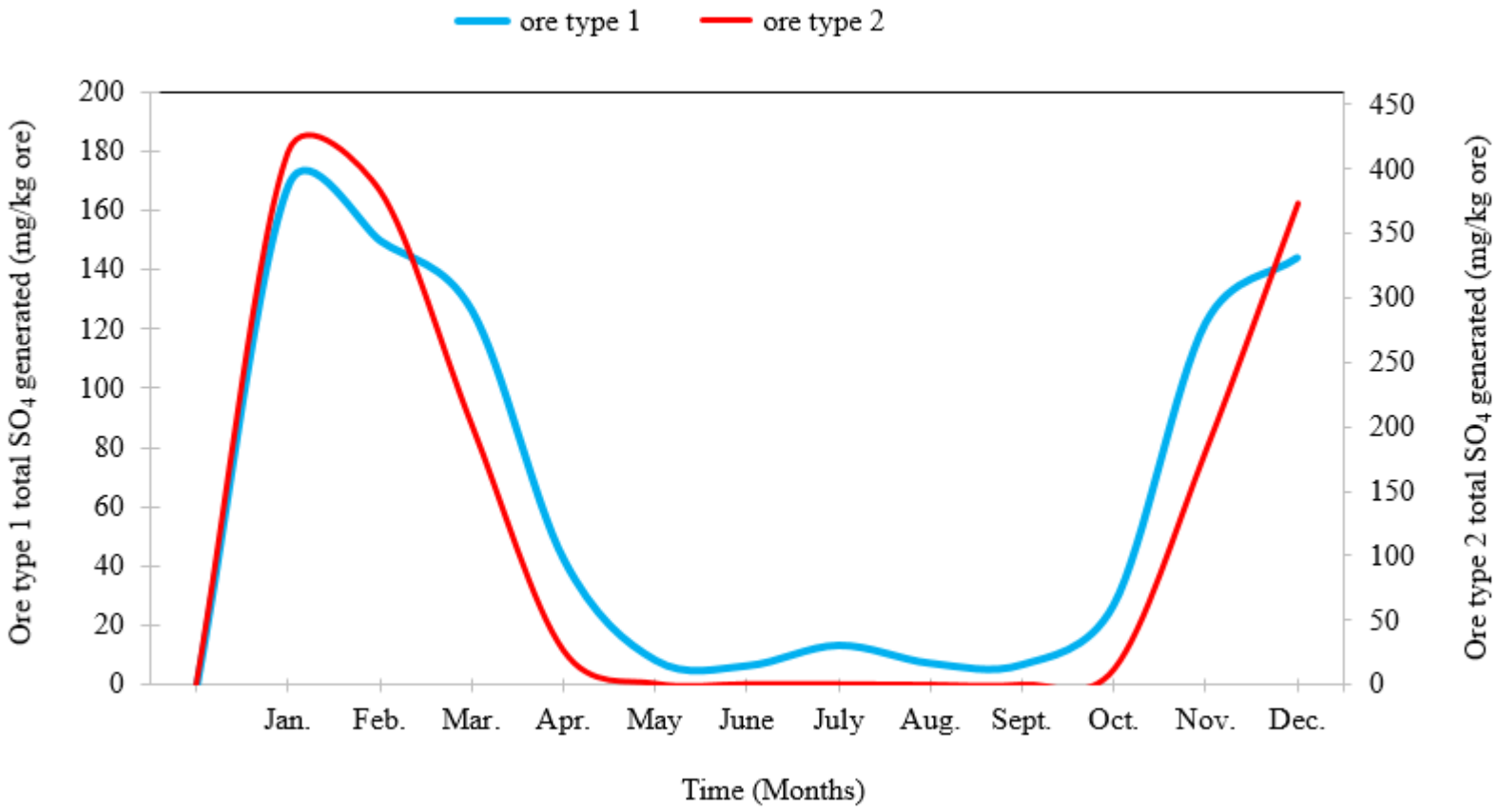

Figure H. 23: Multiple particle size model predictions with silicate minerals effects – 1 full year predictions